Journal of Life Sciences & Biomedicine, vol. 1(74), No 1, p. 5-17 (2019)

Mutation cases in the paternity tests using 15 autosomal STR markers

N.Sh.Mustafayev[1,2,*], E.R. Mammadov[2], A.Ch. Mammadov[1,2], A.B. Hasanov[2], I.M. Huseynova[1]

[1] *Institute of Molecular Biology & Biotechnologies, Azerbaijan National Academy of Sciences, 11 Izzat Nabiyev, Baku AZ 1073, Azerbaijan*

[2] *Biology Department, Scientific-Practical and Educational Unit of Forensic Medical Expertize and Pathological Anatomy, Ministry of Health of the Azerbaijan Republic; 1 M.Mirgasimov, Baku AZ1022, Azerbaijan; *For correspondence: mustafayevn02@yahoo.co.uk*

Accepted for publication: 15 October 2019

As well known, the mutations of the STR loci revealed in resolving the identification, disputed paternity/mothernity, kinship, etc. cases reduce to some extent the reliability of the results and deliver a certain difficulty in preparation of an accurate expert opinion. Therefore, information on the facts of detection of such allelic variations has great practical importance. In this study among 250 family cases of disputed paternity we found mutated alleles in two cases on FGA, in two cases on D19S433, in one case on D13S317 and in one case on D5S818 locus. In five cases more likely these mutations affected the paternal alleles, in one case the maternal allele. For each case possible mutation formation ways scheme was proposed. Moreover, in one case three-allelic profile on D21S11 locus has been observed indicating three copies of chromosome 21, which supported existing Down's syndrome phenotype.

Keywords: *STR marker, crossingover, insertion, deletion, null-allele, stepwise mutation, gene conversion, strand-slippage replication, paternity testing, maternal meiosis*

INTRODUCTION

The main directions of the use of STR-markers located on autosomal and sexual choromosomes is forensic examination in order to solve identification problems and, most importantly, disputed paternity/maternity, relationship or kinship tests (Botstein et al., 1980; Sprecher et al., 1994; Urquhart et al., 1994, 1995; Wang et al., 1996; Dupy et al., 1997; Dauber et al., 2004; Butler, 2006; Schneider, 2012; Dogan et al., 2014). In previous studies we (Mustafayev et al., 2016, 2017a, 2017b) applied of STR-markers in various areas of practical molecular biology and medicine, population studies. All these studies were based on the high hypervariability of these loci.

Currently for these purposes different sets of commercial markers, for example Promega PowerPlex 16®, Promega Geneprint FFFL® kit, Applied Biosystems SGM Plus® kit, AmpFlSTR® Identifiler® PCR Amplification Kit, AmpFlSTR® Y-filer® PCR Amplification Kit, etc are used. Studies are intensively conducted to assess the suitability of these markers for use in solving of abovementioned problems. This necessity is primarily associated with the detection of mutations in deciding the questions of disputed paternity/maternity at all loci included in these kits (Hammond et al., 1994; Geada et al., 2003; Aşıcıoğlu et al., 2004; Opolska-Bogusz et al., 2006; Zhao et al., 2007; 2015; Deucher et al.., 2010; Dinesh et al., 2013; Zhang et al., 2014, etc.). Such assessment of 18 frequently used loci in conducting maternity/paternity and kinship tests was regularly conducted American Association of Blood Banks (AABB) from 2001 to 2013 (Annual Report Summary..., 2001, 2002, 2003, 2004, 2006, 2008, 2010, 2013; for details see: https://strbase.nist.gov/mutation.htm, table 1).

As it is known mutations arise mainly in meiosis, i.e. more precisely it occur in pachytene (pachyneme) phase of prophase I (the final phase of genetic recombination or third phase of prophase I) of the meiosis I with the participation of the

synaptoneme complex. In this stage of meiosis occur exchange of genetic material/or information between homologous chromosomes. It should be noted that all types of chromosomal rearrangements – deletions/ insertions, inversions, duplications, translocations, etc., occur in this phase The chance of autosomal chromosome mutations in meiosis is always great compared to sex chromosomes. When the meiotic mutation affects the maternal genetic material it is called maternal meiosis, when paternal genetic material - paternal meiosis.

There are several different approaches for describing mutations in these microsatellite loci which are used in performing of paternity tests (Fan and Chu, 2007). All these points of views theoretically based on stepwise mutation model of T.Ohta and M.Kimura (see: H.Ellegren, 2004). U-D.Immel et al. (2004) showed that the most obvious explanation for a mutation in an STR locus would be a contraction of the repeat stretch due to polymerase slippage and these mutations are almost invariably confined to a single repeat. Based to the experimental data they proposed a gene conversion and DNA crossover model (see: Fig. 3 in Immel et al., 2004). By M.A.Jobling (2004) preferred other – strand-slippage replication mechanism of mutation formation (Fig. 1). It should be noted that larger contractions or expansions are considered extremely rare, and to be the consequence of recombination rather than slippage.

In the literature there is a large amount of data on identified mutations almost for each autosomal STR locus (Boutrand et al., 2001; Leibelt et al., 2003; Ricci et al., 2003; Immela et al., 2004; Edwards and Allen, 2004a, 2004b; Singh et al., 2006; Huel et al., 2007; Narkuti et al., 2007, 2008; Balloch et al., 2008; Natsuko et al., 2008; Eunus et al., 2009; Venkanna et al., 2009; Burkhard et al., 2011; Li et al., 2014; Liu et al., 2015; Cabezas et al., 2016, etc.). For example, in study performed by H.Geada et al. (2003) 511 paternity cases were investigated using SGM Plus and PowerPlex 16 Kits, 18 paternal and maternal mutation cases have been detected in 13 STR loci and types of mutations (one-step, two-step and null allele-mutations) were indicated.

In another sudy of paternity testing by K.J.D.Balloch et al. (2008) 2 exclusions are encountered at D8S1179 and CSF1PO STR loci has been reported. Paternity test repeated using PowerPlex16®, FFFL System® and SGM Plus® kits and detected exclusions were observed. Interestingly, the alleles observed at CSF1PO: alleged father (11, 12), child (10, 11), mother (11, 12) arose as a result of a mutation from either the mother or father. Paternity has been proven Y-chromosome testing using PowerPlex Y® kit which result showed that Y-chromosome haplotypes of alleged father and child are matched.

Табле 1. Apparent mutations observed at STR loci in the course of paternity testing (https://strbase.nist.gov/mutation.htm).

STR System	Maternal Meioses (%)	Paternal Meioses (%)	Number from either	Total Number of Mutations	Mutation Rate
CSF1PO	95/304,307 (0.03)	982/643,118 (0.15)	410	1,487/947,425	0.16%
FGA	205/408,230 (0.05)	2,210/692,776 (0.32)	710	3,125/1,101,006	0.28%
TH01	31/327,172 (0.009)	41/452,382 (0.009)	28	100/779,554	0.01%
TPOX	18/400,061 (0.004)	54/457,420 (0.012)	28	100/857,481	0.01%
VWA	184/564,398 (0.03)	1,482/873,547 (0.17)	814	2,480/1,437,945	0.17%
D3S1358	60/405,452 (0.015)	713/558,836 (0.13)	379	1,152/964,288	0.12%
D5S818	111/451,736 (0.025)	763/655,603 (0.12)	385	1,259/1,107,339	0.11%
D7S820	59/440,562 (0.013)	745/644,743 (0.12)	285	1,089/1,085,305	0.10%
D8S1179	96/409,869 (0.02)	779/489,968 (0.16)	364	1,239/899,837	0.14%
D13S317	192/482,136 (0.04)	881/621,146 (0.14)	485	1,558/1,103,282	0.14%
D16S539	129/467,774 (0.03)	540/494,465 (0.11)	372	1,041/962,239	0.11%
D18S51	186/296,244 (0.06)	1,094/494,098 (0.22)	466	1,746/790,342	0.22%
D21S11	464/435,388 (0.11)	772/526,708 (0.15)	580	1,816/962,096	0.19%
Penta D	12/18,701 (0.06)	21/22,501 (0.09)	24	57/41,202	0.14%
Penta E	29/44,311 (0.065)	75/55,719 (0.135)	59	163/100,030	0.16%
D2S1338	15/72,830 (0.021)	157/152,310 (0.10)	90	262/225,140	0.12%
D19S433	38/70,001 (0.05)	78/103,489 (0.075)	71	187/173,490	0.11%
SE33 (ACTBP2)	0/330 (<0.30)	330/51,610 (0.64)	None reported	330/51,940	0.64%

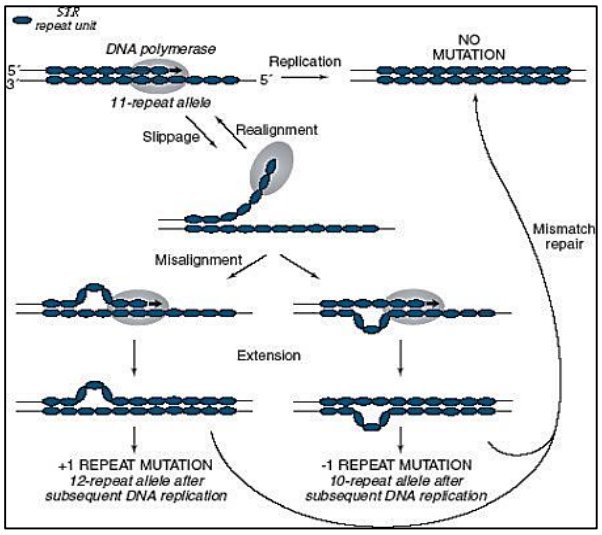

Fig. 1. Schematic illustration of the strand-slippage replication at STR (M.A.Jobling, 2004).

The mutation case in paternity test – two repeat decrease at FGA locus was reported in Turkish family (Canturk et al., 2015). Because of mother and alleged father are homozygous (25, 25) at this loci, but child is heterozygous (23, 25)) the authors failed to establish the source of the reduced allele.

During a population study of 128 Korean families (626 persons) with the AmpF*l*STR Profiler Plus PCR amplification system by G-R.Han et al. (2001) was found an unusual homozygous genotype at the D8S1179 locus in 4 families. To evaluate the cause newly designed primers designed for the D8S1179 locus from GenBank data (GenBank Accession No. G08710) amplified alleles that were not amplified with the AmpF*l*STR Profiler Plus PCR amplification system. Authors sequenced alleles of the family members who had non-amplified alleles and found the point mutation - a G-to-A transition at the position of the 147th base of the GenBank sequence.

In three paternity tests performed by U.Ricci et al. (2003) with a set of autosomal STRs discovered three separate incompatibilities for the loci D3S1358, D8S1179 and D18S51 which was probably due to mutation events. Since in these three cases disputed children were males the paternity of the alleged fathers was confirmed with set of 10 Y-STR markers.

As can be seen from the analysis of the above cited literature data, the study of mutations at the practical application of STR-markers have a great importance. Considering this factor we decided to provide information about the mutational cases revealed at the disputed paternity tests using 15 autosomal STR markers including in the AmpF*l*STR®Identifiler®Plus PCR Amplification Kit during 2012-2018 years, classify them and give a brief analysis of each case.

MATERIAL AND METHODS

Blood samples: Blood samples were collected for paternity tests in period of 2012-2018 (250 tests) from citizens living in territory of Azerbaijan Republic and whose ancestores presumably are Azerbaijan residents for several generations. All blood samples were collected in accordance with international ethics rules: signed consent from all donors collected and further anonymity of individuals were provided. All the chromosomal DNA samples isolated from these blood samples were used only for research purposes based on decision of local ethical committees of both institutions only for research purposes.

DNA samples: DNA were extracted from liquid or dried blood samples using PrepFiler ®DNA Extraction Kit (Applied Biosystems, Life Technologies, USA) according manufacturer's instuctions. Concentrations and purity DNA simples were determined using Quantifiler®Human DNA Quantification Kit in 7500 RealTime PCR System (Applied Biosystems, USA).

Multiple PCR amplification and genotyping: Multiple amplification reactions (total reaction volume is 25 μl) using 0.1 ng genomic DNA were carried out in an ABI 9700 PCR system (Thermo Fisher Scientific Company, USA) for all 15 STR loci (D8S1179, D21S11, D7S820, CSF1PO, D3S1358, THO1, D13S317, D16S539, D2S1338, D18S51, D19S433, vWA, TPOX, D18S51, D5S818 and FGA) included in the AmpF*l*STR®Identifiler®Plus PCR Amplification Kit (Identifiler_V2). After PCR amplification the reaction products were denatured with formamide (Hi-Di) and internal size standard GeneScan ™-500 LIZ®SizeStandard (Thermo Fisher Scientific Company, USA). Electrophoresis of all amplified PCR products and genotype profiling were performed using HITACHI ABI 3130 DNA Genetic Analyzer (Applied Biosystems, USA) and GeneMapper ID software v. 3.2 (Applied Bio-systems, USA) respectively. All PCR amplification, denatu-

ration, electrophoresis and gene profiling experimental procedures were carried out according to the manufacturer's guidelines (AmpF*l*STR® Identifiler®Direct PCR Amplification Kit User Guide, 2015). At performance of the work were met all conditions of accuracy and taken into account the DNA Commission of the International Society for Forensic Genetics (ISFG) recommendations (Prinz et al., 2007; Genetic diversity analysis…, 2003; Gusmao et al., 2006; Schneider, 2007, 2012).

RESULTS AND DISCUSSION

It is known that mutations in STR loci occur both in maternal and paternal meiosis. But, the mutation rate for paternal meiosis is higher than maternal meisosis (see: Annual Reports…, 2001-2013). It should be noted that the chance (probability) of one-step mutations is much higher than 2, 3- and multi-sttep mutations. For example, Brinkmann et al. (1998) reported that in 10,844 parent/child allelic transfers at nine STR loci 23 isolated STR mismatches observed and of 23 STR mutations found, 22 were by a single step; one by a double step. C.H.Brenner (2009) based on numerous literary reports, suggested that there is no common formula for description of the of STR marker mutation cases, therefore it can be assumed that:

- 50% of all mutations increase by one step;
- 50% decrease by one step;
- 5% increase by two steps;
- 5% decrease by two steps;
- 0.5% increase by three steps;
- 0.5% decrease by three steps;
- ... etc.

We observed 6 mutation events during paternity tests in period of 2012-2018 (~250 tests). These cases have not been proven either directly or indirectly (for example, isolating and sequencing a mutated allele, involvement of additional autosomal markers, using markers of X- or Y-chromosomes etc.). Therefore, we present the DNA profiles of each case for persuasiveness. Below we will try to discuss and interpret each case separately according to the existing literature data, generally accepted models and mechanisms of formation of such mutations.

2 cases of mutation at the FGA locus were found (Fig. 2a and 2b, table 2). The FGA loci have complex tetranucleotide repeat: $[TTTC]_3TTTTTTCT[CTTT]_nCTCC[TTCC]_2$. Total mutation rate is 0.28%.

In the first case assuming that the maternal allele is not mutated (i.e. Child1 inherited allele **21** from mother), then based on the literature data (Ali et al., 2009), the more likely scheme of mutation formation can be represented as multi-step mutation process: (1) Ch1(17)=AF1(20) – 3 repeat or Ch1(17)=AF1(23) – 6 repeat (hereinafter Ch-child, AF – alleged father, AM – alleged mother). First scheme is more reasonable. Note that it is not excluded and such a mutation scheme, according to which the mutation affects both the maternal and the paternal alleles simultaneously, i.e. occurs double one-step mutation – one with reducing allele size (deletion), another with increasing allele size (insertion), for example: Ch1(17)=AM1(18) – 1 repeat and Ch1(21)=AF(20) + 1 repeat.

Below the DNA sequences of the all alleles that are present in the DNA profiles at the FGA locus of the tested individuals are shown.

Allele	Sequence	Owner
17	$[TTTC]_3TTTT\ TTCT[CTTT]_9CTCC[TTCC]_2$	**Ch1**
18	$[TTTC]_3TTTT\ TTCT[CTTT]_{10}CTCC[TTCC]_2$	**AM1**
20	$[TTTC]_3TTTT\ TTCT[CTTT]_{12}CTCC[TTCC]_2$	**AF1**
21	$[TTTC]_3TTTT\ TTCT[CTTT]_{13}CTCC[TTCC]_2$	**AM1/ Ch1**
23	$[TTTC]_3TTTT\ TTCT[CTTT]_{15}CTCC[TTCC]_2$	**AF1**

Analogically, the second case of mutation at this locus can be explained more simply: Ch2(25)=AF2(26) – 1 repeat (one-step mutation).

During paternity testing another 2 cases of mutation were detected at the D19S433 locus (Fig. 3a and b, table 3). The locus have repeat structure: $(AAGG)(AAAG)(AAGG)(TAGG)[AAGG]_n$. Total mutation rate for this loci is 0.11%. First mutational event is paternal allele mismatch and second event is maternal allele mismatch. For the first case more reasonable mutation scheme can be presented as a deletion: Ch1(15.2)=AF1(16.2) – 1 repeat (one-step mutation "del" type).

Second mutational case on D19S433 locus represent maternal allele mutation with more complex character. Mother (AM2) and child (Ch2) on this locus are homozygous. One way of mutation can be represented as insertion of 2 repeats and 2 nucleotides: Ch2(15.2)=AM2(13) + 2 repeat+2 b.p. or as insertion of 3 repeats and subsequential loss of 2 nucleotides: Ch2(15.2)=AM2(13) + 3 repeat – 2 b.p. But the probability of such conversion schemes is very low.

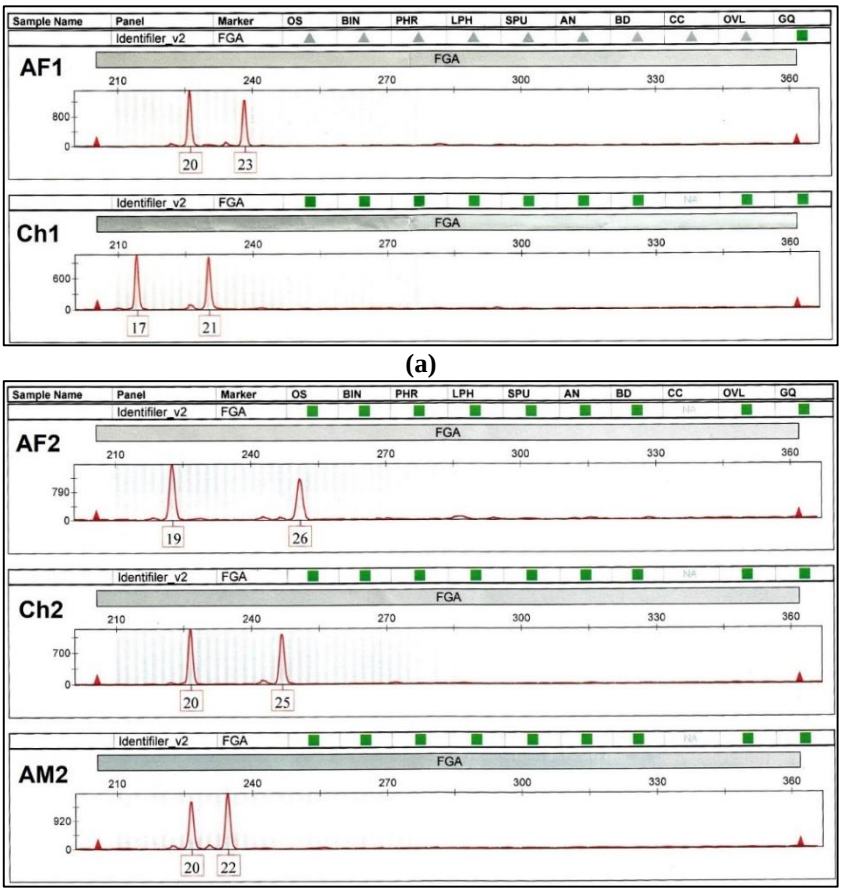

(a)

(b)

Fig. 2. The mutation cases observed on FGA locus in the form of paternal allele mismatch. Hereinafter: AM – alleged mother; Ch – child; AF – alleged father. Note: in case (a) since the data on mother DNA profiles are presented to us by the applicants, therefore the picture of the DNA profile is missing.

Table 2. The mutation cases at the FGA locus observed in two paternity tests.

No	STR loci	Family 1				Family 2			
		*AM1	Ch1	AF1	Status	AM2	Ch2	AF2	Status
1	D8S1179	14, 16	14, 16	13, 14	match	13, 14	13, 15	15, 15	match
2	D21S11	30, 31.2	31.2, 31.2	30.2, 31.2	match	31.2, 31.2	31.2, 32.2	31.2, 32.2	match
3	D7S820	11, 11	10, 11	9, 10	match	11, 13	11, 13	8, 13	match
4	CSF1PO	10, 11	11, 11	10, 11	match	12, 13	12, 12	12, 12	matsch
5	D3S1358	15, 19	15, 17	17, 17	match	16, 17	17, 17	17, 17	match
6	THO1	8, 9.3	6, 8	6, 8	match	6, 8	8, 9	9, 9	match
7	D13S317	12, 12	11, 12	11, 12	match	10, 11	10, 11	11, 11	match
8	D16S539	11, 13	11, 11	11, 13	match	10, 12	10, 10	9, 10	match
9	D2S1338	17, 20	17, 25	22, 25	match	17, 25	17, 25	17, 20	match
10	D19S433	14.2, 15.2	13, 15.2	12, 13	match	14, 14	14, 15	15, 16.2	match
11	vWA	16, 17	14, 17	14, 15	match	15, 15	15, 18	14, 18	match
12	TPOX	8, 11	8, 11	8, 11	match	10, 12	10, 12	8, 10	match
13	D18S51	12, 14	12, 15	12, 15	match	13, 16	13, 16	13, 13	match
14	D5S818	11, 13	11, 11	11, 11	match	11, 12	11, 11	9, 11	match
15	FGA	18, **21**	17, **21**	20, 23	**mismatch**	**20**, 22	**20**, 25	19, 26	**mismatch**
16	Amelogenin	X, X	X, X	X, Y		X, X	X, Y	X, Y	

Notes: **Hereinafter:** AM – alleged mother; Ch – child; AF – alleged father; Possible parental alleles marked in bold, mutated alleles indicated in box; * - DNA profiles of the mother (AM1) were presented to us by the aplicants on the disputed paternity test.

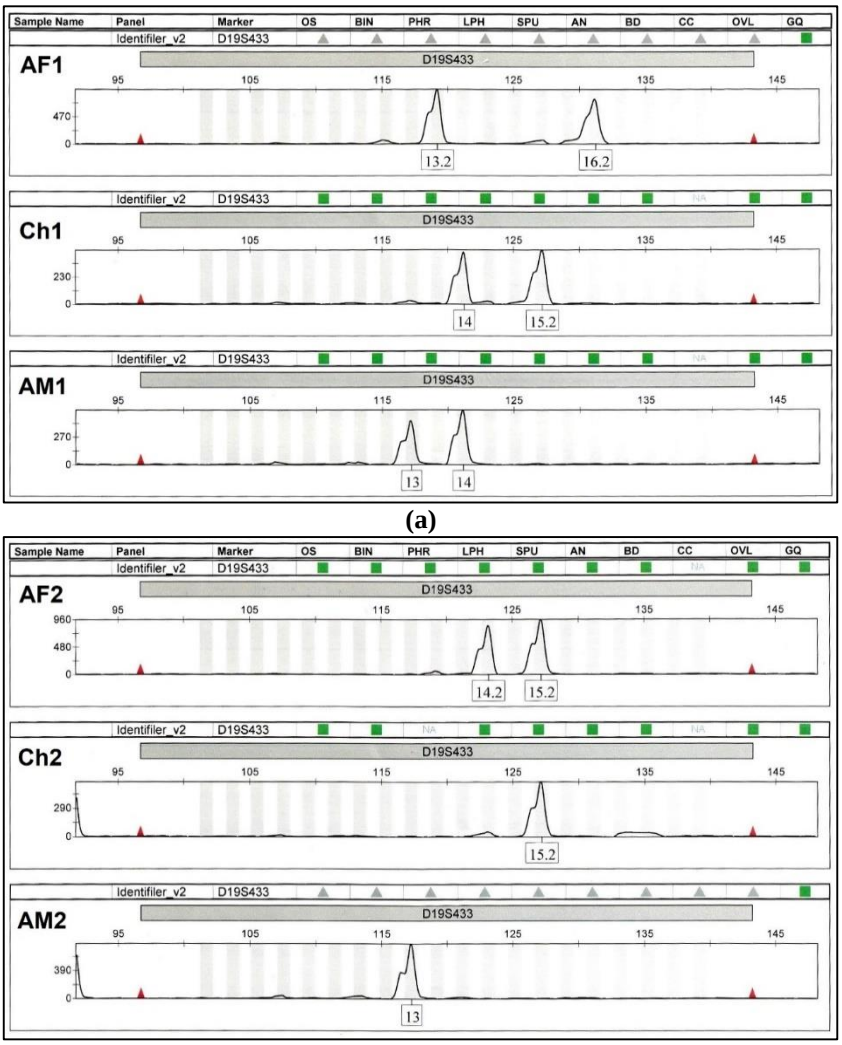

Fig. 3. The mutation cases observed on D19S433 locus: (a) paternal allele mismatch; (b) maternal allele mismatch.

Table 3. The mutation cases at the D19S433 locus observed in two paternity tests.

No	STR loci	Family 1				Family 2			
		AM1	**Ch1**	**AF1**	**Status**	**AM2**	**Ch2**	**AF2**	**Status**
1	D8S1179	11, 15	15, 17	11, 17	match	10, 12	12, 14	11, 14	match
2	D21S11	27, 30	27, 30	30, 31.2	matsch	29, 31	29, 29	29, 32	matsch
3	D7S820	10, 12	10, 12	10, 11	match	8, 12	8, 11	11, 12	match
4	CSF1PO	12, 13	10, 12	10, 11	match	9, 12	10, 12	10, 10	match
5	D3S1358	14, 15	15, 16	16, 17	match	15, 17	17, 18	15, 18	match
6	THO1	6, 9	9, 9.3	6, 9.3	match	8, 9	9, 9.3	6, 9.3	match
7	D13S317	8, 13	8, 12	12, 12	match	11, 12	9, 11	9, 11	match
8	D16S539	11, 12	11, 12	12, 13	match	12, 12	11, 12	11, 12	match
9	D2S1338	21, 23	17, 23	17, 17	match	18, 25	22, 25	17, 22	match
10	D19S433	13, **14**	**14**, 15.2	13.2, 16.2	**mismatch**	13, 13	15.2, **15.2**	14.2, **15.2**	**mismatch**
11	vWA	17, 19	15, 17	15, 15	match	15, 19	15, 19	15, 16	match
12	TPOX	8, 11	11, 11	8, 11	match	11, 11	8, 11	8, 8	match
13	D18S51	14, 16	12, 14	12, 14	match	16, 18	15, 16	15, 15	match
14	D5S818	11, 15	12, 15	12, 12	match	13, 13	11, 13	11, 12	match
15	FGA	21, 21	21, 24	22, 24	match	21, 23	21, 24	21, 24	match
16	Amelogenin	X, X	X, Y	X, Y		X, X	X, Y	X, Y	

Table 4. The mutation case at the D13S317 locus observed in paternity tests.

No	STR loci	AM	AF	Ch1	Status	Ch2	Status
1	D8S1179	15, 15	14, 14	14, 15	match	14, 15	match
2	D21S11	29, 33.2	31.2, 31.2	31.2, 33.2	match	31.2, 33.2	match
3	D7S820	10, 11	8, 10	10, 10	match	8, 10	match
4	CSF1PO	10, 10	11, 11	10, 11	match	10, 11	match
5	D3S1358	15, 18	16, 18	15, 18	matsch	18, 18	match
6	THO1	7, 9.3	7, 9.3	9.3, 9.3	match	7, 7	match
7	D13S317	**10**, 11	**8**, 13	**8**, **10**	match	**10**, 12	mismatch
8	D16S539	11, 12	11, 12	11, 12	match	11, 11	match
9	D2S1338	20, 24	17, 18	17, 20	match	18, 20	match
10	D19S433	15, 15	14, 15	14, 15	match	15, 15	match
11	vWA	14, 16	16, 17	16, 17	match	14, 16	match
12	TPOX	9, 11	8, 11	9, 11	match	8, 11	match
13	D18S51	15, 16	12, 12	12, 16	match	12, 16	match
14	D5S818	12, 13	9, 12	12, 13	match	9, 12	match
15	FGA	19, 25	20, 23	19, 20	match	20, 25	match
16	Amelogenin	X, X	X, Y	X, Y		X, X	

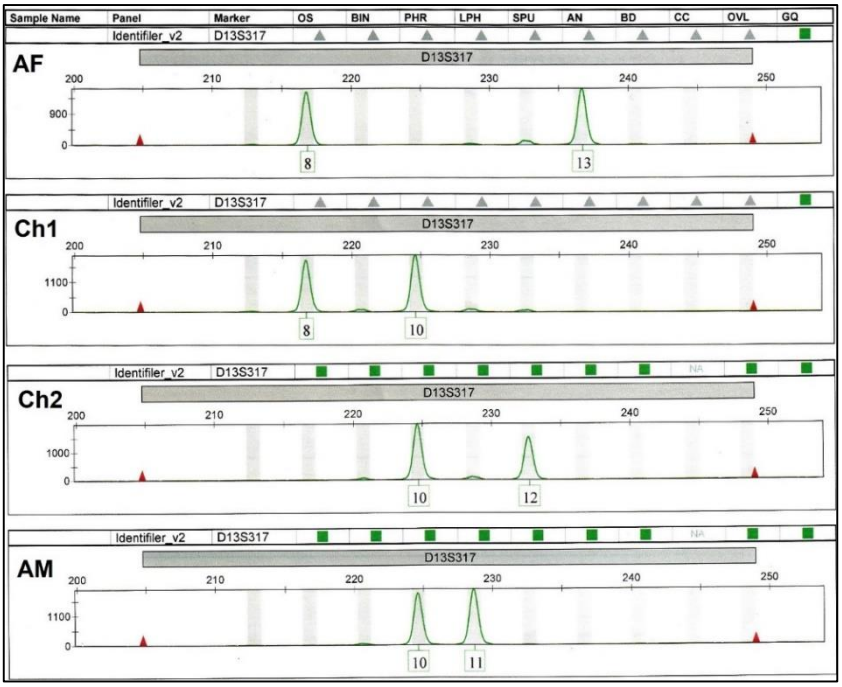

Fig. 4. The mutation case observed on D13S317 locus – paternal allele mismatch in second child.

However, the point mutations (basically in the form of nucleotide transitions or transversions) in flanking regions of locus, i.e. in primer-binding sites, that leads to non-amplification and lost of maternal allele, in other words probability of conversion of maternal allele to the null-allele also is very high. It should be noted that allele frequencies of 14.2 and 16.2 (0.0248 and 0.0149 respectively) are much less than allele 15.2 (0.1225) for our population (Mustafayev et al., 2017b).

Allele	Sequence	Owner
13	(AAGG)(AAAG)(AAGG)(TAGG)(**AAGG**)$_{11}$	**AM1/ AM2**
14	(AAGG)(AAAG)(AAGG)(TAGG)(**AAGG**)$_{12}$	**AM1/ Ch1**
14.2	Sequence no available	**AF2**
15.2	Sequence no available	**Ch1/ Ch2/ AF2**
16.2	Sequence no avaliable	**AF1**

Next mutation event is observed at the D13S317 locus (Fig. 4, table 4). Total mutation rate for this loci is 0.14%. The locus have repeat structure [**GATA**] (bottom strand (commonly used)) or [**TATC**] (GenBank top strand). As it is seen from the table 4, the mutation affected only the second child allele. More reasonable mutation scheme can be represented as one-step mutation with deletion leading to reduction of paternal allele size: Ch1(12)=AM(13) – 1 repeat. Below the DNA sequences of the all alleles that are present in the DNA profiles of the tested individuals are shown.

Allele	Sequence	Owner
8	**(TATC)**$_8$	**AF/Ch1**
10	**(TATC)**$_{10}$	**AM/Ch1/Ch2**
11	**(TATC)**$_{11}$	**AM**
12	**(TATC)**$_{12}$	**Ch2**
13	**(TATC)**$_{13}$	**AF**

Another mutation case was detected on D5S818 locus (table 5, Fig. 5). Total mutation rate on this locus is 0.11% (0.025% during maternal and 0.12% paternal meiotic stages). The locus repeat structure is [**AGAT**]$_n$ (GeneBank top strand).

If it is assumed that allele 14 in the child's DNA profile is inherited from the mother, then the presence of allele 12 can be explained as follows: (1) as a result of one-step mutagenesis with the addition of one repeat as Ch(12)=AF(11) + 1 repeat (allele size extension) and (2) as a result of one-step mutagenesis with the loss of one repeat as Ch(12)=AF(13) – 1 repeat (allele size reduction). For clarity, below the DNA sequences of all alleles present on the DNA profiles of the mother, child and alleged father are presented.

Allele	Sequence	Owner
10	**(AGAT)**$_{10}$	**AM**
11	**(AGAT)**$_{11}$	**AF**
12	**(AGAT)**$_{12}$	**Ch**
13	**(AGAT)**$_{13}$	**AF**
14	**(AGAT)**$_{14}$	**AM/Ch**

Table 5. The mutation case at the D5S818 locus observed in paternity tests..

No	STR loci	AM	Ch	AF	Status
1	D8S1179	12, 14	14, 14	14, 14	match
2	D21S11	30, 30	30, 33.2	31, 33.2	match
3	D7S820	10, 11	10, 11	10, 11	match
4	CSF1PO	10, 12	12, 13	12, 13	match
5	D3S1358	16, 16	15, 16	13, 15	match
6	THO1	6, 9.3	6, 9.3	6, 7	match
7	D13S317	8, 11	8, 11	8, 8	match
8	D16S539	9, 13	9, 9	9, 12	match
9	D2S1338	17, 20	17, 25	20, 25	match
10	D19S433	12, 13	12, 14.2	13, 14.2	match
11	vWA	16, 19	19, 19	17, 19	match
12	TPOX	8, 8	8, 8	8, 8	match
13	D18S51	15, 17	17, 21	16, 21	match
14	D5S818	10, **14**	12, **14**	11, 13	mismatch
15	FGA	23, 23	23, 23	23, 23	match
16	Amelogenin	X, X	X, X	X, Y	---

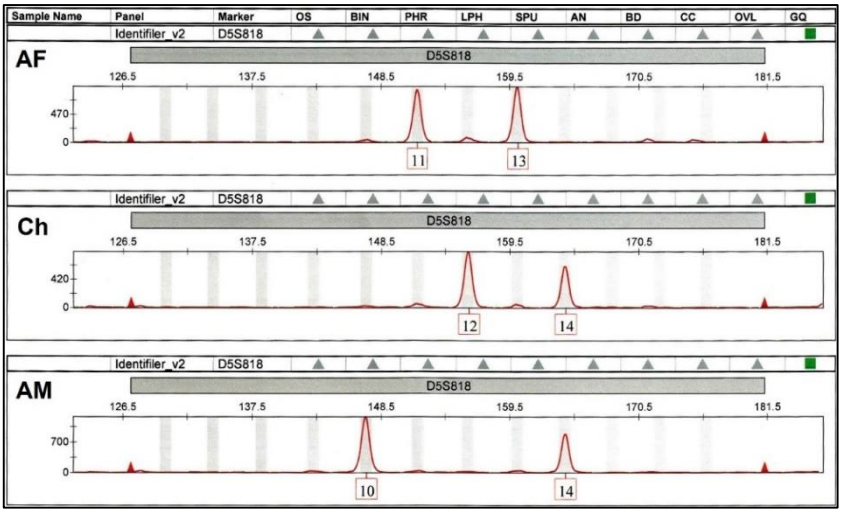

Fig. 5. The mutation case observed on D5S818 locus – paternal allele mismatch.

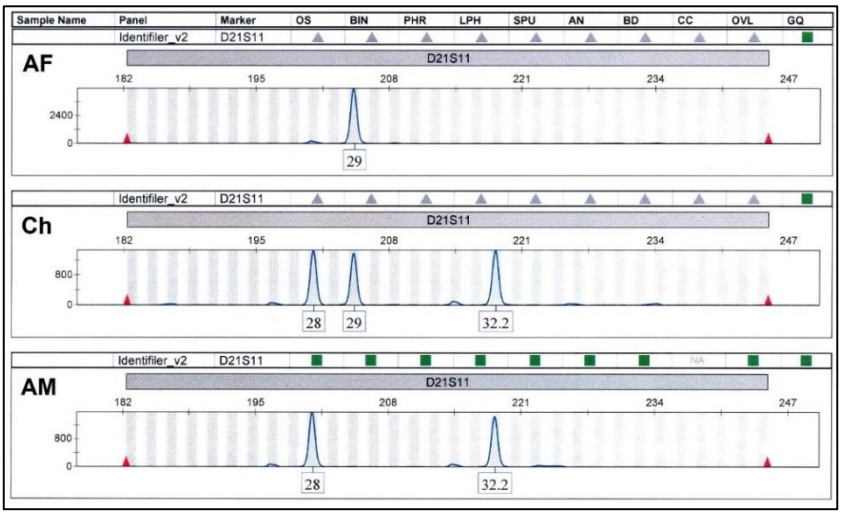

Fig. 6. The mutation case observed on D21S11 locus – trialleic variant indicating Downs syndrome.

Most interesting mutation case observed by us is trialleic variant revealed in the child's DNA profile on the D21S11 locus (Fig. 6, table 6). This indicated the chromosome 21 trisomy, which was in agreement with existing Down's syndrome phenotype. Since the father was homozygous for allele 29 and mother had alleles 28 and 32.2 in D21S11 STR locus, we assumed that child inherited extra chromosome 21 from the mother.

Table 6. The triallelic mutation case at the D21S11 locus observed in paternity tests.

No	STR loci	AM	Ch	AF	Status
1	D8S1179	12, 13	12, 14	14, 15	match
2	D21S11	**28**, **32.2**	**28**, **29**, **32.2**	**29**, **29**	**match (trialleic variant)**
3	D7S820	10, 11	7, 11	7, 9	match
4	CSF1PO	12, 12	12, 12	10, 12	match
5	D3S1358	16, 18	16, 16	16, 18	match
6	THO1	6, 9.3	6, 9.3	6, 9	match
7	D13S317	9, 10	10, 12	11, 12	match
8	D16S539	12, 12	10, 12	9, 10	match
9	D2S1338	20, 23	20, 23	22, 23	match
10	D19S433	12, 13	13, 14	14, 15	match
11	vWA	16, 19	16, 16	16, 17	match
12	TPOX	8, 11	11, 11	8, 11	match
13	D18S51	11, 15	14, 15	13, 14	match
14	D5S818	9, 12	12, 12	11, 12	match
15	FGA	21, 22	19, 21	19, 27	match
16	Amelogenin	X, X	X, X	X, Y	---

Patterson et al. (2009) described in detail the Down syndrome arising mechanisms and its different forms. Basically the trisomy of 21st chromosome is caused by a failure of the this chromosome to separate during egg or sperm development. Due to the chromosome nondisjunction a sperm or egg cell have an extra copy of 21st chromosome, therefore when this cell combined with a normal cell from the other parent, the baby has 47 chromosomes. It should be noted that about 88% of cases of the 21st chromosome trisomy happens due to nondisjunction of the maternal, 8% cases due to nondisjunction of the paternal chromosomes, and in 3% cases after the egg and sperm have merged.

CONCLUSIONS

As well known, the allele variants due to mutations of the STR loci revealed during resolving the identification, disputed paternity/mothernity, kinship, etc. problems to some extent reduce the reliability of the results and deliver a certain difficulty in preparation of an accurate expert opinion. Therefore, information regarding the facts of detection such allelic variations has great importance. Given this, we found it appropriate to inform the scientific community and practicing specialists in this area about the mutations identified by us over a certain period by using of 15 autosomal STR markers including in the AmpF*l*STR® Identifiler®Plus PCR Amplification Kit.

Analyzing the observed mutational cases based on literary data, we can conclude that 5 cases of

them (2 cases on FGA, first case on D19S433, 1 case on D13S317 and 1 case on D5S818 locus) are ins/del type mutations with reducing/increasing of an allele size the occurrence of which can be explained by a step-wise mutation model or strand-slippage replication model. For the one case (the second case on D19S433 locus) a more reasonable explanation is that the point mutation(s) affected the primer binding site which led to maternal allele lost or to conversion it into a null allele. The trialleic variant revealed in the child DNA profile on the D21S11 locus indicates the existence of 21st chromosome trisomy (i.e. Down's syndrome), which can be explained that the existence of extra copy of 21st chromosome the child DNA profile is inherited from the mother. Summarizing the foregoing we assume that our report on detected mutations is important not only in terms of statistics, but will be also off grate value for practicing experts.

AKNOWLEDGEMENTS

Authors express their gratitude to Dr. Agshin F. Taghiyev for the kind assistance rendered at the contribution of this work.

REFERENCES

Ali M.E., Alam S., Ferdous A. et al. (2009) Mutation in the FGA locus of father causing allele mismatch in the child in a DNA paternity test. *Dhaka Univ. J. Biol. Sci.,* **18(2):** 91-98.

AmpF*l*STR®Identifiler®Direct PCR Amplification Kit (2015) User Guide. Thermo Fisher Scientific Inc., 126 p.; **Chapter 5:** Experiments and Results, pp. 66-72; Population data, pp. 86-93.

Annual Report Summary For Testing In 2001, 2002, 2003 (2001, 2002, 2003) *Prepared by the Parentage Testing Program Unit,* 2001: 12 p.; 2002: 51 p.; 2003, 53 p.

Annual Report Summary For Testing In 2004, 2006 (2004, 2006) *Prepared by the Relationship Testing Program Unit and Accreditation Program Units,* 2004: 62 p.; 2006, 102 p;

Annual Report Summary For Testing In 2008, 2010, 2013 (2008, 2010, 2013) *Prepared by the Relationship Testing Program Unit*, 2008: 64 p; 2010: 9 p; 2013; 4 p.

Aşıcıoğlu F., Oguz-Savran F., Ozbek U. (2004) Mutation rate at commonly used forensic STR loci: Paternity testing experience. *Disease Markers*, **20:** 313-315.

Balloch K.J.D., Marshall J., Clugston J., Gow J.W. (2008) Reporting paternity testing results when 2 exclusions are encountered. *Forensic Science International: Genetics Supplement Series*, **1:** 492-493

Botstein D., White R.L., Skolnick M., Davis R.W. (1980) Construction of a genetic linkage map in man using restriction fragment length polymorphisms. *Am. J. Hum. Genet.,* **32(3):** 314-331.

Boutrand L., Egyed B., Füredi S., Mommers N., Mertens G., Vandenberghe A. (2001) Variations in primer sequences are the origin of allele drop-out at loci D13S317 and CD4. *Int. J. Legal Med.,* **114(4-5):** 295-297.

Brenner C.H. (2009) Mutations in Paternity: http//www.dna-view.com/ mudisc.htm.

Brinkmann B., Klintschar M., Neuhuber F., Hoehne J., Burkhard R. (1998) Mutation rate in human microsatellites: Influence of the structure and length of the tandem repeat. *Am. J. Hum. Genet*., **62:**1408-1415.

Burkhard R., Nicole B., Peter W. (2011) Insertion-/deletion polymorphisms close to the repeat region of STR loci can cause discordant genotypes with different STR kits. *Forensic. Sci. Int. Genet.,* **5(4):** 339-341.

Butler J.M. (2006) Genetics and genomics of core Short Tandem Repeat loci used in human identity testing. *J. Forensic Sci.,* **51(No 2):** 253-265.

Cabezas S.R., Ribeiro T., Lucas I. et al. (2016) Analysis of 17 STR data on 5362 southern Portuguese individuals-an update on reference database. *Forensic Sci. Int. Genet.,* **21:** e10-12.

Canturk K.M., Emre R., Müslümanoğlu Ö. et al. (2015) Two repeat decrease at FGA locus in a paternity test: A case of mutation. *J. of Forensic Medicine*, **29(1):** 56-59.

Dauber E.M., Bärb W., Klintschar M. et al. (2004) New sequence data of allelic variants at the STR loci ACTBP2 (SE33), D21S11, FGA, vWA, CSF1PO, D2S1338, D16S539, D18S51 and D19S433 in Caucasoids. *International Congress Series*, **1261:** 191-193.

Deucher A., Chiang T., Schrijver I. (2010) Consultations in Molecular Diagnostics: Rare sequence variation in the genome flanking a short tandem repeat locus can lead to a question of "nonmaternity". *Journal of Molecular Diagnostics,* **12(3):** 385-389.

Dinesh K.J., Jiwan P.R., Bhinu S.T., Basanta R.P. (2013) Mutations or exclusion: an uncommon parentage assessment case. *Scientific World*, **11(11):** 74-76.

Dogan S., Asic A., Muhovic I. et al. (2014) Overview of the genetic STR clustering among worldwide human populations. *Int. J. Hum. Genet.*, **14(3,4):** 131-142.

Dupuy B.M., Olaisen B. (1997) Sequenced alleles as internal standard in STR fragment analysis. *Proceedings from the First European Symposium on Human İdentification,* pp. 71-80.

Edwards M., Allen R.W. (2004a) Characteristics of mutations at the D5S818 locus studied with a tightly linked marker. *Transfusion.*, **44(No 1):** 83-90.

Edwards M., Allen R.W. (2004b) Characteristics of D5S818 mutations revealed through study of a flanking marker. *International Congress Series*, **1261:** 33-35.

Ellegren H. (2004) Microsatellites: simple sequences with complex evolution. *Nature Rev. Genet.*, **5(6):** 435-445.

Eunus A., Shafiul A., Ahmad F., Mahamud H., Tania H., Sharif A. (2009) Mutation in paternally transmitted alleles at FGA microsatellite locus: A case of allele mismatch in child. *Indian Journal of Forensic Medicine and Toxicology,* **3(3):** 41-43.

Fan H., Chu J.-Y. (2007) A brief review of Short Tandem Repeat mutation. *Genomics, Proteomics. Bioinformatics*, **5(1):** 7-14.

Geada H., Viriato L., Vieira-Silva C., Cruz C., Lucas I., Ribeiro T., Espinheira R. (2003) STR mutations in paternity investigations: a study of 1-year consecutive cases. *International Congress Series*, **1239:** 657-660.

Genetic diversity analysis with molecular marker data: Learning module. Measures of genetic Diversity (2003) IPGRI and Cornell University, 71 p.

Gusmao L., Butler J.M., Carracedo A. et al. (2006) DNA commission of the international society of forensic genetics (ISFG): An update of the recommendations on the use of Y-STRS in forensic analysis. *Forensic Sci. Int.,* **157(2-3):** 187-197.

Hammond H.A., Jin L., Zhong Y., Caskey C.T., Chakraborty R. (1994) Evaluation of 13 short tandem repeat loci for use in personal identification applications. *Am. J. Hum. Genet.*, **55:** 175-189.

Han G-R., Song E-S., Hwang J-J. (2001) Non-amplification of an allele of the D8S1179 locus due to a point mutation. *Int. J. Legal Med.,* **115:** 45-47.

http://www.cstl.nist.gov/strbase/mutation.htm

Huel R.L.M., Bašić L., Madacki-Todorović K. et al. (2007) Variant alleles, triallelic patterns, and point mutations observed in nuclear short tandem repeat typing of populations in Bosnia and Serbia. *Croat Med. J.*, **48:** 494-502.

Immela U.-D., Kleibera M., Neerman-Arbezb M., Klintschara M. (2004) An isolated exclusion in the FGA system. *International Congress Series*, **1261:** 148-150.

Jobling M.A. (2004) The diversity of the human genome. In *Human Evolutionary Genetics: Origins, Peoples & Disease* (eds. Jobling, M.A., *et al*.). USA: New York, Garland Science, pp. 67.

Leibelt C., Budowle B., Collins P. et al. (2003) Identification of a D8S1179 primer binding site mutation and the validation of a primer designed to recover null alleles. *Forensic Science International*, **133:** 220-227.

Li F., Xuan J., Xing J., Ding M., Wang B., Pang H. (2014) Identification of new primer binding site mutations at TH01 and D13S317 loci and determination of their corresponding STR alleles by allele-specific PCR. *Forensic Sci. Int. Genet.*, **8(1):** 143-146.

Liu Y.X., Zhang W.Q., Jia Y.S. et al. (2015) Multistep microsatellite mutation in a case of non-exclusion parentage. *Forensic Science International: Genetics*, **16:** 205-207.

Mustafayev N.Sh. Mammadov A.Ch., Mammadov E.R., Hasanov A.B., Huseynova I.M. (2016) Study of the Azerbaijan population by the STR markers: I. Definition of basic population-genetic parameters of the STR markers. *Proc. of ANAS (biol. and med. sci.)*, **71(2):** 5-16.

Mustafayev N.Sh., Mammadov A.Ch., Mammadov E.R., Huseynova F.R., Hasanov A.B., Huseynova I.M. (2017a) Study of the Azerbaijan population by the STR Markers: II. Interpopulation analysis on the basis of STR markers' allele structure. *Proc. of Azerbaijan NAS, (biol. and med. sci.)*, **72(2):** 5-20.

Mustafayev N.Sh., Mammadov E.R., Huseynova F.R., Mammadov A.Ch., Hasanov A.B., Huseynova I.M. (2017b) Population-genetic and

comparative interpopulation studies of Azerbaijan population based on the 15 autosomal STR markers. *Transactions of the Institute of Mol. Biol. & Biotechnol.*, **1:** 72-79.

Narkuti V., Vellanki R.N., Gandhi K.P. et al. (2007) Microsatellite mutation in the maternally/paternally transmitted D18S51 locus: two cases of allele mismatch in the child. *Clin. Chim. Acta.*, **381(2):** 171-175.

Narkuti V., Vellanki R.N., Anubrolu N. et al. (2008) Single and double incompatibility at vWA and D8S1179/D21S11 loci between mother and child: Implications in kinship analysis. *Clinica Chimica Acta*, **395:** 162-165.

Natsuko M., Tetsushi K., Koji F. et al. (2008) A D19S433 primer binding site mutation and the frequency in Japanese of the silent allele it causes. *J. of Foresic Sci.*, **53(5):** 1068-1073.

Nutini A.L., Mariottini A., Giunti L., Torricelli F., Ricci U. (2003) Double incompatibility at human alpha fibrinogen and Penta E loci in paternity testing. *Croat. Med. J.*, **44:** 342-346.

Opolska-Bogusz B., Kaczmarczyk G., Piniewska D. et al. (2006) Allelic variant 6' at locus D13S317 in a paternity casework; a semi-automatic genotyping problem. *Arch. Med. Sadowej Kryminol.*, 2006, **56(2):** 115-118.

Patterson D. (2009) Molecular genetic analysis of Down syndrome. *Human Genetics*, **126(1):** 195-214.

Prinz M., Carracedo A., Mayr W.R. et al. (2007) DNA Commission of the International Society for Forensic Genetics (ISFG): Recommendations regarding the role of forensic genetics for disaster victim identification (DVI). *Forensic Science International: Genetics*, **1:** 3–12.

Ricci U., Cerri N., Sani I. et al. (2003) De novo mutations at D3S1358, D8S1179 and D18S51 loci emerged during paternity testing: confirmation of biological paternal lineage by using a panel of Y-chromosome STRs. *Progress in Forensic Genetics 9. Int. Congr. Ser.*, 1239: 643-646.

Ricci U., Melean G., Robino C., Genuardi M. (2007) A single mutation in the FGA locus responsible for false homozygosities and discrepancies between commercial kits in an unusual paternity test case. *J. Forensic Sci.*, **52(2):** 393-396.

Schneider P.M. (2007) Scientific standards for studies in forensic genetics. *Forensic Sci. Int.*, **165(2-3):** 238-243.

Schneider P.M. (2012) Beyond STRs: The role of diallelic markers in forensic genetics. *Transfus. Med. Hemother.*, **39:** 176-180.

Singh Negi D., Alam M., Bhavani S.A., Nagaraju J. (2006) Multistep microsatellite mutation in the maternally transmitted locus D13S317: a case of maternal allele mismatch in the child. *Int. J. Legal Med.*, **120(5):** 286-292.

Sprecher C.J., Puers C., Lins A.M., Schumm J.W. (1996) General approach to analysis of polymorphic short tandem repeat loci. *BioTechniques*, **20:** 266-276.

Turchi C., Pesaresi M., Alessandrini F. et al. (2004) Unusual association of three rare alleles and a mismatch in a case of paternity testing. *J. Forensic Sci.*, **49(2):** 260-262.

Urquhart A., Kimpton C.P., Downes T.J., Gill P. (1994) Variation in short tandem repeat sequences – a survey of twelve microsatellite loci for use as forensic identification markers. *Int. J. Leg. Med.* **107:** 13-20.

Urquhart A., Oldroyd N.J., Kimpton C.P., Gill P. (1995) Highly discriminating heptaplex short tandem repeat PCR system for forensic identification. *BioTechniques* **18:** 116-121.

Venkanna N., Ravi N.V., Narasimha M.O., Lakshmi N.M. (2009) *De novo* deletion at D13S317 locus: A case of paternal-child allele mismatch identified by microsatellite typing. *Clin. Chim. Acta*, **403(1-2):** 264-265.

Wang W., Fukuda M., Kishida T., Tamaki Y. (1996) Quintuplex PCR-amplification of microsatellites. *Jpn. J. Legal Med.*, **50:** 231-236.

Zhang M.X., Gao H.M., Han S.Y. et al. (2014) Risk analysis of duo parentage testing with limited STR loci. *Genetics and Molecular Research*, **13(1):** 1179-1186.

Zhao Z.M., Liu Y., Lin Y. (2007) Mutations of short tandem repeat loci in Identifiler system. *Fa Yi Xue Za Zhi*, **23(4):** 290-291, 294.

Zhao Z., Zhang J., Wang H. et al. (2015) Mutation rate estimation for 15 autosomal STR loci in a large population from Mainland China. *Meta Gene*, **5:** 150-156.

15 Autosom STR marker istifadə edilən atalıq testlərində mutasiya halları

N. Ş. Mustafayev[1,2,*], E. R. Məmmədov[2], Ə. Ç. Məmmədov[1,2], Ə.B. Həsənov[2], İ.M. Hüseynova[1]

[1] AMEA Molekulyar Biologiya və Biotexnologiyalar İnstitutu
[2] Azərbaycan Respublikası Səhiyyə Nazirliyi Məhkəmə Tibbi Ekspertiza və Patoloji Anatomiya Elmi-Təcrübi və Tədris Birliyinin Biologiya Şöbəsi

Məlumdur ki, identifikasiya, mübahisəli atalıq/analıq, qohumluq və s. məsələlərin həlli zamanı STR lokuslarda aşkarlanan mutasiyalar müəyyən dərəcədə nəticələrin etibarlılığını aşağı salır və dəqiq ekspert rəyinin tərtibində müəyyən çətinliklər yaradır. Buna görə də belə allel variantlarının aşkarlanması haqqında məlumatlar mühüm praktiki əhəmiyyət kəsb edir. Bu tədqiqatda bizim tərəfimizdən 250 ailədən ibarət mübahisəli atalıq testlərində iki halda FGA, iki halda D19S433, bir halda D13S317 və bir halda D5S818 STR lokusu üzrə mutant allellər aşkarlanmışdır. Beş halda bu mutasiyaların daha böyük ehtimalla atadan mənimsənilən allellərdə, bir halda isə anadan mənimsənilən alleldə baş verməsi güman edilir. Hər bir hal üçün mutasiyaların yaranma yollarının mümkün sxemləri təklif edilmişdir. Bunlardan başqa bir halda 21-ci xromosomun trisomiyasını göstərən D21S11 STR lokusu üzrə üç allelli profil aşkarlanmışdır ki, bu da real olaraq Daun sindromunu müəyyən edən edən mutasiyanın baş verməsini təsdiq etmişdir.

Açar sözlər: *STR marker, krossinqover, insersiya, delesiya, null-allel, mərhələli mutasiya, genlərin konversiyası, zəncir-sürüşməli replikasiyası, atalıq testi, ana meyozu*

Случаи мутаций в тестах на отцовство с использованием 15 аутосомных STR-маркеров

Н.Ш. Мустафаев[1,2], Э.Р. Маммадов[2], А.Ч. Маммадов[1,2], А.И. Гасанов[2], И.М. Гусейнова[1]

[1] Институт молекулярной биологии и биотехнологий НАН Азербайджана
[2] Биологическое отделение Научно-практического и учебного объединения Судебно-медицинской экспертизы и патологической анатомии Министерства Здравоохранения Азербайджанской Республики

Известно, что мутации STR локусов, выявленные при решении задач идентификации, спорного отцовства/материнства, родства и др. приводят в некоторой степени к снижению достоверности результатов, что представляет определенную трудность в составлении точного экспертного заключения. Поэтому информация о фактах обнаружения таких аллельных вариаций имеет большое практическое значение. В данном исследовании из 250 семейных случаев спорного отцовства, нами был выявлен мутантный аллель в двух случаях по локусу FGA, в двух случаях по D19S433, в одном случае по D13S317 и в одном случае по локусу D5S818. В пяти случаях более вероятно, что эти мутации затронули отцовские аллели, в одном случае - материнский аллель. Для каждого случая была предложена схема возможных путей образования мутаций. Более того, в одном случае был обнаружен трехаллельный профиль по локусу D21S11, что указывает на трисомию 21-ой хромосомы, что подтверждает существующий фенотип синдрома Дауна.

Ключевы слова: *STR маркер, кроссинговер, инсерция, делеция, нуль-аллель, ступенчатое мутирование, конверсия генов, репликация с проскальзыванием цепи, тест на отцовство, материнский мейоз*

Life Sciences and Biomedicine, vol. 1 (74), No 1, p. 18-28 (2019)

Chlorophyll fluorescence and "Maximum Quantum Efficiency" of photosystem II in plant sciences

Y.M. Feyziyev*

*Institute of Molecular Biology & Biotechnologies, Azerbaijan National Academy of Sciences, 11 Izzat Nabiyev, Baku AZ 1073, Azerbaijan; *For correspondence: y.feyziyev@imbb.science.az*
Accepted for publication: 20 November 2019

The fluorescence of chlorophyll *a* is widely used as an indicator of the state of photosystem II (PSII) in plants, algae and cyanobacteria. There were reports on ~ 20 various parameters of fluorescence of PSII chlorophyll. Three of these characteristics, the initial (F_0), maximum (F_M) and variable (F_V) fluorescence of chlorophyll, and the derivative value (F_M-F_0)/F_M, called by different authors a "maximum quantum efficiency" of PSII, are reviewed in this paper. A brief and comparative analysis of the Duysens hypothesis (Duysens and Sweers, 1963) and Klimov's hypothesis of recombination luminescence (Klimov et al., 1978) widely used to describe the processes in the PSII reaction center was carried out. Eventual errors due to inaccuracy in the applications of the parameter "maximum quantum efficiency" of PSII used to evaluate the photochemical activity of the photosynthetic apparatus and the physiological state of plants are discussed.

Keywords: *Photosystem II, chlorophyll fluorescence, maximum quantum efficiency*

Abbreviations:

Chl – Chlorophyll; **CP43, CP47 –** 43 and 47 kDa PSII core antenna proteins, Chl *a* proteins; **Cyt b_6f –** Cytochrome b_6f complex; **D_1, D_2 –** PSII reaction center proteins; **F_0, F_M, F_V –** Initial, maximal and variable fluorescence of Chl *a*; **k_f, k_d, k_e –** Rate constants of fluorescence, thermal dissipation and photochemical quenching, respectively; **LHCII –** Light harvesting complex II; **$NADP^+$ –** Nikotinamide-adenine dinucleotide phosphate, oxidized; **Q_A –** Plastoquinone, primary electron acceptor of PSII, $Q_A^{-\bullet}$ (semiquinone) reduced form; **Q_B –** Plastoquinone, secondary electron acceptor of PSII; **Pheo –**Pheophytin, $Pheo^{-\bullet}$ reduced form; **P_{680} –** Primary electron donor, P_{680}* and $P_{680}^{+\bullet}$ excited and oxidised forms; **PQH_2 –** Plastoquinole; **PSI, PSII –** Photosystem I, Photosystem II; **RC –** Reaction center; **Y –**"Maximum quantum efficiency" of photosystem II, (F_M-F_0)/F_M; **Y_Z, Y_D –** Redox active tyrosines of PSII: Y_Z is a redox intermediate between PSII reaction center and water oxidation; **φ_f, φ_d, φ_p –** Quantum yield of fluorescence, thermal dissipation and photochemistry.

INTRODUCTION

The photosynthetic apparatus of oxygen-evolving species converting light energy to the chemical energy of organic compounds includes several protein complexes located in the thylakoid membrane. These are complexes: photosystem I and II (PSI and PSII), cytochrome $b_6 f$ (Cyt $b_6 f$), ATP-synthase and $NADP^+$. A combined action of the photosystem II and I results in the electron transfer through the thylakoid membrane, from H_2O ($E_{m\ (pH\ 7.0)}$ = +0.82 V) to $NADP^+$ ($E_{m\ (pH\ 7.0)}$ = –0.32 V), using two light quanta (one for each photosystem) for the transfer of each electron. In the redox potential scale, the photosynthetic electron transfer is represented by the Z-scheme of photosynthesis in which the photochemical reactions of PSII and PSI interact through the electron transfer chain consisting of the pool of plastoquinols (PQH_2), Cyt b_6 f and plastocyanin (Hill, 1965; Govindjee et al., 2017).

The photosystem II of oxygenic organisms couples the photochemical excitation of chlorophyll with the electron transfer from water to PQH_2. Stu-

dies of the molecular architecture of PSII in cyanobacteria and red algae have revealed ~20 proteins and a number of cofactors in the structure of this complex (Zouni et al., 2001; Ferreira et al., 2004; Umena et al., 2011, Ago et al., 2016). The transmembrane D_1 and D_2 proteins (32-34 kDa), α- and β-subunits of cytochrome b_{559}, core antenna proteins CP47 and CP43 carrying Chl *a*, and three peripheral proteins of 33-, 23- and17 kDa located on the lumen surface of thylakoid membranes are the most important proteins of photosystem II in plants. Cyanobacteria and red algae contain cytochrome c_{550} and 12 kDa PsbU polypeptide, instead of plant 23 and 17 kDa polypeptides.

D_1/D_2 heterodimer of the PSII complex binds an initial electron donor P_{680}, pheophytin (Pheo) and two plastoquinones (plastoquinone O_A and Q_B) electron acceptors, two redox active tyrosines Y_Z (D_1-Tyr^{161}) and Y_D (D_2-Tyr^{161}) as an electron donor to the photooxidized P_{680} (Barber, 2006; Muh and Zouni, 2011). During excitation, P_{680} oxidizes and the electron is transferred to the pheophytin molecule, resulting in the formation of oxidized $P_{680}^{+\bullet}$ and reduced $Pheo^{-\bullet}$ radicals (Klimov et al., 1977) in the PSII reaction center (RC). The quantum yield of charge separation in the PSII reaction center is ~1.0 (Groot et al., 1997). From $Pheo^{-\bullet}$ the electron is transferred sequentially to plastoquinones Q_A and Q_B, and then to the pool of plastoquinols, which serves as a reservoir for electrons leaving PSII. The oxidized primary donor of photosystem II, $P_{680}^{+\bullet}$ is a strong oxidant (E_m ~ 1.2 V) which is reduced by an electron transferred from tyrosine Y_Z. This leads to the oxidation of tyrosine Y_Z and forming $Y_Z^{+\bullet}$ radical. Oxidized tyrosine ($Y_Z^{+\bullet}$) is ultimately reduced by an electron from water (Debus, 1992; Nelson and Yocum, 2006; Muh and Zouni, 2011).

Among the components of the photosynthetic apparatus, PSII is a most sensitive to the extreme factors, and therefore, the characteristic reactions of PSII including the fluorescence of chlorophyll *a* are attracted to research as an indicator the physiological state of oxygenic species. About 20 components of chl *a* fluorescence, applied to the study of oxygenic photosynthesis, are described in different studies. However, most of the components of chlorophyll *a* fluorescence are not characterized sufficiently, that does not allow determining the state of PSII adequately.

In this paper the constant and variable components of chlorophyll fluorescence (F_0 and F_V, respectively), as well as the derivative parameter called the "maximum quantum efficiency" of PSII designated as Y have been considered briefly in the context of their correct interpretation in studies of photosynthesis and various problems of plant science.

2. The fluorescence of chlorophyll a

Photosynthesis starts with the absorption of light quanta by the antenna pigments. A small part of the absorbed light energy (~ 2%) is not used in photosynthesis and lost as a fluorescence of chlorophyll. At room temperatures, fluorescence emitted by chloroplasts and thylakoid membranes has a major band with a maximum at 685 nm and a non-intense broad band (≤ 10% of total intensity) in the red spectral region extending up to 760 nm. At low temperatures (77 K), three emission bands with maxima at 685, 695 and 735 nm are resolved. It is assumed that the 685 and 695 nm bands are emitted by the PSII components, and the 735-nm band is associated with photosystem I (Briantais et al., 1986).

The intensity of PSII chlorophyll fluorescence is sensitive to the redox state of its components. Depending on the redox state of the PSII electron transport chain, several components are distinguished in the yield of chlorophyll fluorescence of oxygenic species. Among them, the most interesting are the parameters such as the "initial" (F_0) and "variable" fluorescence of chlorophyll (F_V), and the "maximum quantum efficiency" of photosystem II (Y), widely used by researchers as a tool in monitoring the physiological state of plants. The use of fluorescence in studies of oxygenic species is well reviewed in several articles (Krause and Weis, 1984, 1991, Horton and Bowyer, 1990; Campbell et al., 1998; Lazar, 1999; Maxwell and Johnson, 2000; Baker, 2008; Brestic and Zivcak, 2013; Kalaji et al., 2014, 2016; Goltsev et al., 2019).

2.1. The initial fluorescence of chlorophyll, F_0

The initial fluorescence of chlorophyll F_0, often referred as a constant, zero or prompt fluorescence, can be observed when the primary electron acceptor of the photosystem II plastoquinone Q_A is in the oxidized state and the PSII reaction cen-

ters are "open". In this state, the yield of chlorophyll fluorescence is minimal. F_0 can be observed under a weak measuring light (which prevents the accumulation of Q_A in the reduced state) in photosynthetic organelles or the suspensions containing PSII (in leaves, chloroplasts, plant thylakoid membranes, green algae and cyanobacteria) after prolonged dark adaptation.

F_0 represents the radiative deactivation of the excited state of antenna chlorophylls during the energy transfer to the PSII reaction centers, i.e. loss of the part of the excitation energy before it reaches the RC (Fig. 1, a). The fluorescence of the chlorophyll of photosystem I (> 700 nm) can also contribute to F_0. However, at a wavelength < 700 nm this contribution is negligible (Schreiber et al., 1998) and may not be taken into account. The lifetime of chlorophyll fluorescence determined by time-resolved fluorometry in dark adapted and quinone oxidized samples shows the decay components in the range of few hundred picoseconds which attributed to F_0 (Haehnel et al., 1982; 1983; Nairn et al., 1982; Karukstis and Sauer, 1985; Mauzerall, 1985; Holzwarth et al., 1985; Moya et al., 1986; Hozwarth, 1986).

2.2. Variable fluorescence of chlorophyll, F_V

When the primary electron acceptor of photosystem II, plastoquinone Q_A, is reduced (photochemically, under strong excitation light, or chemically, for example, in the presence of dithionite), the intensity of chlorophyll fluorescence increases 4-5-fold, from the initial F_0 level to the maximum F_M (Klimov et al., 1977). The state of RC when Q_A becomes reduced is often referred as a "closed" state of PSII, although such terminology is not quite true (see section 2.3). The difference $F_V = F_M - F_0$ is called the variable fluorescence of chlorophyll. Variable fluorescence of chlorophyll is observable in plant leaves, chloroplasts, thylakoid membranes, enriched with PSII complexes, as well as in cyanobacteria and algae. It is intensively used in the study of the photosynthetic apparatus and physiological state of the oxygenic species. Below we will compare two different views of the mechanism of increasing chlorophyll *a* fluorescence, proposed by Duysens and Sweers (1963), and Klimov et al. (1977).

Duysens and Sweers (1963). The hypothesis of Duysens and Sweers (1963) explains the increase of the fluorescence intensity due to blockage of the photochemical quenching of the excited chlorophyll molecules of the light-harvesting antenna after the reduction of plastoquinone Q_A. According to this hypothesis, the quantum yields of fluorescence for "open" (φ_0) and "closed" (φ_m) reaction centers may be determined as follows:

$$\varphi_0 = \frac{k_f}{k_f + k_d + k_p} \quad (1)$$

$$\varphi_m = \frac{k_f}{k_f + k_p} \quad (2)$$

where k_f, k_d and k_p are the rate constants of fluorescence, radiationless transition to the ground state, and photochemical quenching (photochemical electron transfer), respectively.
Simple calculations using equations 1 and 2, and the relation,

$$\varphi_p + \varphi_d + \varphi_f = 1$$

which includes the quantum yields of three basic processes involved in the utilization of the energy of the absorbed light quanta, photochemistry (φ_p), thermal dissipation (φ_d) and fluorescence (φ_f), give the following result for the quantum yield of photochemistry (Borisov and Godik, 1973):

$$\varphi_p = 1 - \frac{\varphi_0}{\varphi_m} \quad (3a)$$

Considering the proportionality of the fluorescence intensity (F) and its quantum yield ($F \propto \varphi_f$), the last equation can be expressed as:

$$\varphi_p = 1 - \frac{F_0}{F_M} \quad (3b)$$

Equations (3a) and (3b) are easily transformed into the following equivalent equations:

$$\frac{\varphi_m}{\varphi_0} = \frac{1}{1 - \varphi_p} \quad (4a)$$

$$\frac{F_M}{F_0} = \frac{1}{1 - \varphi_p} \quad (4b)$$

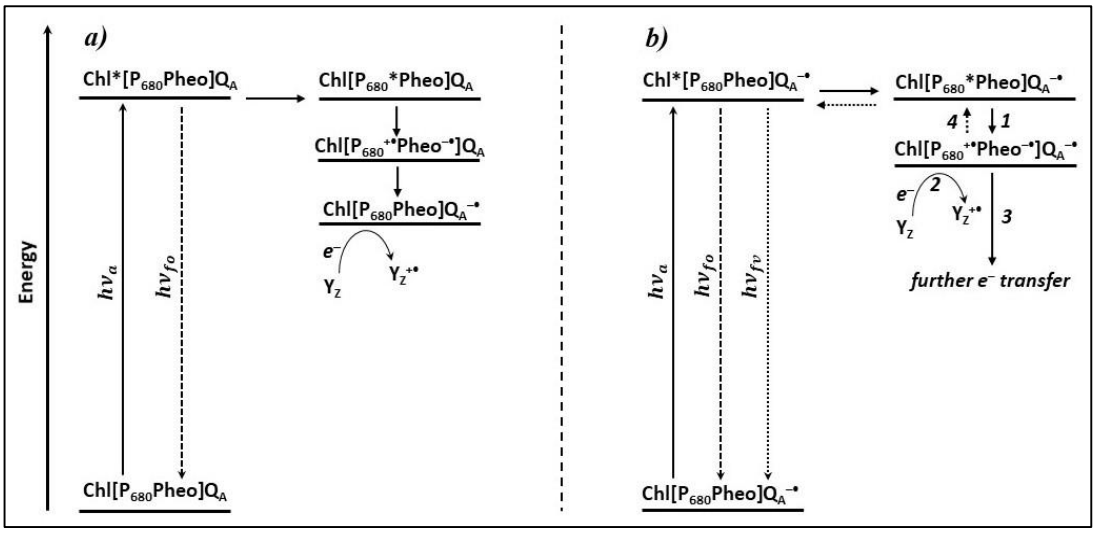

Figure 1. a) – Appearance of prompt fluorescence. b) – Appearance of variable fluorescence of chlorophyll by the mechanism of recombination luminescence (Klimov et al., 1978): $h\nu_a$ - absorption of light quantum, $h\nu_{f_0}$, $h\nu_{f_v}$ - emission of initial and variable fluorescence, respectively. The states of $[P_{680}^{+\bullet}Pheo^{-\bullet}]Q_A^{-\bullet}$ (scheme b) can be stabilized in two ways: 1) electron transfer from Y_Z to $P_{680}^{+\bullet}$: $Y_ZP_{680}^{+\bullet} \rightarrow Y_Z^{+\bullet}P_{680}$ (transition 2), and from pheophytin to plastoquinones: $Pheo^{-\bullet}Q_A^{-\bullet}Q_B \rightarrow PheoQ_A^{-\bullet}Q_B^{-\bullet}$ (transition 3); 2) recombination of the pair $[P_{680}^{+\bullet}Pheo^{-\bullet}]$ (transition 4) which can be accompanied by the emission of light. The ultimate electron donor to $Y_Z^{+\bullet}$ is H_2O.

Thus, the hypothesis, which suggests inhibition of the photochemical quenching of excitation energy during reduction of Q_A (Duysens and Sweers, 1963) leads to relations (4a) and (4b). Furthermore, the model considers F_V as prompt fluorescence (see also: Kitajima and Butler, 1975).

However, this model cannot explain the following: according to the equation (4b), complete blockage of the photochemical reaction, having a quantum yield of $\varphi_p \geq 98\%$ should lead to an increase of fluorescence intensity by a factor of ~50. Nevertheless, experimentally 4-5-fold increase of chlorophyll fluorescence is observed (Klimov et al., 1977), which questioned this approach for explanation of the mechanism of the increase of chlorophyll fluorescence (or appearance of variable fluorescence).

Klimov's recombination luminescence. According to the Duysens hypothesis (Duysens and Sweers, 1963), chlorophyll fluorescence in the presence of both oxidized (F_0), or reduced plastoquinone Q_A (F_M) in the PSII reaction center have the same nature, i.e., they are represented by prompt fluorescence emitted at the same time range. However, it has been shown experimentally that the part of fluorescence emitted from the so-called "closed" centers ($[P_{680}Pheo]Q_A^{-\bullet}$ state) has a lifetime in the nanosecond range. In different studies, the lifetime of 2-4 ns was reported for the slow component of chlorophyll fluorescence (Klimov et al., 1978; Haehnel et al., 1982; 1983; Nairn et al., 1982; Karukstis and Sauer, 1985; Mauzerall, 1985; Holzwarth et al., 1985; Holzwarth, 1986; Moya et al., 1986). The appearance of the slow component of chlorophyll fluorescence after the reduction of plastoquinone Q_A, also contradicts the above-mentioned Duysens hypothesis.

A more attractive mechanism explaining the increase of chlorophyll fluorescence upon reduction of Q_A is a model proposed by Klimov (Klimov et al., 1978; see also: Klevanik et al., 1991). Unlike the above hypothesis, this model considers functionality of the photochemical pathway of utilization of the excitation energy in the PSII reaction centers after reduction of Q_A. According to the model, an increase of chlorophyll fluorescence when Q_A becomes reduced, i.e. induction of the variable fluorescence of chlorophyll may occur in the following way: the transformation of the energy starts with the excitation of the primary electron donor P_{680} (P_{680}*) and subsequent fast (for ~ 3 ps) electron

transfer from the excited P_{680}* to the pheophytin molecule, which leads to the formation of the unstable [$P_{680}^{+\bullet}$Pheo$^{-\bullet}$] pair (Klimov et al., 1977; Wasielevski et al., 1989a; 1989b; Hasting et al., 1992; Schelvis et al., 1994; Visser et al., 1995). According to other authors, for the formation of the [$P_{680}^{+\bullet}$Pheo$^{-\bullet}$] pair 8 ps are required (Greenfield et al., 1997). Stabilization of the [$P_{680}^{+\bullet}$Pheo$^{-\bullet}$] pair occurs due to electron transfer from Pheo$^{-\bullet}$ to plastoquinone Q_A for ~ 200 ps (Nuijs et al., 1986; Eckert et al., 1988; Leibl et al., 1989) and the reduction of $P_{680}^{+\bullet}$ by the electron transferred from tyrosine Y_Z for 20-260 ns (Brettel et al 1984, Sclodder et al., 1984; Meyer et al., 1989). When Q_A is reduced photochemically, stabilization of the [$P_{680}^{+\bullet}$Pheo$^{-\bullet}$] pair may occur as a result of charge recombination between $P_{680}^{+\bullet}$ and Pheo$^{-\bullet}$ (Klimov et al., 1978; Klevanik et al., 1991), which proceeds in the time scale of 2-30 ns depending on the molecular size of PSII preparation used in the study (Shuvalov et al., 1980; Danielius et al., 1987; Hansson et al., 1998). The decay of the [$P_{680}^{+\bullet}$Pheo$^{-\bullet}$] state due to charge recombination can occur through the excited state of P_{680}* (Fig. 1, b). In this case, conversion of P_{680}* to the ground state is accompanied by the emission of light quanta, which represents the variable fluorescence of chlorophyll (Klimov et al., 1978; Klimov and Krasnovskii, 1981; Klevanik et al., 1991).

Thus, the hypothesis includes a molecular mechanism. According to this hypothesis, the variable fluorescence is a delayed luminescence emitted during charge recombination in the PSII reaction center.

2.3. Fluorescence of chlorophyll is a loss of excitation energy

Being part of the excitation energy of antenna pigments, which cannot be utilized by the PSII reaction centers, chlorophyll fluorescence represents a loss of excitation energy. As shown above, it comprises ~2% (2-5%, Kitajima and Butler, 1975) of the excitation energy of the antenna. Since F_0 is emitted by the "open" centers at low intensity of excitation light when the energy transfer to the PSII reaction center balances with electron transfer events in reaction centers from P_{680} to plastoquinones Q_A, Q_B and further. In the case of maximal (or variable) fluorescence of chlorophyll, differences in the rate of electron transfer from P_{680} to plastoquinone Q_A (~ 200 ps: Nuijs et al., 1986, Eckert et al., 1988; Leibl et al., 1989), and from $Q_A^{-\bullet}$ to plastoquinone Q_B (100-200 μs: Bowes and Crofts, 1980; Crofts and Wraight, 1983; Robinson and Crofts, 1983; De Wijn and van Gorkom, 2001) leads to the accumulation (increase in the quasi-stationary concentration) of $Q_A^{-\bullet}$ in the PSII reaction centers under strong excitation ("actinic") light. In this circumstance only a part of the separated charges is stabilized through the charge recombination, during which the energy of the redox pair [$P_{680}^{+\bullet}$Pheo$^{-\bullet}$] may be lost as a luminescence. However, a part of the separated charges is involved in maintaining the electron transfer along the redox chain, thereby performing photosynthesis. Thus, in this sense, the concept of "closed" centers becomes meaningless.

Nevertheless, the variable fluorescence is closely related to the processes of electron transfer from water to plastoquinones, and therefore its intensity can be tuned by the factors affecting the electron transfer in PSII from the P_{680} to Q_A (in the reaction center), from H_2O to $P_{680}^{+\bullet}$, and from $Q_A^{-\bullet}$ to Q_B. Thus, the variable fluorescence of chlorophyll may be successfully applied to the study of the photosynthetic apparatus, and to the study of the problems of plant physiology.

2.4. "Maximum quantum efficiency" of photosystem II

Chlorophyll *a* in oxygenic species represents an intrinsic fluorescence probe. Considering the complex response against different external factors, chlorophyll fluorescence is widely used in various fields of plant biology. As mentioned above, about 20 different parameters (amplitude, kinetic and derivatives) characterizing complex changes of chlorophyll fluorescence were reported by different authors in the literature (Kromkamp and Forster 2003, Baker, 2008, Brestic and Zivcak, 2013). Among these parameters, a particular interest represents "maximum quantum efficiency" of PSII, determined on the basis of the F_0, F_V and F_M.

The "maximum quantum efficiency" of photosystem II, denoted sometimes as "maximum quantum yield" or "potential quantum yield", is defined by the ratio of variable and maximum fluorescence of chlorophyll:

$$Y = \frac{F_M - F_0}{F_M} = \frac{F_V}{F_M} \quad (5)$$

Usually the parameter Y (**Y**ield) is determined in the dark-adapted leaves, and used as an indicator of the photochemical activity of the plant photosynthetic apparatus thereby the physiological state of the plants. It is considered as the most sensitive indicator characterizing the effects of different stresses on plants. For most plants grown under non-stressed conditions, the maximum measured value of *Y* is 0.83 (Björkman and Demmig, 1987). Under stressful conditions, usually a significant decrease in this value is observed. Using Y and its characteristic terminology, many authors disregard the mechanisms of photosystem II during the studies, which in turn may lead to misinterpretation of the results. Indeed, according to the expressions 4b and 5 when the value F_M/F_0 is equal to 5.0, the quantum yield of photochemistry (φ_p) is 0.8, and this result may be perceived as a true result. However, this seeming "success" arises from the mechanistic assumption used in deriving equation 4b (see also below, point 4). Thus, when using the parameters F_V, F_M and Y for the estimation of photochemical processes and the PSII state, the following comments should be considered as useful:

1) Chlorophyll fluorescence F_0, F_V, and maximal fluorescence F_M refer to the loss of excitation energy in photosystem II. The ratio of the values of these two radiative losses (F_V/F_M) cannot be used as an indicator of the quantum yield (efficiency) of photosystem II, i.e. photochemical electron transport in PSII.

2) Quantum yield of chlorophyll fluorescence does not represent the quantum yield of photochemical electron transfer in PSII. Identifying the quantum yields of the photochemical reaction and chlorophyll fluorescence, can lead to the errors during interpretation of the results. In photosynthetic systems under constant illumination, the quantum yield of chlorophyll fluorescence is ~ 2% (2-5% in: Kitajima and Butler, 1975), and it consists of the sum of F_0 and F_V. Therefore, the ratio of the parameters, which total values (2-5%) are far from the quantum yield of photochemistry (≥95%), cannot be used as an indicator of the quantum yield of photosystem II.

3) Above (paragraph 2.1-2.3) it was shown that the constant (F_0) and the variable fluorescence of the chlorophyll F_V include different mechanisms: F_0 is emitted directly by the antenna before the excitation energy reaches the RC, and F_V is emitted by the antenna through the processes occurring in RC. Maximum fluorescence (F_M) includes F_0 ($F_M = F_0+F_V$). Therefore, the "maximum quantum efficiency" of photosystem II estimated by the F_V/F_M ratio will lead to incorrect results. This can be confirmed by simple examples:

a) In plants, which are not subjected to stress, the value of F_V/F_M is ~0.8 (Klimov et al., 1977; Björkman and Demmig, 1987). However, according to expression 5, a twofold (50%) decrease in the intensity of the variable fluorescence of chlorophyll at a constant F_0 results in F_V/F_M value of ~0.66 (~80% of the maximum Y), the correctness of the use of the parameter Y as an indicator and for evaluating the stress of plants may cause doubts.

b) Inhibition of the donor side of photosystem II, for example, when Mn cluster is removed, leads to the decreases in F_V almost to zero (Klimov et al., 1982). According to equation 5, in this case the "maximum quantum efficiency" of PSII should also decrease to zero. However, it was experimentally found that in this case the photochemical activity of the PSII reaction center, thus the quantum yield of photosystem II remains high.

4) Another reason pointing to the incorrectness of using F_V/F_M to determine the "maximum quantum efficiency" of PSII is that this approach includes the mechanisms proposed by Duysens and Sweers (1963), which accept the concept of "closed" PSII centers and cannot explain the RC mechanisms properly. However, as shown above (Klimov et al., 1978, Klevanik et al., 1991), the PSII reaction centers remain open when Q_A is reduced. In this case, part of the redox energy stored in the RC is consumed photosynthetically, and only a small part of the energy can be lost in the form of luminescence.

5) During the determination of quantum efficiency using the above method, it is impossible to obtain detailed information about the sites and mechanisms of inhibition of the photosynthetic electron transport chain of plants under stressfull conditions. However, F_V itself carries information about photoinduced electron transfer in photosystem II, from water to plastoquinones. When using suspensions, combining with other available met-

hods, it is relatively easy to identify the mechanism of inhibition. In addition, in suspensions, it is possible to equalize the concentration of chlorophyll accurately, which allows, without difficulty, comparing the F_V values of each individual measurement.

3. Conclusion

One of the main properties of photosystem II is the emission of light by chlorophyll *a* in this complex, which provides properties of a fluorescent marker in the study of the physiological state of plants, algae and cyanobacteria. Under continuous illumination, and due to the processes that are not directly related to photosynthesis, the intensity of chlorophyll fluorescence changes in a very complex manner, which allows widespread using of chlorophyll fluorescence in studies of oxygenic species. Among the fluorescence components of F_0, F_V, and the parameter "maximum quantum efficiency", a variable fluorescence of chlorophyll is the most suitable parameter characterizing the state of the photosynthetic apparatus. Despite the fluorescence of chlorophyll is the loss of the absorbed light energy, due to the close relationship between the processes occurring in the PSII reaction centers (growth kinetics of F_V and its amplitude are related to the processes of electron transfer to plastoquinone Q_A and charge recombination in the RC, respectively), F_V may be considered as a more appropriate component of fluorescence in studies of the physiological state of oxygenic species. Changes in its intensity can be easily interpreted upon the influence of different factors on photosystem II in isolated chloroplasts and PSII membranes. However, when plant leaves are being examined, evaluation and comparison of the results of each individual measurement is difficult and requires special attention. Another component of chlorophyll fluorescence, F_0 is not directly related to RC processes. However, this component of fluorescence can be used as an important indicator in stressful situations, for example, due to changes in membrane fluidity under high temperature stress, or during the study of the antenna systems (Yamane et al., 1997). It was mentioned above that the parameter "maximum quantum efficiency" of PSII (parameter Y) is not a true quantum yield and, thus may incorrectly describe the state of the photosynthetic apparatus. The Y concept is based on the concepts of Duysens and Sweers (1963), and Kitajima and Butler (1975) and does not reflect the molecular processes occurring in the photosynthetic apparatus. However, the use of the ratio F_V/F_M without attributing it the name "maximum quantum efficiency", can play an auxiliary role in estimating the photochemical activity of photosystem II. Whereas, the ratio F_V/F_0, representing relative share of two different processes occurring in the PSII reaction centers and in the antenna, which contributes to the chlorophyll fluorescence can be more suitable for characterizing the photosynthetic apparatus.

ACKNOWLEDGMENTS

This work was supported by the Science Development Foundation under the President of the Republic of Azerbaijan – **Grant No EIF-BGM-4-RFTF-1/2017-21/20/3**, and by the Presidium of Azerbaijan National Academy of Sciences – **Grant dated on 15.03.2017**.

REFERENCES

Ago H., Adachi H., Umena Y. et al. (2016) Novel features of eukaryotic photosystem II revealed by its crystal structure analysis from a red alga. *J. Biol. Chem.*, **291:** 5676-5687.

Baker N.R. (2008) Chlorophyll fluorescence: A probe of photosynthesis in vivo. *Annu. Rev. Plant Biol.* 2008, **59:** 89-113.

Barber J. (2006) Photosystem II: An enzyme of global significance. *Biochem. Soc. Trans*., **34:** 619-631.

Björkman O., Demmig B. (1987) Photon yield of O_2 evolution and chlorophyll fluorescence characteristics at 77 K among vascular plants of diverce origins. *Planta,* **170**: 484-504.

Borisov A.Yu., Godik V.I. (1973) Excitation energy transfer in photosynthesis. *Biochim. Biophys. Acta*, **301:** 227-248.

Bowes J.M., Crofts A.R. (1980) Binary oscillations in the rate of reoxidation of the primary acceptor of photosytem II. *Biochim. Biophys. Acta*, **590:** 373-384.

Brestic M, Zivcak M. (2013) PSII fluorescence Techniques for measurement of drought and high temperature stress signal in crop plants:

Protocols and applications. In: G.R.Rout, A.B.Das (Eds.) *Molecular Stress Physiology of Plants.* Springer, Dordrecht, pp. 87-131

Brettel K., Schlodder E., Witt H.T. (1984) Nanosecond reduction kinetics of photooxidized chlorophyll-a_{II} (P-680) in single flashes as a probe for the electron pathway, H^+-release and charge accululation in the O_2-evolving complex. *Biochim. Biophys. Acta*, **766:** 403-415.

Briantais J.M., Vernotte C., Krause G.H., Weis E. (1986) Chlorophyll *a* fluorescence of higher plants: chloroplasts and leaves. In: Govindjee, J.Amesz and D.C.Fork (Eds.) *Light emission by plant and bacteria.* Academic Press, New York, p. 539-577.

Campbell D., Hurpy V., Clarke A.K. et al. (1998) Chlorophyll fluorescence analysis of cyanobacterial photosynthesis and acclimation. *Microbiol. Mol. Biol. Rev.* **62:** 667-683.

Crofts A.R., Wraight C.A. (1983) The electrochemical domain of photosynthesis. *Biochim. Biophys. Acta*, **726:** 149-185.

Danielius R.V., Satoh K., van Kan P.J.M., et al. (1987) The primary reaction of photosystem II in the D1-D2-cytochrome b-559 complex. *FEBS Lett.*, **213:** 241-244.

De Wijn R., van Gorkom H.J. (2001) Kinetics of electron transfer from Q_A to Q_B in photosystem II. *Biochemistry*, **40:** 11912-11922.

Debus R.J. (1992) The manganese and calcium ions of photosynthetic oxygen evolution. *Biochim. Biophys. Acta*, **1102:** 269-352.

Duysens L.N.M., Sweers H.E. (1963) Mechanism of two photochemicals reaction in algae as studied by means of fluorescence. In: S.Miachi (ed.) *Studies on microalgae and photosynthetic bacteria.* Tokyo: Univ. Tokyo press, p. 353-372.

Eckert H.-J., Wiece N., Bernarding J. et al. (1988) Analysis of the electron transfer from $Pheo^-$ to Q_A in PSII membrane fragments from spinach by time-resolved 325 nm absorption changes in the picosecond domain. *FEBS Lett*., **240:** 153-158.

Ferreira K.N., Iverson T.M., Maghlaoui K. et al. (2004) Architecture of the photosynthetic oxygen-evolving center. *Science*, **303:** 1831-1838.

Goltsev V.N., Kalaji H.M., Paunov M. et al. (2016) Variable chlorophyll fluorescence and its use for assessing physiological condition of plant photosynthetic apparatus. Russian J. Plant Phys. 63: 869-893.

Govindjee, Shevela D., Björn L.O. (2017) Evolution of the Z-scheme of photosynthesis: a perspective. *Photosynth. Res.* **133:** 5-15.

Greenfield S.R., Seibert M., Govindjee, Wasielewski M.R. (1997) Direct measurement of the effective rate constant for primary charge separation in isolated photosystem II reaction centers. *J. Phys. Chem.* B, **101:** 2251-2255.

Groot M.L., van Grondelle R., Leegwater J.A., van Mourik F. (1997) Radical pair quantum yield in reaction centers of photosystem II of green plants and of the green bacterium *Rhodobacter sphaeroides*: Saturation behavior with subpicosecond pulses. *J. Phys. Chem.* (B), **101:** 7869-7873.

Haehnel W., Holzwarth A.R., Wendler J. (1983) Picosecond fluorescence kinetics and energy transfer in the antenna chlorophylls of green algae. *Photochem. Photobiol.*, **37:** 435-443.

Haehnel W., Nairn J.A., Reisberg P., Sauer K. (1982) Picosecond fluorescence kinetics and energy transfer in chloroplasts and algae. *Biochim. Biophys. Acta*, **680:** 161-173.

Hansson Ö., Duranton J., Mathis P. (1998) Yield and lifetime of the primary radicals pairs in preparations of photosystem II with different antenna size. *Biochim. Biophys. Acta*, **932:** 91-96.

Hasting G., Durrant J.R., Barber J. et al. (1992) Observation of pheophytin reduction in photosystem II two reaction centers using femtosecond transient absorption spectroscopy. *Biochemistry*, **31:** 7638-7647.

Hill R. (1965) The biochemist's green mansions: the photosynthetic electron-transport chain in plants. In: P.N.Campbell, G.D.Greville (Eds.) *Essays in Biochemistry*. London: Academic Press, **1:** 121-151.

Holzwarth A.R. (1986) Fluorescence lifetime in photosynthetic systems. *Photochem. Photobiol.*, **43:**707-735.

Holzwarth A.R., Wendler J., Haehnel W. (1985) Time resolved fluorescence spectra of the antenna chlorophylls in *Chlorella vulgaris*. Resolution of photosystem I fluorescence. *Biochim. Biophys. Acta*, **807:** 155-167.

Horton P., Bowyer J.R. (1990) Chlorophyll fluorescence transients. *Meth. Plant. Biochem.* 4:259-296.

Kalaji H.M., Jajoo A., Oukarroum A. et al. (2016) Chlorophyll *a* fluorescence as a tool to monitor physiological status of plants under abiotic stress conditions. *Acta. Physiol. Plant.* **38:** 102-113.

Kalaji H.M., Schansker G., Ladle R.J. et al. (2014) Frequently asked questions about in vivo chlorophyll fluorescence: practical issues. Photosynth. Res. 122: 121-158.

Karukstis K.K., Sauer K. (1985) The effect of cation induced and pH-induced membrane stacking on chlorophyll fluorescence decay kinetics. *Biochim. Biophys. Acta,* **806:** 374-388.

Kitajima M., Butler W.L. (1975) Quenching of chlorophyll fluorescence and primary photo-chemistry in chloroplasts by dibromothymoquinone. *Biochim. Biophys. Acta,* **376:** 105-115.

Klevanik A.V., Feyziev Y.M., Allakhverdiev S.I. et al. (1991) The origin of photosystem II variable chlorophyll fluorescence. *Biologicheskie Membrany,* **10:** 1053-1065. (Russian)

Klimov V.V., Allakhverdiev S.I., Pashchenko V.Z. (1978) Measurement of the activation energy and the lifetime of the chlorophyll fluorescence of photosystem II. *Dokl. Acad. Sci. USSR,* **242:** 1204-1208 (Russian)

Klimov V.V., Allakhverdiev S.I., Shuvalov V.A., Krasnovsky A.A. (1982) Effect of extraction and re-addition of manganese on light reactions of photosystem-II preparations. *FEBS Lett*., **148:** 307-312.

Klimov V.V., Klevanik A.V., Shuvalov V.A., Krasnovsky A.A. (1977) Reduction of pheophytin in the primary light reaction of photosystem II. *FEBS Lett*., **82:** 183-186.

Klimov V.V., Krasnovskii A.A. (1981) Pheophytin as the primary electron acceptor in photosystem 2 reaction cnter. *Photosynthetica,* **15:** 592-609.

Krause G.H., Weis E. (1984) Chlorophyll fluorescence as a tool in plant physiology. II. Interpretation of fluorescence signals. *Photosynth. Res.,* **5**: 139-157.

Krause G.H., Weis E. (1991) Chlorophyll fluorescence and photosynthesis. *Annu. Rev. Plant Physiol. Plant Mol. Biol.,* **42:** 313-349.

Kromkamp J.C., Forster R.M. (2003) The use of variable fluorescence measurements in aquatic ecosystems: differences between multiple and single turnover measuring protocols and suggested terminology. *Eur. J. Physiol.,* **38:** 103-112.

Lazár D. (1999) Chlorophyll *a* fluorescence induction. *Biochim. Biophys. Acta,* **1412:** 1-28.

Leibl W., Breton J., Deprez J., Trissl H.-W. (1989) Photoelectric study on the kinetics of trapping and charge stabilization in oriented PSII membranes. *Photosynth. Res*., **22:** 257-275.

Mauzerall D.C. (1985) Evidence that the variable fluorescence of *Chlorella* is recombination luminescence. *Biochim. Biophys. Acta,* **809:** 11-16.

Maxwell K., Johnson G.N. (2000) Chlorophyll fluorescence – a practical guide. *J. Exp. Bot.,* **51:** 659-668.

Meyer B., Schlodder E., Dekker J.P., Witt H.T. (1989) O_2 evolution and Chl-a_{II} (P-680$^+$) nanosecond reduction kinetics in single flashes as a function of pH. *Biochim. Biophys. Acta*, **1974:** 36-43.

Moya I., Hodges V., Barbet J.C. (1986) Modification of room temperature picosecond chlorophyll fluorescence kinetics in green alga by photosystem II trap closure. *FEBS Lett.,* **1986:** 256-262.

Muh F., Zouni A. (2011) Light-induced water oxidation in photosystem II. *Front. Biosci.,* **16:** 3072-3132.

Nairn J.A., Haehnel W., Reisberg P., Sauer K. (1982) Picosecond fluorescence kinetics in spinach chloroplasts at room temperature. Effects of Mg^{2+}. *Biochim. Biophys. Acta,* **682:** 420-429.

Nelson N., Yocum C.F. (2006) Structure and function of photosystems I and II. *Annu. Rev. Plant Biol*., **57:** 521-565.

Nuijs A.M., van Gorkom H.J., Plijter J.J., Duysens L.N.M. (1986) Primary charge separation and excitation of chlorophyll *a* in photosystem II particles from spinach as studied by picosecond absorbance difference spectroscopy. *Biochim. Biophys. Acta,* **848:** 167-175.

Robinson H.-H., Crofts A.R. (1983) Kinetics of the oxidation-reduction reactions of the photosystem II quinine acceptor complex and the pathway for deactivation. *FEBS Lett*., **153:** 221-226.

Schelvis J.P.M., van Noort P.L., Aartsma T.J., van Gorkom H.J. (1994) Energy transfer, charge separation and pigment arrangement in the reaction center of photosystem II. *Biochim. Biophys. Acta*, **1184:** 242-250.

Schlodder E., Brettel K., Schatz G.H., Witt H.T. (1984) Analysis of the Chl-a_{II}^{+} reduction kinetics with nanosecond time resolution in oxygen-evolving photosystem II particles from *Synechococcus* at 680 and 824 nm. *Biochim. Biophys. Acta*, **765:** 178-185.

Schreiber U., Bilger W., Hormann H., Neubauer C. (1998) Chlorophyll fluorescence as a diagnostic toll: basics and some aspects of practical relevance. In: A.S.Raghavendra (Ed.) *Photosynthesis: A comprehensive treatise.* Cambridge Univ. Press, Cambridge, p. 320-336.

Shuvalov V.A., Klimov V.V., Dolan E., et al. (1980) Nanosecond fluorescence and absorbance changes in photosystem II at low redox potential. Pheophytin as an intermediary electron acceptor. *FEBS Lett*., **118:** 279-282.

Umena Y., Kawamaki K., Shen J.R., Kamiya N. (2011) Crystal structure of oxygen evolving photosystem II at an atomic resolution of 1.9 Å. *Nature*, **473:** 55-60.

Visser H.M., Groot M.-L., van Mourik F. et al. (1995) Subpicosecond transient absorption difference spectroscopy on the reaction center of photosystem II: Radical pair formation at 77 K. *J. Phys. Chem.* A, **99:** 15304-15309.

Wasielewski M.R., Johnson D.G., Govindjee et al. (1989a) Determination of the primary charge sepapration rate in photosystem II reaction centers at 15 K. *Photosynth. Res*., **22:** 89-99

Wasielewski M.R., Johnson D.G., Seibert M., Govindjee (1989b) Determination of the primary charge sepapation rate in isolated photosystem II reaction centers with 500-fs resolution. *Proc. Natl. Acad. Sci. USA*, **86**: 524-528.

Yamane Y., Kashino Y., Koike H., Satoh K. (1997) Increase in the fluorescence F_0 level and reversible inhibition of hotosystem II reaction center by high-temperature treatments in higher plants. *Photosynth. Res.*, **52:** 57-64.

Zouni A., Witt H.-T., Kern J. et al. (2001) Crystal structure of photosystem II from *Synechococcus elongatus* at 3.8 Å resolution. *Nature*, **409:** 739-743.

Xlorofil fluoressensiyası və fotosistem II-nin "maksimal kvant effektivliyi" parametrinin bitki tədqiqatlarında istifadəsi

Y.M. Feyziyev

AMEA Molekulyar Biologiya və Biotexnologiyalar İnstitutu

Xlorofilin fluoressensiyası və onun dəyişmələri bitki, birhüceyrəli yosun və sianobakteriyalarda fotosistem II kompleksinin (FSII) fəaliyyətinin indikatoru olaraq geniş istifadə olunur. İndiyədək ədəbiyyatda xlorofilin fluoressensiyasını xarakterizə edən 20-dək parametr məlumdur. Bu işdə FSII fluoressensiyanın bəzi əsas xarakteristikaları – xlorofilin başlanğıc (F_0), maksimal (F_M) və dəyişən fluoressensiyaları (F_V) müqayisə olunmuş, eləcə də FSII-nin maksimal kvant effektivliyi adlanan törəmə (F_M-F_0)/F_M parametrinin критик təhlili aparılmışdır. FSII reaksiya mərkəzi proseslərinin və dəyişən fluoressensiyanın təsvirində istifadə olunan Duysens (Duysens and Sweers, 1963) hipotezi və Klimov tərəfindən irəli sürülmüş rekombinasiya lüminessensiyası hipotezinin (Klimov et al., 1978) qısa, müqayisəli təhlili aparılmış və oksigenli fotosintezdə aparılan fluoressensiya ölçülərinin nəticələrinin interpretasiyasınnın çatışmazlıqları müzakirə olunmuşdur. Bitki fiziologiyası və ekofizioloji tədqiqatlarda geniş istifadə olunan FSII-nin "maksimal kvant effektivliyi" parametrinin tətbiqindəki qeyri-dəqiqliklər göstərilmişdir.

Açar sözlər: *Fotosistem II, xlorofilin fluoressensiyası, maximum kvant effektivliyi*

Флуоресценция хлорофилла и «максимальная квантовая эффективность» фотосистемы II в исследованиях растений

Я.М. Фейзиев

Институт молекулярной биологии и биотехнологий НАН Азербайджана

Флуоресценция хлорофилла *a* широко используется в качестве индикатора состояния фотосистемы II (ФСII) растений, водорослей и цианобактерий. В литературе разными авторами сообщались о 20-и разных параметрах флуоресценции хлорофилла ФСII. В данной работе обсуждены три из этих характеристик: начальная (F_0), максимальная (F_M) и переменная флуоресценция хлорофилла (F_V) и производная величина (F_M-F_0)/F_M, называемая «максимальной квантовой эффективностью» ФСII. Осуществлен краткий и сравнительный анализ гипотезы Дейзенса (1963) и гипотезы рекомбинационной люминесценции Климова (Klimov et al., 1978), применяемых для описания процессов реакционного центра ФСII, и обсуждены возможные ошибки, допущенные в интерпретациях переменной флуоресценции хлорофилла. Обсуждены возможные неточности при применении параметра «максимальной квантовой эффективности» PSII используемой для оценки активности фотосинтетического аппарата и физиологического состояния растений.

Ключевые слова: *Фотосистема II, флуоресценция хлорофилла, максимальная квантовая эффективность*

Journal of Life Sciences and Biomedicine, vol. 1 (74), No 1, p. 29-36 (2019)

Resolution and resolvability in one, two and three dimensions

G.M. Gasimova[1,2]*, R.C. Masmaliyeva[1], G.N. Murshudov[1,3]*****

[1]Institute of Molecular Biology & Biotechnologies, Azerbaijan National Academy of Sciences, Azerbaijan
[2]Azerbaijan State Oil and Industry University, 34 Azadliq ave., Baku AZ1010, Azerbaijan
[3]MRC Laboratory of Molecular Biology, Cambridge, UK
** For correspondence: GXG557@alumni.bham.ac.uk*
*** For correspondence: r.masmaliyeva@gmail.com*
****For correspondence: garib@mrc-lmb.cam.ac.uk*
Accepted for publication: 10 August 2019

This contribution describes an approach to the problem of resolution and resolvability in scattering methods (*e.g.* X-ray diffraction, electron microscopy) in the presence of series termination and blurring. One-, two- and three-dimensional cases are considered separately. Formulas relating the effects of nominal resolution and blurring to peak resolvability are derived and analysed. We show that both blurring and series termination widen point source peaks thus reducing their resolvability.

Keywords: *Refinement, electron cryo-microscopy, Fourier shell correlation, Fourier transformation, Gaussian distribution*

INTRODUCTION

Macromolecular crystallography (MX) and single particle cryo electron microscopy (cryo-EM) are two widely used scattering methods used to derive atomic models of biological molecules (Rupp, 2010; Frank, 2005). Both techniques produce density maps that are interpreted as atomic models (Emsley and Cowtan, 2006). Derived atomic models are deposited to the Protein Data Bank (PDB) via which they are made available to the community free of charge (Berman et al., 2002). Maps can be represented equivalently either in image space as a function sampled on a regular three-dimensional grid points or as Fourier coefficients of these maps. In crystallography observations are related to the Fourier coefficients (Harker and Kasper, 1948), whereas in cryo-EM usually observations are made for images themselves (Frank, 2005). Details that can be seen in these maps and therefore accuracy of atomic models depend on the amount and quality Fourier coefficients.

There are some confusion and controversy on the definition and use of resolution concept: current definition only uses the highest frequency terms of the Fourier coefficients used for map calculations (Wlodawer et al., 2017). This definition does not account for the noise in the data, absolute and relative mobility of the objects under study. It only states the radius of a sphere within which observations reside. Although it does seem that in crystallography, since observations are directly related to the Fourier coefficients, the highest observed frequency term should define the resolution provided that all Fourier coefficients have been measured with high accuracy. This definition has been successfully used for last 100 years. However now increasingly more and more noisy data are used for structure determination and old definition is no longer applicable: this definition only defines the radius in the Fourier space where data reside. Another problem arises when the resolution of structure used as an indication of their accuracies and different structures are compared with reference to resolution; e.g. for selection of the "best" atomic models, for comparison of accuracy of atomic models to typical models in the PDB corresponding to the same resolution.

In cryo-EM resolution is defined by analogy to that in crystallography: the highest frequency of observed Fourier coefficient are defined for which Fourier shell correlation (fsc) is more than 0.143 where fsc is calculated in narrow shells between Fourier coefficients of two independently reconstructed maps (Rosenthal and Henderson, 2003;

Scheres, 2012). Both of these definitions, to a certain degree, make use of the signal to noise ratio. Information about the signal-noise ratio should also be used in structure determination and refinement (Murshudov, 2016). Usage of the highest observed significant frequency terms as a definition of the resolution does not account for the behaviour of the noise and the signal over the Fourier space: it is time to make these definitions more precise that accounts for the quality of all available information in the data.

Moreover, both of these definitions do not fully account for the signal the noise level in the data, they also do not use the fact that molecules oscillate resulting in the blurred image and therefore reducing the visibility of them in the map affecting different parts of the density differently in accordance with varying mobility of molecules.

In this paper, we will address this problem theoretically with some certain simplifying assumptions that make calculations manageable. Here we consider one-, two- and three-dimensional cases and show that objective measure can be calculated to measure resolvability that would reflect the information contained in the data about the object under study.

1. Resolution and Resolvability

Let us assume that we have observations in the Fourier space up to a nominal resolution s_{nom}. Our observations are Fourier coefficients that are sum of two components $F_{obs}(s)$=$F_{true}(s) + F_{noise}(s)$, where $F_{obs}(s)$ is observed, $F_{true}(s)$ is the "true" and $F_{noise}(s)$ is the noise Fourier coefficients. We also assume that "true" image is a blurred version of the object we would like to observe, where blurring is linear. *I.e.* true part of the observed image is:

$$\rho_{true}(x) = \int_y \rho_0(y) g(x,y) dy \qquad (1)$$

where *g(x,y)* is a blurring function that is normalised everywhere:

$$\int_y g(x,y) dy = 1 \qquad (2)$$

where $\rho_{true}(x)$ is the true image, $\rho_0(x)$ is the image we would like to observe.

Basic image processing and modelling problem is that our data have noise and blurred then we would like to solve the equation (1) so that as much as possible details in the map can be visualised and modelled. This problem can be considered as Wiener filtering problem (Vega and Rey, 2012). In general, a solution of the equation (1) requires solving very large linear systems which is not possible in practice. In addition, since we do not know the blurring function then the problem becomes even more complex; we must find blurring function as well as solving the equation (1). When blurring is position independent, *i.e.* $g(x,y) = g(x-y)$ then the problem becomes simpler, "true" image is just a convolution of the unblurred image with the blurring function. In this case, it is known that $F_{blur}(s) = F_0(s)F_g(s)$, i.e. Fourier coefficients of the blurred image is the product of Fourier coefficients of the unblurred image and that of blurring function.

So, the observation in the Fourier space can be written as:

$$F_{obs}(s) = F_0(s)F_g(s) + F_{noise}(s)$$

Recall that our observations are within the nominal resolution sphere $|s| < s_{nom}$. We assume that we know the blurring function - $F_g(s)$, the variance and covariance of the noise in the Fourier space - F_{noise}. We want to know what are the details in the image that can be seen (distinguish from each other) for a given nominal resolution, blurring function and noise level. We will approach to this problem step by step. First, we will assume that there is no noise $F_{noise}(s) = 0$, no blur $F_g = 1$ and the only shortcoming of our observations is that we observe only within a resolution sphere $|s| < s_{nom}$, the only problem is the series termination effect. After analysis of this problem we will move on to assume that there is a position independent blurring and we know blurring function. We also will assume that the blurring function is Gaussian and we know the blurring parameter. Then we will consider the cases when there is noise and we know the variance and covariance of the noise. Then we assume that we do know the shape of blurring function but we do not know its parameters (e.g. blurring is Gaussian but we do not know variance of the Gaussian). Our problem then will be a) what level of details can be seen; b) what are the optimal parameters of blurring function. Then we will move on and assume that blurring is position dependent. However, in this work we will

only consider only limited resolution data (series termination effect) and position independent Gaussian blurring. Remaining problems will be dealt with in future works.

To define the resolvability in the scattering data we will assume that there are two point sources, however because of observational deficiencies or intrinsic properties, *e.g.* mobility of the objects observed sources are broadened. We will consider two reasons for peak broadening: a) our observations are within a certain resolution limit - $|s| < s_{nom}$; b) sources oscillate during observations and we observe blurred version of these sources.

We will define resolvability as follows: With a given nominal resolution limit, blurring and noise level resolvability is the minimum distance between like point sources that can be distinguished in the map.

We assume that we have two point sources in n-dimensional space and they are blurred by a Gaussian blur with the variance $u = \frac{B}{8\pi^2}$. Then the observed peak for one point source would have the form:

$$f_B(x) = \int_{|s|<s_{nom}} e^{-\frac{B|s|^2}{4}} e^{i2\pi xs} ds \qquad (3)$$

where integral is in n-dimensional space. *xs* is the bilinear form formed with the vectors in image (x) and Fourier space (s), $i = \sqrt{-1}$ is the imaginary number. We would like to find minimal non-zero root of this equation:

$$f_B(0) + f_B(x) - 2f_B\left(\frac{x}{2}\right) = 0 \qquad (4)$$

i.e. we want to find such a distance between point sources that image values at the positions of the peaks are bigger than in the middle of the vector connecting them.

In the following sections, we will consider this equation for one, two and three dimensions with and without blurring.

2. Peak widening and resolvability in 1D

Let us assume that we have a point source: $\delta(x)$ in one dimensional case. Its Fourier transformation for all s $F(s) = 1$. Now let us assume that we cut the data $s \in [-s_{nom}, s_{nom}]$. Let us calculate the inverse Fourier transformation which is the following integral:

$$f_0(x) = \int_{-s_{nom}}^{s_{nom}} e^{i2\pi xs} ds = \frac{2s_{nom}\sin(2\pi x s_{nom})}{2\pi x s_{nom}} = \\ = 2s_{nom} j_0(2\pi x s_{nom}) \qquad (5)$$

Therefore, in this case, the above stated problem is reduced to the solution of the equation:

$$2s_{nom} + 2s_{nom} j_0(2\pi x s_{nom}) - \\ -4s_{nom} j_0(2\pi x s_{nom}/2) = 0 \qquad (6)$$

If we let $y = 2\pi x s_{nom}$ then the solution of (6) is equivalent to finding of the smallest non-zero root of the equation

$$1 + j_0(y) - 2j_0(y/2) = 0 \qquad (7)$$

Solution of this equation is $y_0 = 4.28$ and therefore $x_0 = \frac{y_0}{2\pi s_{nom}} = \frac{0.68}{s_{nom}}$.

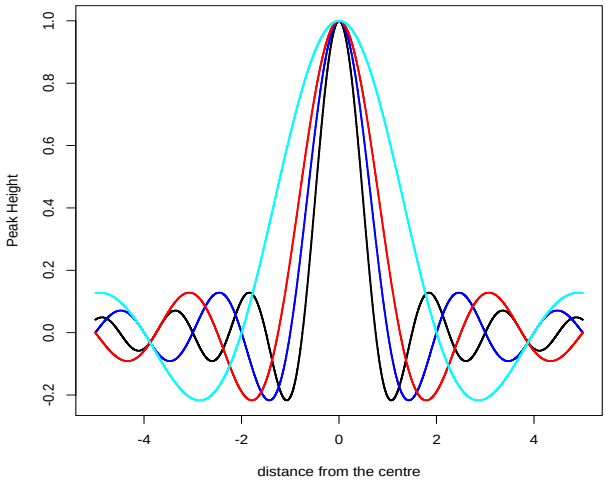

Fig. 1. The graphs of $f(x) = j_0(2\pi x s_{nom})$ function for different values of nominal resolution - s_{nom}. This graph shows that peaks are broadened as s_{nom} decreases. Black line corresponds to $s_{nom} = 0.75$, blue line corresponds to s_{nom} =0.5, red line corresponds to $s_{nom} = 0.4$ and cyan line corresponds to $s_{nom} = 0.25$.

Figure 1 demonstrates the effect of nominal resolution on peak broadening. As it is expected as the nominal resolution increases the calculated peaks become sharper.

If we have two point-sources and observations inside the interval $|s| < s_{nom}$ what is the minimal distance between peaks so that they can be seen as a separate peak. Let us assume that distance between point sources is z. Then we can plot the following function:

$$j_0(2\pi x s_{nom}) + j_0(2\pi(x - z)s_{nom})$$

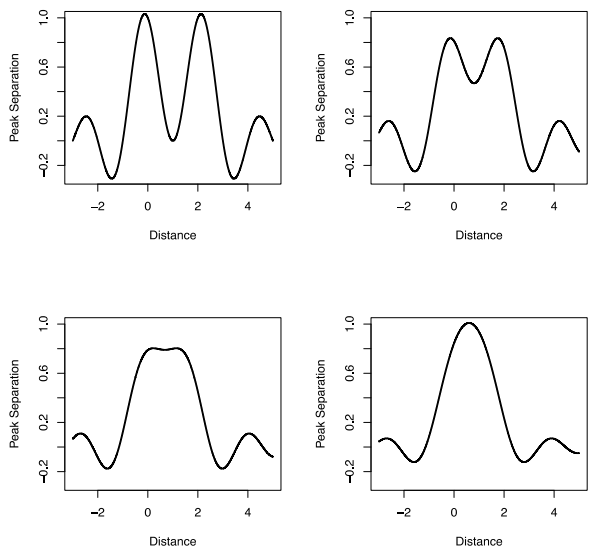

Fig. 2. The graph of two point-sources for one-dimensional case – the function $j_0(2\pi x s_{nom}) + j_0(2\pi(x - z)s_{nom})$. Resolution is s_{nom}=0.5. Top left: distance between sources is 2Å, top right: distance between source is 1.6Å, bottom left: distance between sources 1.36Å, bottom right: distance between sources is 1.2Å

Fig. 2. demonstrate that inside $|s| < 0.5Å^{-1}$ interval when the distance between peaks are decreasing then resolvability power of the map become is reduced. When the distance is 2Å then peaks are clearly visible, when the distance becomes 1.6Å peaks become less separable, when the distance between peaks is 1.36Å then peaks are marginally separable and when the distance is 1.2Å then two peaks are merged together and they are no longer be seen as two different peaks. It should be noted that when the distance is equal to the resolvability – 1.36Å then, although peaks can still be separated they come close to each other - the maxima of peaks are no longer at the original peak positions.

Gaussian blurred source with the variance $u = \frac{B}{8\pi^2}$ has the form:

$$\rho(X) = 2\sqrt{\frac{\pi}{B}}e^{-\frac{x^2}{B}} \quad (8)$$

Fourier transformation of this source is:

$$F(s) = e^{-B|s|^2/4} \quad (9)$$

Now we again assume that the data have been observed within the interval $s \in [-s_{nom}, s_{nom}]$. Inverse Fourier transformation of the Gaussian blurred point source is:

$$f_B(x) = \int_{-s_{nom}}^{s_{nom}} e^{-B|s|^2/4}\, e^{i2\pi x s} ds \quad (10)$$

resulting in

$$f_B(x) = 2\frac{\sqrt{\pi}}{\sqrt{B}}e^{-\frac{(2\pi x)^2}{B}} Re(\mathrm{erf}(\frac{\sqrt{B}s_{nom}}{2} - \frac{i2\pi x}{\sqrt{B}}))$$

We can evaluate this function if we have access to the error function of complex variables. This function can be evaluated efficiently using Faddeeva function (Poppe and Wijers, 1990) defined for complex arguments as:

$$\omega(z) = e^{-z^2}erfc(-iz) = e^{z^2}(1 - erf(-iz))$$

where z is a complex variable and the values of this function, in general, are complex numbers.

Using the relationships between error and Faddeeva functions we can write:

$$f_B(x) = 2\frac{\sqrt{\pi}}{\sqrt{B}}e^{-\frac{(2\pi x)^2}{B}} - 2\frac{\sqrt{\pi}}{\sqrt{B}}e^{-\frac{Bs_{nom}^2}{4}} Re(e^{i2\pi x s_{nom}} w\left(\frac{2\pi x}{\sqrt{B}} + i\frac{\sqrt{B}s_{nom}}{2}\right))$$

Let us compare the effects of different B values on point source broadening.

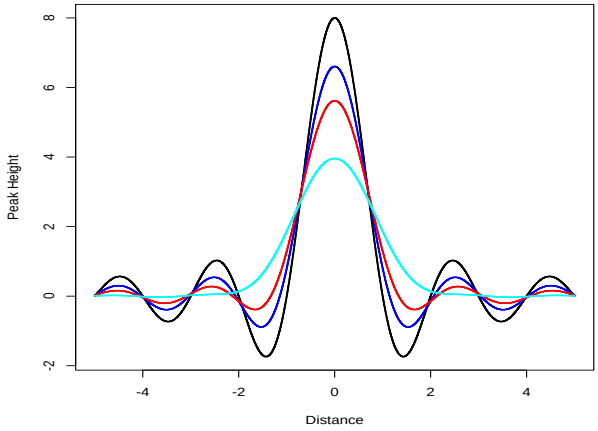

Fig. 3. Point source with blurs**.** All plots correspond to s_{nom} = 0.5, Black line corresponds to B = 0.001Å^{-2}, blue line corresponds to B = 10Å^{-2}, red line corresponds to B=20Å^{-2} and cyan line corresponds to B=50Å^{-2}.

It is clear that as B value increases the peaks are broadening thus reducing resolvability of these peaks. To observe highly oscillating peaks one needs to produce maps with as little as possible noise.

Fig. 4 shows that for the same resolution and distance between Gaussian sources as blurring parameter increases peaks become less and less resolvable. It should be noted that if there would be no noise and blurring parameter would be known then we could remove the effect of blurring without difficulty by simply using deconvolution. The problem becomes more complicated when the noise comes into play. All observations in reality are with noise, the noise level can be reduced it is impossible to remove it completely.

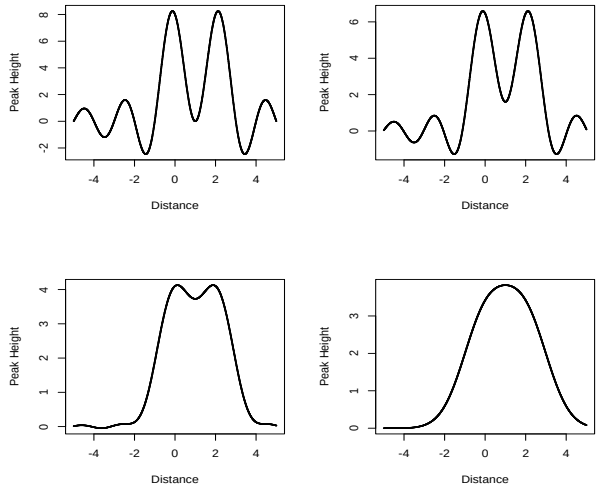

Fig. 4. Sum of two Gaussian blurred sources at $s_{nom} = 0.5, dist = 2$Å for different blurring parameters. Top left: B=0.01Å^{-2}, top right: B=10Å^{-2}, bottom left B=50Å^{-2}, bottom right B=100Å^{-2}.

3. Peak widening and resolvability in 2D

Now let us assume that we have a point source in two dimensions. Its Fourier transformation for all *s* is constant. Now let us assume that we cut the data within $|s| < s_{nom}$. The observed peak will have the form:

$$f_0(x) = \int_{|s|<s_{nom}} e^{i2\pi xs} ds = \\ = 2\pi s_{nom}^2 \frac{J_1(2\pi|x|s_{nom})}{2\pi|x|s_{nom}} \quad (11)$$

where J_1 is the 1st order Bessel function of first kind. All other terms are the same as defined above. Since $\lim_{t\to 0} \frac{J_1(t)}{t} = \frac{1}{2}$ we can write $f_0(0) = \pi s_{nom}^2$. If we use $t = 2\pi|x|s_{nom}$ then the equation (4) is reduced to:

$$1 + \frac{J_1(t)}{t} - 2\frac{J_1(t/2)}{t/2} = 0 \quad (12)$$

The solution of this equation is $t_0 \approx 4.7715$ and we obtain that: $t_0 = 2\pi s_{nom} x$ and therefore in the absence of blurring resolvability in two-dimensional case is: $x_0 = \frac{t_0}{2\pi s_{nom}} = 0.7594\frac{1}{s_{nom}}$. Since these functions have qualitatively the same form as in one-dimensional case we do not show figures for unblurred cases in two dimensions.

The observed peak with the blurring parameter B and nominal resolution s_{nom} is calculated using the following integral:

$$f_B(x) = \\ = \int_0^{2\pi} \int_0^{s_{nom}} e^{-B|s|^2/4} |s| \cos(2\pi|x||s|\cos(\phi)) d\phi ds$$

To our knowledge there is no closed form expression for this integral, therefore this integral is calculated numerically using the statistics package R (R core team, 2018) that uses QUADPACK for numerical integration (Piessens et al., 1983).

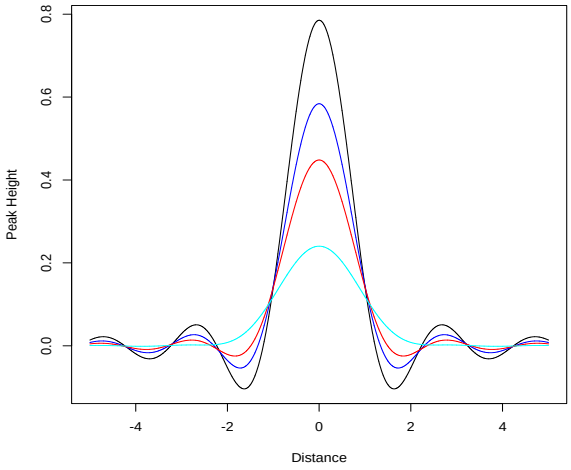

Fig. 5. Point source with blur in 2D, $s_{nom} = 0.5$Å^{-1}. Black line corresponds to B = 0.001, for blue line B = 10, for red line B=20 and for cyan line B=50.

The figure 5 illustrates that for a given resolution the observed peaks are broadened as blurring increases.

Again, as in one-dimensional case, let us consider the blurred image with two point sources and with the observations within the circle $|s| < s_{nom}$. We assume that the distance between these point sources is *z*. Now we can plot the following function:

$$f_B(2\pi x s_{nom}) + f_B(2\pi(x-z)s_{nom})$$

to see how peaks widen and become unsolvable as blurring parameter increases (figure 6).

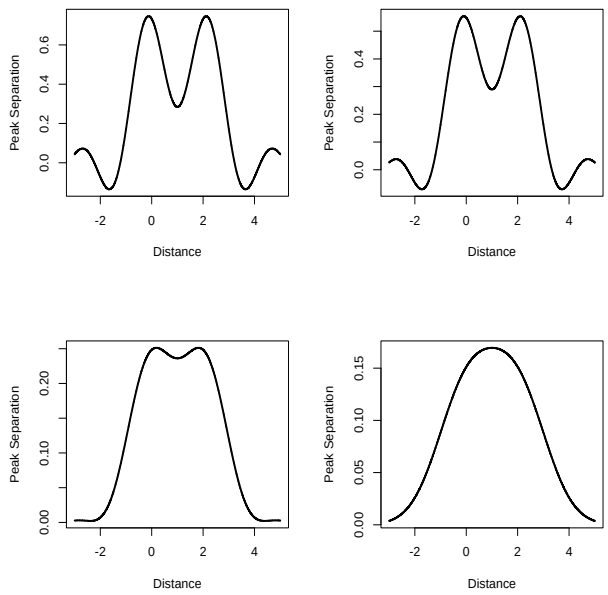

Fig. 6. The graph of two point sources in two dimensions with resolution $s_{nom} = 0.5Å^{-1}$ and distance between sources $d = 2.0Å$ for different blurring parameters. Top left: B=0.01Å^{-2}, top right: B=10Å^{-2}, bottom left B=50Å^{-2}, bottom right B=100Å^{-2}.

The Figure 6 illustrates again that in two dimensions also as blurring parameter – B increases peaks become less and less resolvable.

4. Peak widening and resolvability in 3D

Now let us consider three-dimensional case with point sources. Peaks for which Fourier coefficients observed within a nominal resolution will have the form:

$$f_0(x) = \int_{|s|<s_{nom}} e^{2\pi i x s} ds = 4\pi \frac{-2\pi|x|s_{nom}\cos(2\pi|x|s_{nom}) + \sin(2\pi|x|s_{nom})}{(2\pi|x|)^3} = \frac{4\pi s_{nom}^3 j_1(2\pi|x|s_{nom})}{2\pi s_{nom} x}.$$

where j_1 is the spherical Bessel function of first order. All other notations are the same as defined above.

In this case, the solution of equation (4) gives: $x_{res} = \frac{0.8322}{s_{nom}}$. It is the maximum attainable resolvability in three dimensions in the absence of blurring. We will consider blurring with various parameters, although in this case the results will be qualitatively similar to one- and two-dimensional cases. Indeed, it can be seen in figure 7 and 8.

We next consider the case when the density is blurred with a Gaussian blurring function with the parameter B. To add the effect of blurring we again need to calculate the integral:

$$f_B(x) = \int_{|s|<s_{nom}} e^{-\frac{B|s|^2}{4}} e^{(2\pi i x s) ds} = \left(\frac{8\pi}{B}\right)^{\frac{3}{2}} e^{-\frac{(2\pi|x|)^2}{B}} - e^{-\frac{Bs_{nom}^2}{4}} \left(\frac{4\sin 2\pi|x|s_{nom}}{|x|B} + \right.$$

$$\left. + \left(\frac{8\pi}{B}\right)^{\frac{3}{2}} Re\left(e^{i2\pi|x|s_{nom}} w\left(\frac{2\pi|x|}{\sqrt{B}} + i\frac{\sqrt{B}s_{nom}}{2}\right)\right)\right)$$

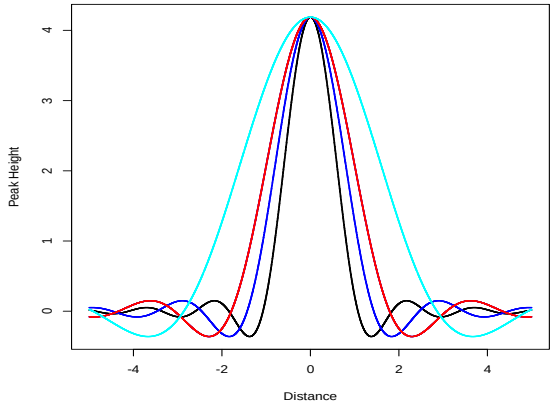

Fig. 7. Peak broadening in the case of no blurring corresponding to different nominal resolution. These graph shows peaks are broadened as s_{nom} decreases. Black line corresponds to $s_{nom} = 0.75$, blue line s_{nom} =0.5, reac line $s_{nom} = 0.4$ and cyan line $s_{nom} = 0.25$.

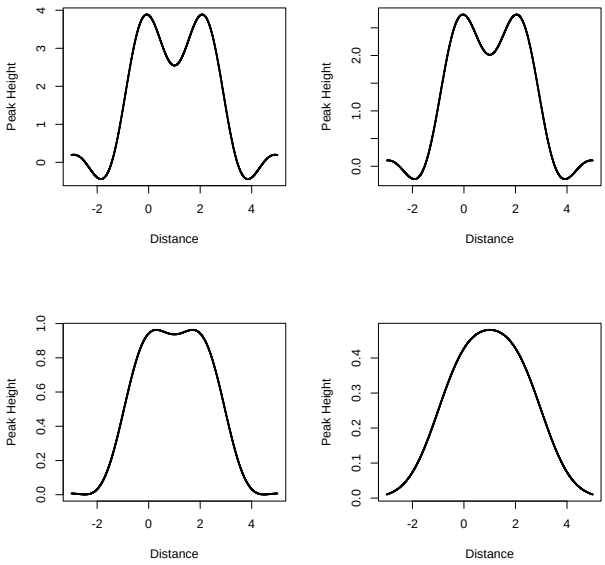

Fig. 8. Sum of two peaks for three-dimensional case with Gaussian blurring. Top left corresponds to B=0.001Å^{-2}, top right corresponds to B=10Å^{-2}, bottom left corresponds to B =50Å^{-2} and bottom right corresponds to B=100Å^{-2}

All terms and variables are as defined before. The first term on the right side of this equation is the peak if there is no series termination and the second terms accounts for the series termination.

Again, we need to plug in this function into the equation (4) and solve it. As expected as B values increase the solution of this equation gives larger and larger distances meaning that when amplitude of blurring increases the resolvability of peaks decreases.

Again, the figure 8 shows that as blurring amplitude increases peak separability and therefore resolvability decreases. Detailed analyses of cases with noise and anisotropic mobility will be the subject of future study.

Conclusion and Future Perspectives

In this work, we presented an approach to the problem of resolution and resolvability for scattering methods used in macromolecular structural biology. We focused on the cases without noise. We assumed that there are only two shortcomings of the observations: 1) diffraction limit, i.e. observations are made within the nominal resolution $|s| < s_{nom}$; 2) sources for which we are doing observations are oscillating and as a result we observe a blurred version of the object. We considered both cases for one-, two- and three-dimensional cases. We showed that as resolution decreases peaks get broader and thus becoming less resolvable as expected. We also found a closed form relationship between the nominal resolution and peak resolvability for one-, two- and three-dimensional cases. Similar effects are observed when objects are blurred with a Gaussian function – peaks get broader as the amplitude of oscillation increases and they become less resolvable. It has already an implication to structural biology that signal level in different parts of the observed density will be different and will correspond to the amplitude of oscillation of the molecule corresponding to these parts of the density.

Future work will focus on a theoretical treatment of the effect of noise on the peak resolvability. Ultimate purpose of this work, that will be dealt in future works, is to derive an algorithm to calculate position and orientation dependent resolvability in the density corresponding to noisy data with anisotropic signal strengths. The planned work will answer to one of the long-standing questions in structural biology: what are the details that can be observed in the map if we do know the nominal resolution, the noise level, relative and absolute amplitudes of mobility for different parts of the calculated (observed) maps. The result of this work will help the unification of resolvability used in different scattering methods. However, we would like to stress that our main concern is macromolecular crystallography and single particle cryo-electron microscopy.

ACKNOWLEDGEMENTS

We would like to thank Laboratory of Computational Structural Biology, Institute of Molecular Biology and Biotechnologies of ANAS. Part of this work was supported by Presidium of Azerbaijan National Academy of Sciences grant of decree № 5/9 dated on 15.03.2017. GNM also thanks **MRC grant MC_US_A025_0104**. We would also like to thank to Prof. Irada Huseynova for her support.

REFERENCES

Berman H.M., Battistuz T., Bhat T.N. et al (2002) The Protein Data Bank. *Acta Crystallogr.*, **D58**: 899-907.

Rupp B. (2010) Biomolecular crystallography: principles, practice and applications to structural biology. Abingdon, New York: Garland Science, Taylor & Francis Group, Pp. 808.

Emsley P., Cowtan K.D. (2004) Coot: model-building tools for molecular graphics. *Acta Crystallogr. D,* **60:** 2126-2132.

Harker D., Kasper J.S. (1948) Phases of fourier coefficients directly from crystal diffraction data, *Acta Cryst.*, **1:** 70.

Frank, J (2005) Three-dimensional electron microscopy of macromolecular assemblies: visualization of biological molecules in their Native state. New York, Oxford University Press.

Murshudov G.N. (2016) Refinement of atomic models against cryoEM maps. *Methods in Enzymology*, **579:** 277-305.

Piessens R., de Doncker-Kapenga E., Uberhuber C., Kahaner D. (1983) Quadpack: a Subroutine Package for Automatic Integration. Springer Verlag.

Poppe G.P.M., Wijers C.M.J. (1990) More efficient computation of the complex error function. *ACM Transactions on Mathematical Software*, **16:** 38-46.

Rosenthal P.B., Henderson R. (2003) Optimal determination of particle orientation, absolute hand, and contrast loss in single-particle electron cryomicroscopy. *J. Mol. Biol.*, **333:** 721-745.

Scheres S.H.W. (2012) RELION: Implementation of a Bayesian approach to cryo-EM structure determination. *Journal of Structural Biology*, **180(3):** 519-530.

R Core Team (2018) R: A Language and Environment for Statistical Computing. R Foundation for Statistical Computing, Viena, Austria.

Vega L.R., Rey H. (2012) A Rapid Introduction to Adaptive Filtering, 7 Springer Briefs in Electrical and Computer Engineering.

Wlodawer A., Li M., Dauter Z. (2017) High-resolution cryo-EM maps and models: A crystallographer's perspective. *Structure*, **25:** 1587-1597.

Bir-, iki və üçölçülü fəzalarda ayırdetmə və ayırdetmə qabiliyyəti

G.M. Qasımova[1,2], R. Ç. Məsməliyeva[1], Q. N. Mürşüdov[1,3]

[1] AMEA Molekulyar Biologiya və Biotexnologiyalar İnstitutu
[2]Azərbaycan Dövlət Neft və Sənayə Universiteti
[3] TTM Molekulyar Biologiya Laboratoriyası, Kembric, Böyük Britaniya

Bu məqalə difraksiya məhdudluğu və bulanıqlıq mövcud olan hallarda səpilmə eksperimental metodlarının (məsələn, kristal diffraksiyası, elektron mikroskopiyası) ayırdetmə və ayırdetmə qabiliyyəti probleminə bir yanaşmaya həsr olunur. Birölçülü, ikiölçülü və üçölçülü halların hər biri ayrı-ayrılıqda nəzəri analiz edilmişdir. Nominal ayırdetmə bulanıqlıqdan asılı olan zirvə ayırdetmə qabiliyyətinin ifadələri alınmış və tədbiq olunmuşdurlar. Biz difraksiya məhdudluğu və bulanıqlıq böyüdükcə nöqtə mənbələrinin bir-birindən ayrı görünməsinin çətinləşdiyini göstərdik.

Açar sözlər: *Saflaşdırılma, elektron kriomikroskopiyası, Furye qabığının korrelyasiyası, Furye çevirməsi, Qauss paylanması*

Разрешение и разрешимость в одном, двух и трех измерениях

Г.М. Гасымова[1,2], Р.Дж. Масмалиева[1], Г.Н. Муршудов[1,3]

[1] Институт молекулярной биологии и биотехнологий НАН Азербайджана
[2] Азербайджанский государственный нефтяной и промышленный университет
[3]MRC Лаборатория молекулярной биологии, Кембридж, Великобритания

В этой статье описывается подход к проблеме разрешения и разрешимости в методах рассеяния (например, дифракция рентгеновских лучей, электронная микроскопия) при наличии разрыва ряда Фурье и размытия. Одно-, двух- и трехмерные случаи рассматриваются отдельно. Получены и проанализированы формулы, связывающие эффекты номинального разрешения и размытия с максимальной разрешающей способностью. Мы показываем, что как размытие, так и разрыв ряда Фурье расширяют пики точечного источника, тем самым снижают их разрешающую способность.

Ключевые слова: *Уточнение, электронная крио-микроскопия, корреляция оболочек Фурье, преобразование Фурье, распределение Гаусса*

Journal of Life Sciences & Biomedicine, vol. 1(74), No 1, p. 37-46 (2019)

Study of genomic variation in bread wheat collection based on next generation sequencing data

Z.İ. Akparov, M.A. Abbasov*

*Genetic Resources Institute, Azerbaijan National Academy of Sciences, 155 Azadlig ave., Baku AZ 1106, Azerbaijan; *For correspondence:mehraj_genetic@yahoo.com*
Accepted for publication: 18 September 2019

Genotyping by Sequencing (GBS) is a Next Generation Sequencing (NGS) technique widely applied in plant breeding that uses restriction enzymes to reduce the complexity of the genome. In the current study the genomic diversity of 87 local and introduced bread wheat genotypes was evaluated using GBS technology. A total of 411 single-nucleotide polymorphisms (SNPs) were obtained for three genomes. The SNP range within each genome was 15–29, 10–36 and 3–17 for A, B and D genome, respectively. The highest number of SNP markers was recorded on the B (48.8%) and the lowest on the D genome (14%). In total, 70.2% of SNPs were transitions (Ts) and 29.8% transversions (Tv). The largest Delta K value was recorded at K = 2, indicating the existence of 2 groups in the collection. The I group contained 68.5% of the introduced accessions, whereas 82% of local genotypes fell into the II group. The average ancestral contribution of the genotypes in I and II groups were 86.4% and 83.6%, respectively. The results of cluster and PCoA analyses were consistent with the STRUCTURE, indicating a sharp differentiation between local and introduced germplasm. Other factors determining the grouping of samples were traits of botanical varieties and genealogy. The SNP markers, revealed in the current study will be used as a genetic source for genotyping and marker-trait association analyzes. The data can be successfully applied in the development and implementation of new strategies for subsequent genetic analysis and breeding.

Keywords: *Bread wheat, genome, genotyping by sequencing, SNP, transition, transversion*

INTRODUCTION

Bread wheat (*Triticum aestivum* L.) (AABBDD) is one of the most important cereal crops ensuring food security at the global level (Tadesse, 2016). It occupies more than 90% of the total area cultivated with wheat and mainly used for preparing bread and biscuits. The production of wheat has dramatically increased and continues to increase to meet the steadily growing needs of the world population. To make this increase sustainable new genetic sources must be identified and involved into the breeding process. Wheat genetic resources are the main sources in wheat improvement programs. To date, more than 900,000 wheat accessions, including wild relatives, landraces and breeding lines are conserved in different genebanks at the global level. Management of these genetic resources is a big challenge and requires the use of modern strategies, such as genomic tools and techniques (Tadesse, 2016). The whole genome of bread wheat (Chinese Spring [CS42]) was sequenced in 2012 by Brenchley and co-workers with the Roche 454 Next Generation Sequencer (NGS) and 94,000-96,000 genes were identified in its 17 GB genome. The gradual decline in the financial cost of the sequencing technologies has facilitated the use of the NGS and prompted the creation of new genotyping methods, such as genotyping by sequencing (GBS). GBS is the most successful genotyping method applied to plant breeding (Poland and Rife, 2012; Singh et al., 2019). The method is used in a wide range of breeding programs, including genome selection, Genome Wide Association Mapping, and new marker detection (Poland and Rife, 2012; Narum et al., 2013). It is a high-throughput multiplex genotyping technique that uses restriction enzymes

to reduce the complexity of the genome. GBS has a number of advantages to investigate polyploid species such as bread wheat. The wheat genome is composed of 80% repeated sequences, which can be avoided using methylation-sensitive restriction enzymes during GBS. Due to barcoding, GBS allows the genotyping of hundreds of samples at the same time, depending on the platform (Elshire et al., 2011). Genomic data obtained during genotyping by sequencing are equivalent to the information provided by thousands of molecular markers.

Azerbaijan is considered to be one of the major origin countries and has a large biodiversity of wheat and its wild relatives. This biodiversity has been collected for many years, characterized and evaluated by various methods and involved into breeding processes. As a result, hundreds of landraces and new varieties have been created, a large portion of which along with collected and introduced accessions have been conserved at the National Genebank in the Genetic Resources Institute. Despite various molecular techniques were used to study genetic diversity in this germplasm, the application of NGS technologies, which is considered the most modern genomic approach worldwide is very relevant (Abbasov et al., 2018). Thus the main objective of the study is to characterize the allelic and genetic diversity of local and introduced bread wheat genotypes from National Genebank using NGS-based GBS technology.

MATERIALS AND METHODS

Eighty-seven local and introduced bread wheat accessions conserved at the National Genebank of the Genetic Resources Institute of ANAS were used in the study. The list and characteristics of the studied accessions are given in Table 1.

Table 1. The list of used bread wheat genotypes

№	Botanical variety	№	Botanical variety	№	Botanical variety
6847	v. *erythrospermum*	6983	v. *lutescens*	10425	
6920	v. *graecum*	6984	v. *lutescens*	10430	
6926	v. *graecum*	6985	v. *lutescens*	20125	
6927	v. *graecum*	6987	v. *lutescens*	20783	
6936	v. *milturum*	6989	v. *lutescens*	20785	
6937	v. *milturum*	6992	v. *lutescens*	21134	
6938	v. *milturum*	7008	v. *albidum*	21139	
6939	v. *milturum*	7010	v. *albidum*	21338	
6941	v. *milturum*	7012	v. *albidum*	21339	
6942	v. *milturum*	7014	v. *albidum*	Akinchi 84	v. *erythrospermum*
6944	v. *erythrospermum*	7016	-	Azametli 95	v. *graecum*
6945	v. *erythrospermum*	7017	-	Azeri	v. *lutescens*
6948	v. *erythrospermum*	7019	v. *barbarossa*	Chinese spring	
6949	v. *erythrospermum*	7020	v. *barbarossa*	Giymetli2/17	v. *velutinum*
6950	v. *erythrospermum*	7021	v. *barbarossa*	Graekum75/50	v. *graecum*
6959	v. *alborubrum*	7023	v. *barbarossa*	Guneshli	v. *erythrospermum*
6960	v. *alborubrum*	7027	v. *hostianum*	Gurgene 1	v. *erythrospermum*
6961	v. *alborubrum*	7028	v. *hostianum*	Jagger	
6962	v. *alborubrum*	7029	v. *hostianum*	Mirbashir 128	v. *erythrospermum*
6963	v. *alborubrum*	7032	v. *meridionale*	Morocco	
6964	v. *ferrugineum*	7033	v. *meridionale*	Girmizigul	v. *erythrospermum*
6965	v. *ferrugineum*	7034	v. *leucospermum*	Gobustan	v. *graecum*
6966	v. *ferrugineum*	7036	v. *velutinum*	Ruzi 84	v. *graecum*
6968	v. *ferrugineum*	10377		Shafaq	v. *lutescens*
6969	v. *ferrugineum*	10378		Sheki1	v. *lutescens*
6970	v. *ferrugineum*	10380		Taraqqi	v. *lutescens*
6971	v. *ferrugineum*	10381		Turkey	
6972	v. *ferrugineum*	10383		Yegane	v. *ferrugineum*
6973	v. *ferrugineum*	10384		Zerdabi	

The DNA from young leaves of each accession was extracted using the CTAB procedure (Doyle and Doyle, 1987). The genomic DNA was co-digested with the restriction enzymes *Pst*I (CTGCAG) and *Msp*I (CCGG) (New England BioLabs, Inc., Ipswich, MA, USA) after which barcoded adapters were ligated using T4 ligase. Samples were pooled by plate into libraries, purified using the QIAquick PCR Purification Kit (Qiagen, Inc., Valencia, CA, USA) and polymerase chain reaction amplified. The PCR products were again cleaned up using the same kit, and size-selected in an E-gel system (Life Technologies, Inc.). Each 95-plex library was sequenced on Illumina HiSeq 2500. Sequence results were analyzed using the UNEAK GBS pipeline, TASSEL 3.0. The obtained single nucleotide polymorphism (SNP) markers were filtered and SNPs with more than 40% missing data and with a minor allele frequency (MAF) less than 10% were excluded from the analysis. Nei genetic distances among individuals and botanical varieties were calculated using PoweMarker V3.25 software (Liu and Muse, 2005). PCoA and cluster analyses based on Nei genetic distances (Nei, 1972) among individuals and botanical varieties were performed using DARwin 6.0 (Perrier and Jacquemoud-Collet, 2006). Population structure analysis was done using ADMIXTURE software.

RESULTS AND DISCUSSION

A total of 411 single-nucleotide polymorphisms (SNPs) were obtained for three genomes (ABD) based on GBS analysis of 87 local and introduced wheat varieties and accessions. The distribution pattern of SNPs over the three genomes differed, with the highest number of markers on the B (48.8%) and the lowest marker number on the D genome (14%) (Figure 1). This could be due to the relatively recent introgression of the D genome.

The distribution pattern of SNP markers across the A, B and D genomes is consistent with previous studies (Akhunov et al., 2010; Marcussen et al., 2014; Shavrukov et al., 2014; Edae et al., 2015). Pour et al. (2017) genotyped 369 Iranian hexaploid wheat accessions using 16506 GBS-derived SNPs and found that most of the SNPs were located on the B genome, while the D genome had the least number of markers. The uneven distribution of genetic variation over the *T. aestivum* genome is associated with reduced genetic recombination due to the self-pollination and genetic mechanisms that prevent the pairing of homoelogical chromosomes during meiosis.

The A/D or B/D SNP ratio in the current study was lower than several other studies (Allen et al., 2011; Cavanagh et al., 2013), indicating that the bread wheat accessions of Azerbaijan have a relatively higher SNP variation on the D genome. The presence of D genome largely determines the high baking properties of bread wheat. The high diversity found on the D genome ensures that the collection can be used as a source of new, desirable alleles for traits of agronomic importance, including high baking quality (Jia et al., 2013).

Figure 1. Number of SNP markers mapped on the hexaploid wheat genome.

The number of SNPs on each chromosome varied widely (3-36), with a maximum number on chromosome 5B and minimum on chromosome 5D. The SNP range within each genome was 15–29, 10–36 and 3–17 for A, B and D genome, respectively. Within each genome the least number of SNPs was observed on the homoeologous group 4. Chromosomes of homoeologous group 4 are relatively conservative, with some significant genes located there; for example, one recessive gene responsible for male sterility is located on the short arm of the chromosome 4B (Barlow and Driscoll, 1981). Therefore, any large variation or mutation that occurs on these chromosomes can cause the death of plants. In addition, homoeologous group 4 has a lower number of genes than the remaining homoeologous groups. Since recombination occurs primarily in genes, the low number of genes on this group may also lead to a low frequency of crossover and subsequently to the decrease of polymorphism and variation (Dvorak and McGuire, 1981).

In total, 70.2% of SNPs were transitions (Ts) and 29.8% transversions (Tv). The majority of SNPs were A→G and C→T transitions, with only 3 transitions in the reverse direction detected on the A genome. The highest number of transition-type SNPs was identified on the B (134 SNPs), while the lowest was on the D genome (42 SNPs). Transversion-type substitutions were in 5 directions (C/G, A/C, G/T, A/T and T/A); the only T/A transversion was detected on the B genome. A Ts/Tv ratio over the three genomes of hexaploid wheat was 2.36.

The most common mechanism of transition is the mutation of methylcytosine to uracil and its subsequent replacement with thymine. Genome-wide methylation is considered to be the direct result of polyploidy (Charmet, 2011). The high number of transitions observed on A and B genomes may be due to the two rounds of polyploidy and methylation events during the evolution of the hexaploid wheat (Buckler and Holtsford, 1996).

After filtration 313 SNP markers were used to evaluate the genetic diversity and population structure of bread wheat collection. Genetic diversity index (GDI) and the polymorphism information content (PIC) for 87 genotypes varied between 0.245-0.50 and 0.215-0.375; the average for the collection was 0.422 and 0.331, respectively. For the vast majority of SNP data, GDI is characterized by high values, and for 42% of SNPs maximum value was recorded. A similar tendency was also observed for the PIC value, indicating the presence of rich genome diversity in the collection, the majority (78.2%) of which comprised of Azerbaijani varieties and accessions.

Dvorak et al. (2006) suggested that compared to other places, *T. aestivum* in East Asia represents more original genepool than anywhere else. The spread of this genepool to eastern Turkey through the South Caucasus or south-west coast of the Caspian Sea, caused to the sympatry of the specie with wild emmer, the gene flow from wild emmer to *T. aestivum* and lead to the increase of the genetic variation and to changes in the geographic form of genetic diversity in *T. aestivum*.

The highest polymorphism among the bread wheat botanical varieties was recorded in var. *ferrugineum*, while the least polymorphism was in var. *hostianum* (Table 2). In general, the PIC value depended on the number of samples per botanical varieties.

Table 2. PIC values in bread wheat botanical varieites

Botanical varieties	Sample size	PIC
var. *albidum*	4	0.175
var. *alborubrum*	5	0.203
var. *barbarossa*	4	0.190
var. *erythrospermum*	12	0.276
var. *ferrugineum*	10	0.283
var. *graecum*	7	0.217
var. *hostianum*	3	0.075
var. *lutescens*	10	0.243
var. *meridionale*	2	0.163
var. *milturum*	6	0.245
var. *velutinum*	2	0.111

The delta K value was used to identify subpopulations in a bread wheat collection. The largest Delta K was recorded at K = 2, indicating the existence of 2 groups in the collection (Figure 2). The I group called “Introduction Group” consisted of 25 accessions (red stripe), 13 of which were samples from different countries and 12 were local genotypes. In total, 68.5% of the introduced accessions and only 2 out of 20 varieties (Chinese spring and Morocco) were included in this group. The average ancestral contribution of the genotypes was 86.4%. Of the 25 accessions, five, including Morocco variety had a high proportion of admixture.

The second group (Local Group) contained the remaining 62 accessions (green stripe), including 6 introduced genotypes and 18 varieties. The average ancestral contribution of the samples was 83.6%. Genetic diversity within the Local group (GDI=0.385; PIC=0.305) was higher than the Introduced group (GDI=0.336; PIC=0.268).

The genetic relationship among bread wheat accessions was further studied based on the cluster (Figure 3) and PCoA analyses (Figure 4). Among the samples, the Nei Genetic Distance Index (GD) index varied between 0.0-1.0 and averaged 0.57. Based on the SNP data, 100% similarity was observed between groups of genotypes, while the most genetically remote genotypes were 6926 and 20125. The average genetic distance between varieties and genebank accessions was 0.047. This indicates that there is no sharp differentiation between the two groups. The highest similarity among the varieties was recorded between the Azamatli 95 and Gobustan (GD=0.27), and the least between Mirbashir 128 and the Morocco variety (GD=0.776).

In a dendrogram developed by cluster analysis, bread wheat accessions were grouped into 3 clusters. In general, the results of the cluster analysis were consistent with the STRUCTURE analysis. Thus, the first cluster consists of 27 accessions and resembles the "Introduction group". Similarly, 13 of the 19 introduced accessions, including the Chinese spring and Morocco varieties, were grouped in this cluster. Within the group, the genotypes from the same country (e.g., Iran and Afghanistan) were placed closer.

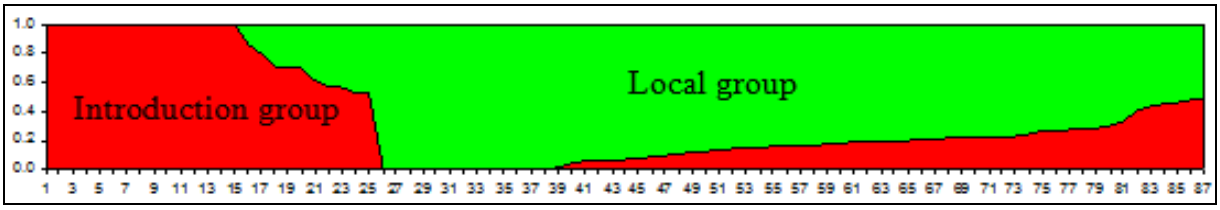

Figure 2. STRUCTURE analysis of bread wheat collection

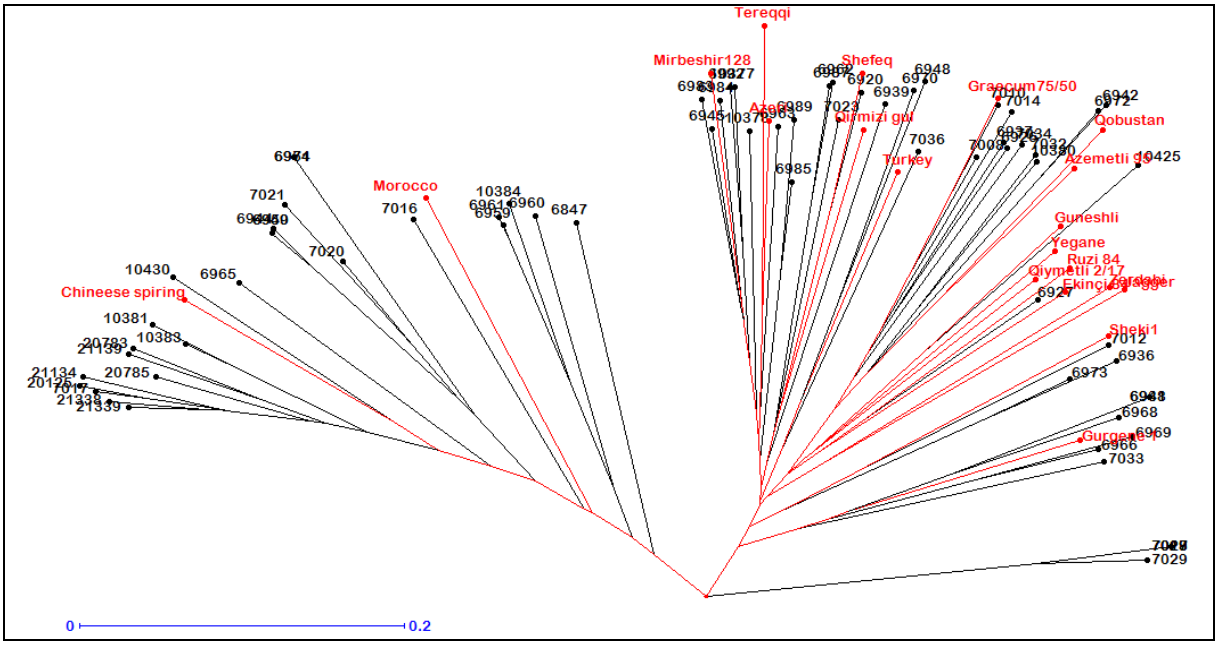

Figure 3. The dendrogram representing the genetic relationship among *T. aestivum* accessions based on GBS-SNP data. The varieties are given in red.

Cluster II consisted of 50 local and only 6 introduced genotypes, as was in "Local group" in Structure analysis. All local (16 varieties) and 2 foreign varieties (Turkey and Jagger) were also included into the cluster.

Finally, the III cluster contained only four genotypes. The genotypes included into the cluster had the highest admixture proportion according to STRUCTURE analysis. Of the four samples, three showed complete similarity.

Several irregularities can be underlined in the grouping pattern of genotypes in the dendrogram.

a) Differentiation of introduced and local accessions. The results of both cluster and Structure analyzes were able to differentiate between local and introduced accessions; with the exception of one accession, the introduced genotypes formed a homogenous subcluster in cluster I. Although 6 introduced accessions were included in another cluster, only two of them were genetically close to the local genotypes.

b) Joint grouping of genotypes of the same botanical varieties. There was a tendency of close grouping for most of the botanical varieties involved in the study. Thus, all 3 var. *hostianum* accessions were tightly grouped in cluster III and 100% similarity was observed between the 2 of them. In addition, 7 out of 10 var. *lutescens* genotypes, 5 out of 6 var. *graecum*, 3 out of 4 var. *alborubrum* and 3 out of 4 var. *albidum* genotypes were located in separate sub-clusters of clusters II and III. The joint grouping was also noted for var. *barbadosa*, var. *milturum* and other botanical varieties. Similar analyses have not been conducted since the botanical variety of introduced genotypes was unknown. The taxonomy on botanical variety had a significant impact on the overall view of the dendrogram.

c) Joint grouping of varieties. Twenty varieties, including 16 local ones were used in the current study, of which 18 were grouped in cluster II (group II) as a result of both analyzes. Although 1 of the 2 introduced varieties (Jagger) was grouped together with the local Zardabi variety, the genetic distance between them was quite high (0.42). The fact that the majority of varieties fell into the same cluster indicates the presence of common or shared alleles among them. The main priority in creating new varieties in local breeding programs was to obtain high-yielding and shorter (dwarf or semi-dwarf) varieties. Most of the studied accessions had short or medium (74-110 cm) height. It seems that the use of similar breeding programs and genetic resources has ultimately led to the creation of a genepool of local varieties with a common genetic background. However, no homogeneity was observed in the distribution of the species within the cluster, and they were placed in combination with genebank accessions.

d) Relationship between the grouping of varieties and genealogy. Some varieties with shared genealogy tended to group together. For example, the 3 species (Azeri, Taraggi and Mirbashir 128) were located in a separate subcluster of Cluster II, and the genetic distance index between the varieties varied from 0.3-0.36. Azeri and Taraggi varieties had common parent Panonia-45319, while Bezostaya-1 was used as a parent for the Azeri and Mirbashir 128 varieties. In addition, the Azamatli 95 and Gobustan varieties were obtained by individual selection from the ICARDA/CIMMYT genotypes.

There was no link between the grouping of the local samples and the geographical region. It can be assumed that the accessions were not grown for a long period in the regions from where they were collected, and the genepool here was formed as a result of the sowing and multiplication of seeds from certain sources by local people, as well as a result of seed exchange among neighboring regions. Therefore, the lack of the relationship between the genetic structure and the geographic region is expected. It should be reiterated that the samples introduced from the same country were found to be closer to each other genetically, indicating the use of similar and common genetic resources within those countries as well.

The distribution pattern of the bread wheat genotypes on the scatter plot was investigated by PCoA analysis, where the first three coordinates explained 25.7% of the SNP variation.

As shown in the figure, the grouping of the samples was in agreement with the previous analyzes. Varieties were located in the left and the introduced accessions in the lower right quadrant of the plot.

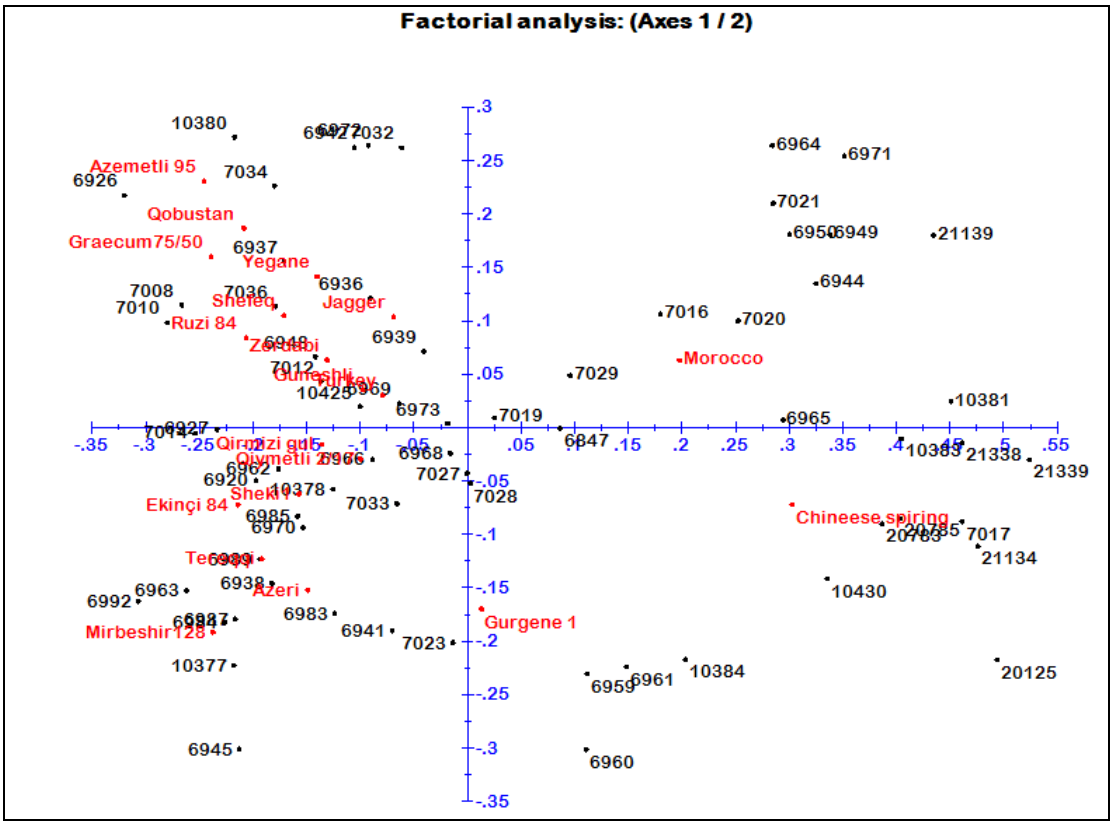

Figure 4. PCoA analysis of 87 bread wheat accessions.

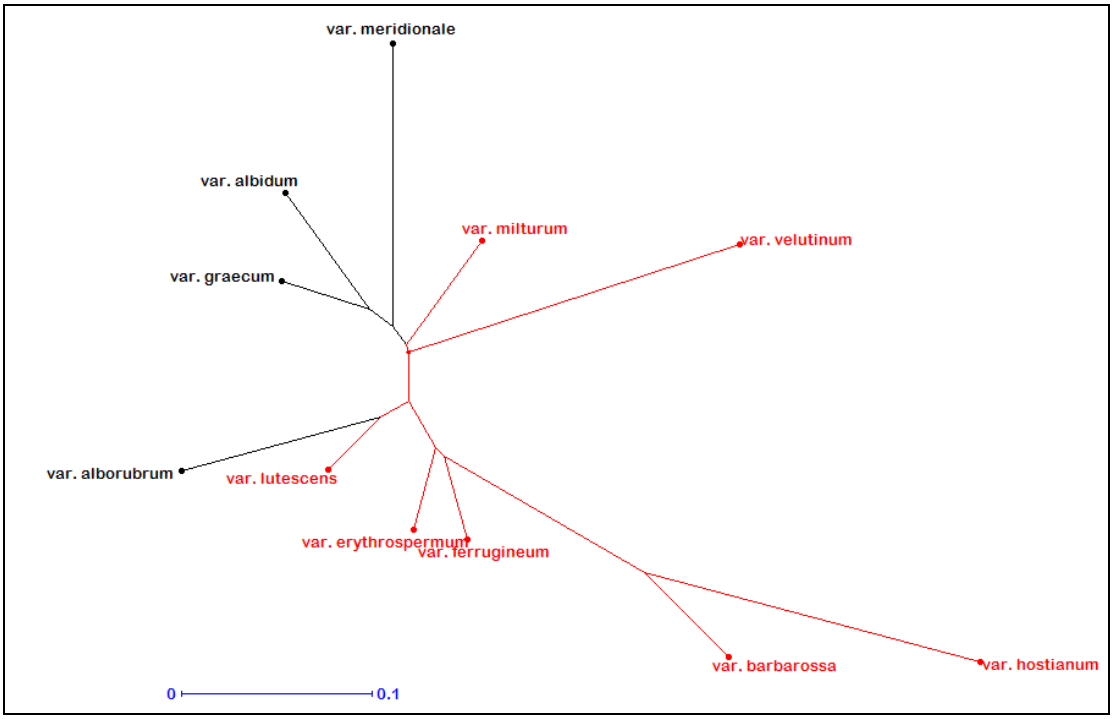

Figure 5. Dendrogram, based on SNP data, reflecting genetic relationship between bread wheat botanical varieties. The botanical varieties with red seeds is shown in red.

The Nei genetic distance index between botanical varieties varied from 0.11-0.68, with an average of 0.29. Var. *velutinum* and var. *hostianum* were the genetically most remote, while var. *ferrugineum* and var. *erythrospermum* have been found to be the closest.

Three clusters were found in the dendrogram representing the genetic relationship between botanical varieties. Var. *velutinum* formed an independent cluster (Figure 5). Unlike the others, the mentioned variety had hairy and white spikes without awns and red seeds.

Of the 6 botanical varieties in cluster II, 5 were red, whereas 3 of the 4 botanical varieties in cluster III had white seeds, suggesting that the seed color had a significant effect on the grouping of botanical varieties.

Summarizing the results of Cluster, STRUCTURE, and PCoA analyses, the use of seed material from the same sources in different geographical regions across the Republic for many years on one hand has resulted in their joint grouping with similar genetic background and, on the other hand, in differentiation from other introduced sources. Other factors determining the grouping of samples were traits of botanical varieties and genealogy. The lack of sharp differentiation between varieties and genebank accessions suggests that local populations are actively used in the breeding process.

So, based on SNP data, a large genomic variation was found among local and introduced bread wheat accessions. Wheat improvement programs are based on the use of molecular markers that significantly increase selective efficiency and allow the accurate transfer of genes and QTLs between different genetic sources. The SNP markers, revealed in the current study will be used as a genetic source and material for genotyping and marker-trait association analyzes. The data can be successfully applied in the development and implementation of new strategies for subsequent genetic analysis and breeding.

REFERENCES

Akhunov E.D., Akhunova A.R., Anderson O.D., Anderson J.A., Blake N., Clegg M.T., et al. (2010) Nucleotide diversity maps reveal variation in diversity among wheat genomes and chromosomes. *BMC Genomics*, **11:** 702. doi: 10.1186/1471-2164-11-702.

Abbasov M., Akparov Z., Gross T., Babayeva S., Izzatullayeva V., Hajiyev E., Rustamov K., Gross P., Tekin M., Akar T., Chao S. (2018) Genetic relationship of diploid wheat (*Triticum* spp.) species assessed by SSR markers. *Genetic resources and crop evolution*, **65(5):**1441-1453.

Singh N., Wu S., Tiwari V.K., Sehgal S.K., Raupp J., Wilson D., Abbasov M., Gill B.S., Poland J. (2019) Genomic analysis confirms population structure and identifies inter-lineage hybrids in *Aegilops tauschii*. *Frontiers in plant science*, **10:** 9.

Alipour H., Bihamta M.R., Mohammadi V., Peyghambari S.A., Bai G., Zhang G. (2017) Genotyping-by-sequencing (GBS) revealed molecular genetic diversity of Iranian wheat landraces and cultivars. *Frontiers in plant science*, **8:** 1293.

Allen A.M., Barker G.L., Berry S.T., Coghill J.A., Gwilliam R., Kirby S., Robinson P., Brenchley R.C., D'Amore R., McKenzie N., Waite D. (2011) Transcript-specific, single-nucleotide polymorphism discovery and linkage analysis in hexaploid bread wheat (*Triticum aestivum* L.). *Plant biotechnology journal*, **9(9):** 1086-1099.

Barlow K.K., Driscoll C.J. (1981) Linkage studies involving two chromosomal male-sterility mutants in hexaploid wheat. *Genetics*, **98(4):** 791-799.

Brenchley R., Spannagl M., Pfeifer M., Barker G.L., D'Amore R., Allen A.M., McKenzie N., Kramer M., Kerhornou A., Bolser D., Kay S. (2012) Analysis of the bread wheat genome using whole-genome shotgun sequencing. *Nature*, **491(7426):** 705.

Buckler E.S., Holtsford T.P. (1996) Zea ribosomal repeat evolution and substitution patterns. *Molecular Biology and Evolution*, **13(4):** 623-632.

Cavanagh C.R., Chao S., Wang S., Huang B.E., Stephen S., Kiani S., Forrest K., Saintenac C., Brown-Guedira G.L., Akhunova A., See D. (2013) Genome-wide comparative diversity uncovers multiple targets of selection for improvement in hexaploid wheat landraces and cultivars. *Proceedings of the national academy of sciences*, **110(20):** 8057-8062.

Charmet G. (2011) Wheat domestication: lessons for the future. *Comptes rendus biologies*, **334(3):** 212-220.

Doyle J.J., Doyle J.L. (1987) A rapid DNA isolation procedure from small quantities of fresh leaf tissues. *Phytochem Bull.,* **19:** 11–15.

Dvorak J., Akhunov E.D., Akhunov A.R., Deal K.R., Luo M.C. (2006) Molecular characterization of a diagnostic DNA marker for domesticated tetraploid wheat provides evidence for gene flow from wild tetraploid wheat to hexaploid wheat. *Molecular biology and evolution*, **23(7):** 1386-1396.

Dvořák J., McGuire P.E. (1981) Nonstructural chromosome differentiation among wheat cultivars, with special reference to differentiation of chromosomes in related species. *Genetics*, **97(2):** 391-414.

Edae E.A., Bowden R.L., Poland J. (2015) Application of population sequencing (POPSEQ) for ordering and imputing genotyping-by-sequencing markers in hexaploid wheat. *G3: Genes, Genomes, Genetics*, **5(12):** 2547-2553.

Elshire R.J., Glaubitz J.C., Sun Q., Poland J.A., Kawamoto K., Buckler E.S., Mitchell S.E. (2011) A robust, simple genotyping-by-sequencing (GBS) approach for high diversity species. *PloS one*, **6(5):** p.e19379.

Jia J., Zhao S., Kong X., Li Y., Zhao G., He W., Appels R., Pfeifer M., Tao Y., Zhang X., Jing R. (2013) *Aegilops tauschii* draft genome sequence reveals a gene repertoire for wheat adaptation. *Nature*, **496 (7443):** 91.

Liu K., Muse S.V. (2005) PowerMarker: Integrated analysis enviornment for genetic marker data. *Bioinformatics*, **21:** 2128–2129.

Marcussen T., Sandve S.R., Heier L., Spannagl M., Pfeifer M. (2014) International Wheat Genome Sequencing Consortium Ancient hybridizations among the ancestral genomes of bread wheat. *Science*, **345:** 1250092. doi: 10.1126/science.1250092.

Narum S.R., Buerkle C.A., Davey J.W., Miller M.R., Hohenlohe P.A. (2013) Genotyping-by-sequencing in ecological and conservation genomics. *Molecular ecology*, **22(11):** 2841-2847.

Perrier X., Jacquemoud-Collet J.P. (2006) DARwin software: Dissimilarity analysis and representation for windows. *Website http://darwin. cirad. fr/darwin*.

Poland J.A., Rife T.W. (2012) Genotyping-by-sequencing for plant breeding and genetics. *Plant Genome*, **5:** 92–102. doi: 10.3835/plantgenome2012.05.0005.

Shavrukov Y., Suchecki R., Eliby S., Abugalieva A., Kenebayev S., Langridge P. (2014) Application of next-generation sequencing technology to study genetic diversity and identify unique SNP markers in bread wheat from Kazakhstan. *BMC plant biology*, **14(1):** 258.

Tadesse W., Amri A., Ogbonnaya F.C., Sanchez-Garcia M., Sohail Q., Baum M. (2016) Wheat. Academic Press. In: *Genetic and Genomic Resources for Grain Cereals Improvement*, 81-124.

Yeni Nəsil Sekvensləmə verilənləri əsasında yumşaq buğda kolleksiyasında genom variasiyasının tədqiqi

Z. İ.Əkpərov, M.Ə.Abbasov

AMEA Genetik Ehtiyatlar İnstitutu

Sekvens əsasında genotipləşdirmə (GBS) genom mürəkkəbliyini azaldılması üçün restriksiya fermentlərdən istifadə edən YNS genotipləşdirmə üsulu olub bitki seleksiyasında uğurla tətbiq olunur. Tədqiqat işində yerli və introduksiya olunmuş 87 yumşaq buğda genotiplərinin genom müxtəlifliyi YNS əsaslı GBS texnologiyasından istifadə edərək qiymətləndirilmişdir. Üç genom üçün ümumilikdə 411 tək nukleotid polimorfizm (TNP) markeri əldə edilmişdir. A, B və D genomu üzrə TNP miqdarı müvafiq olaraq 15–29, 10–36 və 3–17 intervalında dəyişmişdir. SNP markerlərinin ən çox sayı B (48,8%), ən az sayı isə D genomunda (14%) qeydə alınmış, SNP-lərin 70.2% -i tranzisiya (Ts), 29.8% -i isə transversiya (Tv) tipli olmuşdur. Delta K-nın ən böyük dəyəri K = 2 səviyyəsində qeydə alınmışdır ki, bu da kolleksiyada 2

fərqli qrupun mövcudluğunu göstərir. I qrup introduksiya edilmiş genotiplərin 68.5%-ini əhatə etmiş, yerli genotiplərin isə 82% -i II qrupda toplanmışdır. I və II qruplardakı genotiplərin orta əcdad qatqısı müvafiq olaraq 86.4% və 83.6% təşkil etmişdir. Klaster və PCoA analizlərinin nəticələri, STRUCTURE analizi ilə uyğunluq təşkil etməklə yerli və introduksiya olunmuş genotiplər arasındakı kəskin bir fərqliliyin mövcudluğunu göstərmişdir. Nümunələrin qruplaşma xarakterinə təsir edən digər amillər növmüxtəlifliyi əlamətləri və geneologiya olmuşdur. Tədqiqat çərçivəsində aşkar olunmuş TNP markerləri genotipləşdirmə və marker-əlamət asosiasiya analizləri üçün genetik mənbə olaraq istifadə ediləcəkdir. Əldə olunmuş verilənlər gələcək genetik analizlərdə və seleksiya üçün yeni strategiyaların hazırlanmasında və həyata keçirilməsində uğurla tətbiq edilə bilər.

Açar sözlər: *Yumşaq buğda, genom, sekvens əsasında genotipləşdirmə, TNP, tranzisiya, transversiya.*

Изучение геномной вариации в коллекции мягкой пшеницы на основе данных секвенирования нового поколения

З. Акпаров, М.А. Аббасов

Институт генетических ресурсов НАН Азербайджана

Генотипирование путем секвенирования (GBS) - это метод секвенирования следующего поколения (NGS), который использует рестрикционные ферменты для снижения сложности генома и успешно применяется при селекции растений. В настоящем исследовании было оценено геномное разнообразие 87 местных и интродуцированных генотипов мягкой пшеницы с использованием технологии GBS. Всего для трех геномов были получены 411 однонуклеотидных полиморфизмов (ОНП). Диапазон ОНП в геноме A, B и D варьировал в пределах 15–29, 10–36 и 3–17 соответственно. Наибольшее количество маркеров ОНП было установлено для генома B (48,8%), наименьшее – для генома D (14%). В целом, 70.2% ОНП оказались транзиционного (Ts), а 29.8% трансверсионного (Tv) типа. Наибольшее значение Delta K было зарегистрировано при K = 2, что указывает на наличие 2 различных групп в коллекции. I группа охватывала 68.5% интродуцированных образцов, тогда как 82% местных генотипов приходилось на II группу. Средний наследственный вклад генотипов в I и II группах составил 86.4% и 83.6% соответственно. Результаты кластерного и PCoA-анализов в соответствии со структурным анализом показали наличие резкой дифференциации между локальной и интродуцированной гермоплазмой. Другими факторами, определяющими характер группировки образцов, были признаки разновидностей и генеалогия. Маркеры ОНП, выявленные в настоящем исследовании, будут использоваться в качестве генетического источника для генотипирования и анализа ассоциаций маркер-признак. Полученные данные могут быть успешно применены при разработке и внедрении новых стратегий для последующих генетических анализов и селекции.

Ключевые слова: *Мягкая пшеница, геном, генотипирование путем секвенирования, ОНП, транзиция, трансверсия.*

Journal of Life Sciences and Biomedicine, vol. 1 (74), No 1, p. 47-52 (2019)

Morphological studies of seeds of some subgenus (subgen. *Trifolium*, subgen.*Galearia*) of *Trifolium* L.

A.M. Asgarov*, K.A. Mammadyarova

*Genetic Resources Institute, Azerbaijan National Academy of Sciences, 155 Azadlig ave., 155, Baku AZ 1106, Azerbaijan; *For correspondence: askerov1@mail.ru*
Accepted for publication: 23 November 2019

For the first time, micromorphological features of seeds of 6 species of clovers (*Trifolium* L.) of the Talysh flora, collected from the Lankaran-Lerik region of the Azerbaijan Republic, belonging to 2 subgroups and 4 sections were studied on an electron microscope (SEM). The shape of the seeds, their size, color, surface structure, the shape of hilum and their sizes are important taxonomic features. The structure of seeds of the studied species refers to 4 types: seeds with granular surfaces; seeds with tuberculate surfaces; seeds, which have a surface with crystal-like ledges. Features of the structure of the spores can be used, when specifying the status of subgenera; and sections, the remaining morphological features - when determining species of the genus of clover.

Keywords: *Talish, clover, seed, micromorphology, taxonomy*

INTRODUCTION

The genus *Trifolium* L. belongs to the legume family (*Fabaceae*) and includes 255 species (Zohary, 1984). Species of the clover are valuable forage, medicinal, green manure, and also honey plants.

In the Caucasus, 59 species of clover species are widespread (Grossheim, 1952), 43 species of them are found in Azerbaijan (Khalilov, 1952). According to the latest data, there are 50 species of genus *Trifolium* L. s.l. in Azerbaijan (Asgarov, 2016; Gurbanov, Mamedyarova, 2018). According to the same authors data, among the 5 large regions of Azerbaijan, the region with the largest number of clover species is Lankaran-Lerik region-37-39 species, or 76% of the clover species of the whole Azerbaijan. Species that are not found in Talysh mainly belong to the subgenus of *Lotoidea* Grantz. They are widespread in the Caucasus in the higher-altitude floristic complexes that are absent in Talysh.

Lankaran-Lerik region includes 4 botanical and geographical regions: Lankaran lowland, mountainous areas of Lankaran, Diabar (Zuvand) and Lankaran Mugan. In these areas, the spread of clover species is irregular. The most common types of clover spread in the mountainous areas of Lankaran (25 species).

In Flora of Azerbaijan (Khalilov, 1954) subgenera and sections were not indicated. Subgenera of *Trifolium* were adopted by E. Bobrov (1987), A. Grossheim (1954), some of which were later adopted as genus (Bobrov 1987; Roskov, 1990; Askerov, 2016).

Species of *Trifolium* L. of the Lankaran-Lerik region belongs to 4 subgenera and 10 sections. The largest number of species belong to the subgenusof *Trifolium* L. s.str.andcontains 27 species.

It should be mentioned that the statuses of a number of species of the Lankaran-Lerik region and Azerbaijan as a whole are contentious. In addition to general morphological research methods, they were specified by karyological, anatomical and other methods. This paper presents the results of a study of this issue by applying the micromorphological method when using the SEM microscope.

MATERIAL AND METHODS

Materials for our research are the seed samples collected by us during the expedition in the Lankaran-Lerik region in 2017-2018. We also used in our work samples of seeds conserved in the Genebank of the Genetic Resources Institute of the National Academy of Sciences of the Repub-

lic of Azerbaijan. Nomenclature changes were specified according to the monograph "The genus *Trifolium*" (Zohary et. al., 1984) and on the work of A.M.Asgarov (Flora of Azerbaijan, 2016), as well as The International Plant Names Index (IPNI).

For the analysis, samples of seeds on 6 species of clover collected from different populations were taken (*T. angustifolium*, *T. pratense*, *T. lappaceum*, *T. repens*, *T. resupinatum*, *T. tumens*). The collected material was placed in special sterile paper bags and, under laboratory conditions; the moisture was removed by applying silica gel.

Under the scanning electron microscope, (2-3) samples of mature seeds from each species were taken; the seeds were placed on previously prepared tables covered with adhesive carbon tape. Seed samples are sprayed with metal for 1-2x minutes on a JEOL JFC1600 ion sprayer unit. Seed samples were studied from the side surface. The surface of the seeds is photographed with a JEOL JSM6610 lv electron microscope at 4000 times magnification. Under the electron microscope, various structures of the seed surface, the length, and width of the hilum (ribbed) were studied.

RESULTS AND DISCUSSION

Species of *Trifolium* L.in the Lankaran-Lerik region belongs to 4 subgenera and 10 sections. The largest number of species belonging to the subgenus *Trifolium* L. s.str. and contains 27 species.

The statuses of a number of clover species of the Lankaran-Lerik region and Azerbaijan as a whole are contentious. In addition to general morphological research methods, they were specified by karyological, anatomical and other methods. This paper presents the results of a study of this issue by applying the micromorphological method when using the SEM microscope.

Taking into account the morphological features of the seeds and their structural data, a detailed description of 6 species of clovers of the Lankaran-Lerik region is given below. During describing the section, were used the works of M.Zohary et D.Heller and E.G. Bobrova (1987).

Sect. *Stenostoma* Gibelli et Belli

The calyx is closed as a slit with callous thickening in the throat. Corolla deciduous, usually whitish-yellow, rarely pink.

From this section, morphologies of spores of a single species, collected during an expedition of 2018, were studied.

***T. angustifolium* L.**

An annual plant, appressed-hairy, the stem is stiffly erect, and sometimes procumbent, branched, 10-30 cm high. Seeds are ellipsoidal, 0.9-2.2 mm, the surface is smooth, brown. The surface structure is tightly granular. The hilum is bean-shaped, long 0.12 mm. 2n = 14, 16 (Table 2, Figure 1).

They spread in Europe, the Mediterranean, in the countries of South-West Asia. In Azerbaijan, it grows mainly in all regions, and in the Lankaran-Lerik region - in the Lankaran lowland and the Lankaran mountain region (Table 1).

Sect.*Trifolium*

One species was studied. Calyxin the throat without a callous thickening, but with a ring of thick hairs, and sometimes with an annular leathery fold. The corolla is deciduous, with different red or pink, rarely whitish shades.

***T. pretense* L.**

A perennial plant, usually hairy, branched stem, plant height is 15-40 cm. The seeds are ellipsoid or ovate, asymmetrical cordiform or reniform, brown, almost smooth surface, 1.7-2.3 x 1.2-1.5 mm, light or dark, yellowish green, have gray-brown and purple. The surface structure is large-granular. The hilum is oblong-spherical, length - 0.08 mm. 2n = 14 (Table 2, Figure 1).

The plants spread in Europe, the Mediterranean and in Asian countries. They are found in all regions of Azerbaijan, including Lankaran-Lerik region.

It is a valuable forage and medicinal plant (Table 1).

***T. lappaceum* L.**

Annual plant. Stems are often prostrate, hairy, 10-40 cm height. Seeds are oval, hard, slightly shiny, dark brown, 1.2-1.4 x 1-1.2 mm. The structure of the surface with tightly semicircular ledges (forms a network). Hilums are oblong-oval, length 0.14 mm. 2n = 16 (Table 2, Figure 2).

They spread in South-Eastern Europe, the Mediterranean, South-Western and Central Asia. It is found in all regions of Azerbaijan, including Talysh (Table 1).

Table 1. Research species, their location and coordinates

Subgenus	Sections	Species	Collection place and coordinates	Date of collection
I. *Trifolium* L. s. str.	1.*Stenostoma*	*T. angustifolium*	Djalilabad region, Zahmedabad village N39^0 14.954' E048^0 27.420' A 508 m	16.05.2017
	2. *Trifolium*	*T. pratense*	Guba region, Geshresh village N41^0 11.333' E48^0 28.754' A 647 m	13.07.2016
		T. lappaceum	Djalilabad region,, Soltankend village N39^0 41.6' E48^0 16.21' A 536 m	15.06.2017
	3.*Lotoidea*	*T. repens*	Lerik region, Divagach village N38^0 40.014' E048^0 21.663' A 1470 m	03.07.2018
II. *Galearia* (C. Presl) Hossain.	4.*Galearia*	*T. resupinatum*	Lerik region, Lyulakaran village N38^0 74.681' E48^0 39.598' A1300 m	19.05.2017
		T. tumens	Djalilabad region, Zahmedabad village N39^0 14.954' E048^0 27.420' A 508 m	16.05.2017

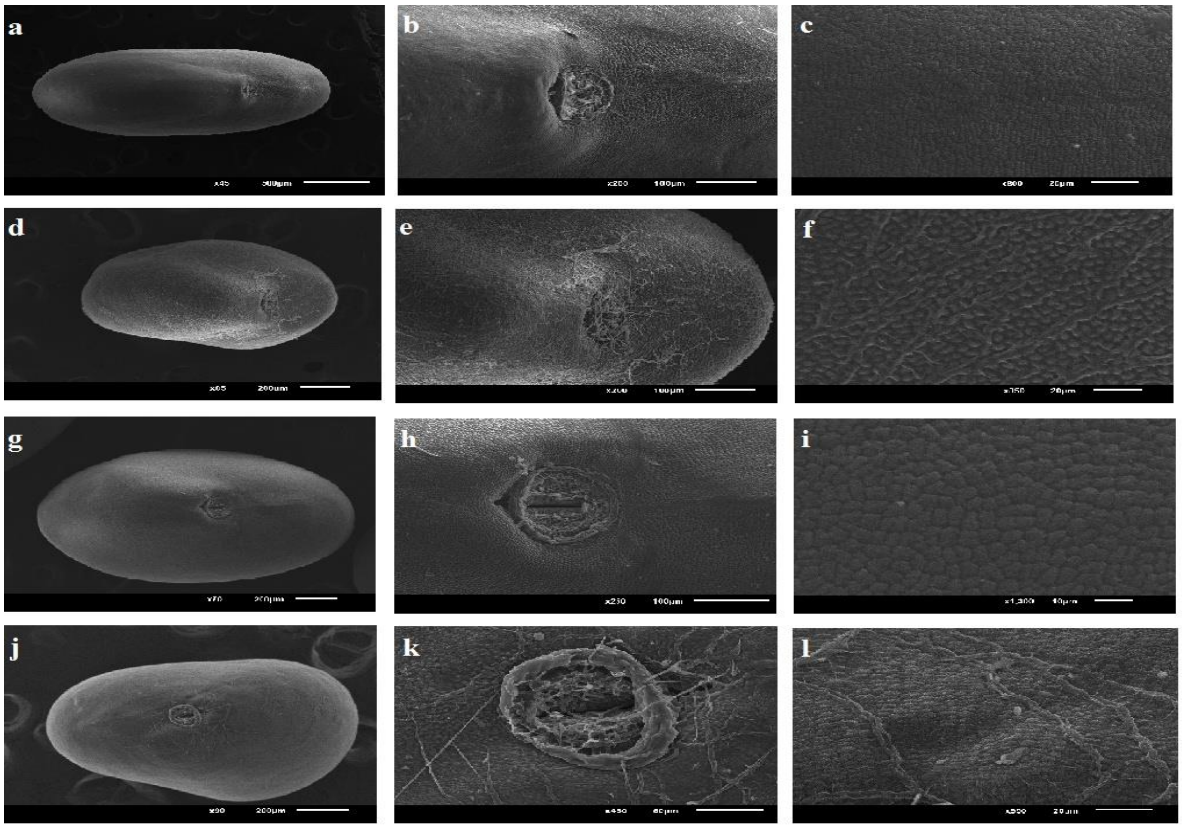

Fig. 1. Shape and structure of seeds under the scan electron microscope (SEM): a – c *T. angustifolium*; d – f *T. repens*; g – I *T. pratense*; j – l *T. tumens.*

Table 2. Seed morphological features

Species	Size(mm) (min-max)	Shape	Color	Surface shape	Surface structure	Hilum forms	Hilum length (mm)
T. angustifolium	0.9-2.2 x 0.7-2.0	ellipsoidal	brown	smooth	tightly granular	bean shaped	0.12
T. repens	1.1-1.5 x 0.9-1.2	cordi or reniform	yellow, yellowish-pink	smooth andshiny	rarely granular	oblong-bean shaped	0.08
T. pratense	1.7-2.3 x 1.2-1.5	ellipsoid or ovate	brown	smooth	large-granular	oblong-spherical	0.08
T. tumens	0.7-1.1 x 0.5-0.9	egg-shaped	white-yellowish	smooth	Densely tuberculate	spherical, indented laterally	0.12
T. resupinatum	1.3-1.8 x 0.9-1.3	ellipsoid or oval	light or dark	smooth	Smooth, semi-annular ledges, forms a network	oval	0.12
T. lappaceum	1.2-1.4 x 1-1.2	oval	dark brown	smooth	tightly semicircular ledges, forms a network	oblong-oval	0.14

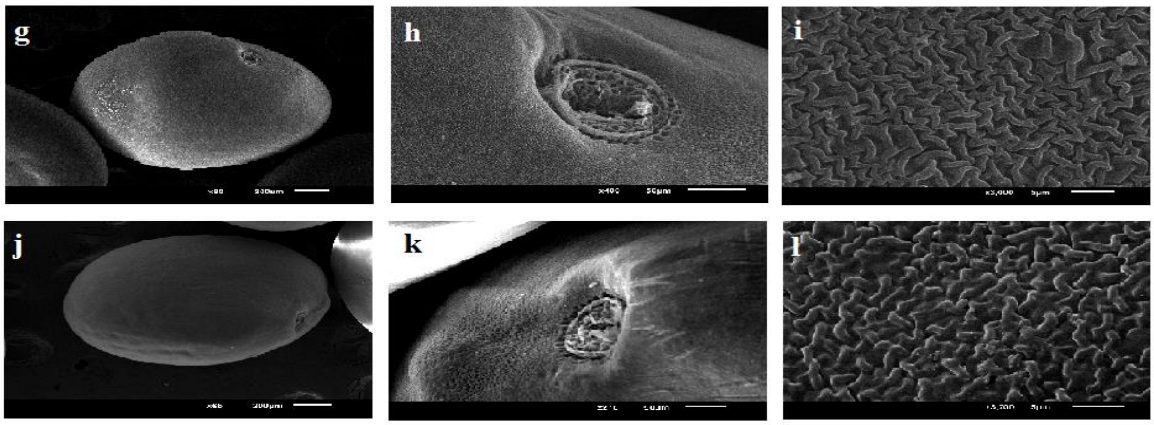

Fig. 2. Shape and structure of seeds under the scan electron microscope (SEM): g – I *T. resupinatum*; j – l *T. lappaceum*.

From this section, the morphology of spores of one species was studied.

Sect. ***Lotoidea*** **Grantz.**

All flowers on peduncle 0.5-3mm long, with well-developed bracts. Calyx with 5 lanceolate or narrow-lanceolate teeth, 2 upper teeth are often longer, not inflated after flowering. The corolla is white,rarely pink or reddish, non-deciduous after flowering.

T. repens **L.**

A perennial plant, creeping stem, plant height is 10-20 cm. The seeds are cords or reniform, 1.1-1.5 x0.9-1.2 mm, the surface is shiny, smooth, immature seeds are yellowish-pink, mature seeds are of light brown. The surface structure is rarely granular. The form of hilum seeds are oblong-bean-shaped, length 0.08 mm. 2n=32 (Table 2, Figure 1).

They spread in Europe, the Mediterranean and in Asian countries. They are found in all regions of Azerbaijan, including Lankaran-Lerik region. It is a valuable pasture and forage plant (Table 1).

Sect. ***Galearia*** **(C. Presl) Godr.**

All blossoms on peduncles up to 1mm long., and located in the axils of the bracts. The calyx is two-lipped; the upper lip is systiform-swelling, membranous during bearing. The corolla is pink, pink-white or reddish, usually deciduous after flowering. From this section, the morphology of two types of spores was studied.

T. resupinatum **L.** - An annual or perennial plant, the stem is branched, bare, plant height is 10 - 40 cm. Seeds ellipsoid or oval, asymmetrical cordiform 1.3-1.8 x 0.9-1.3mm., surface smooth, light or dark, dark yellow or brownish - yellowish, in mature, the seeds are pinkish or blackish.

The structure of the surface with rarely semi-annular ledges (forms a network). The hilum is oval, the length is 0.12 mm. 2n = 16 (Table 2, Figure 2).

Distributed in Asian and Mediterranean countries. It is found in all regions of Azerbaijan, including Talysh. It is a valuable forage plant (Table 1).

***T. tumens* Steven ex M. Bieb.**- A perennial plant, the stem is bare, erect or creeping, height is 10 - 40 cm. Seeds are egg-shaped, 0.7 - 1.1 mm.

The surface is smooth, white-yellowish. The surface structure is densely tuberculate. Hilum is spherical, indented laterally, 0.12 mm long. 2n = 16, 32 (Table 2, Figure 1).

This species spread in South-West Asia (Azerbaijan, Georgia, Armenia, Turkey, and Iran). It grows in all regions of Azerbaijan and Talysh (Table 1).

Thus, researches were conducted on 6 species of clover belonging to 4 sections and 2 subgenus, collected from different populations of the Lankaran-Lerik region.

As a result of the analysis, obtained by us on the study of micromorphological features of seeds, their 3 morphological types were found. The particular focus is paid to the surface features of the seeds and their structural features.

1. Seeds with smooth, covered with dense granules surface. This includes *Trifolium angustifolium*, from section *Stenostoma*; *T. repens*, from section *Lotoidea* and *T. pretense* from section *Trifolium*

2. Seeds whose surface is smooth, densely "tuberculate". This includes *T. tumens* from the *Galearia* section.

3. Seeds with smooth, annular ledges surface. These ledges are tightly annular (forms a network).

This type of seed is characterized by peculiar characteristics and include two types:

T. resupinatum from section *Galearia* and T. *lappaceum* from section *Trifolium.*

According to the micromorphological descriptions of seeds of certain types of clovers, their shapes and sizes (oval, heart-shaped, bud-shaped, etc.), color (brown, yellow, black, etc.), forms and sizes of hilum (bean-shaped, oval, spherical, e) are highly variable and characteristic for the description of species.

And such features of seeds as the shape of their surface, as well as their structural features are valuable in the description of the section and subgenera.

ACKNOWLEDGEMENT

The authors would like to thank the Institute of Geology and Geophysics of ANAS, to Sh. Sh. Bayramova for assisting us to work with the SEM.

REFERENCES

Asgarov A.M (2016) The plant world of Azerbaijan. TEASPRESS, Baku, 444 p.

Bobrov E.G. (1945) *Trifolium* L. In: Flora URSS, **11:** 189-261.

Bobrov E.G. (1947) The species *Trifolium* L. in URSS. In: *Flora et systematica plantae vasculares*. *ACTA Inst. Bot. Acad. Science,* ***ser.* 1, 6:**164-336.

Bobrov E.G. (1987) *Trifolium* L., *Chrysaspis* Desv. In: Flora partis Europaeae URSS, **6:** 195–212.

Bojnansky V., Fargasova A. (2007). Atlas of seeds and fruits of Central and East-European Flora, Springer, 961 p.

Grossheim A.A. (1952) *Trifolium* L. In: Flora Caucasus. vol. 5, p. 194-221.

Gurbanov E.M, Mammadyarova K.A (2018) Taxonomic review of the genus (*Trifolium* L.) in Talish flora. *Proceedings of Azerbaijan NAS (biological and medical sciences)*, **73(1):** 16-28

Khalilov A.K.H. (1954) The genus *Trifolium* L. In: *Flora of Azerbaijan*. Baku, **5:** 272–307

Salimpour F., Mostafavi G., Sharifnia F. (2007) Micromorphologic study of the seed of the genus *Trifolium*, section *Lotoidea*, in Iran. *Pakistan Journal of Biological Sciences*,**10 (3):** 378-382.

Yakovlev G.P. (1991) Legumes of the Earth. *Science*, p. 144

Zohary M. (1970) Genus *Trifolium* L. Flora of Turkey, **3:** 384-448

Zohary M. (1984) Heller D.The genus *Trifolium*.Yerusalem, 606 p.

Zoric L., Merkulov Lj., Lukovic J., Boza P. (2010) Comparative seed morphology of *Trifolium* L. species (*Fabaceae*). *Period Biol.*, **112(3):**26.

Trifolium L. cinsinin bəzi yarımcinslərinə (subgen. *Trifolium,* subgen. *Galearia*) aid növlərin toxumlarının morfoloji öyrənilməsi

A.M. Əsgərov, K.A. Məmmədyarova

AMEA Genetik Ehtiyatlar İnstitutu

Üçyarpaq yonca (*Trifolium* L.) cinsinin 2 yarımcinsinə (subgen. *Trifolium*, subgen. *Galearia*) aid növlərinin toxumlarının mikromorfoloji xüsusiyyətləri skan elektron mikroskopunda tədqiq edilmişdir. Öyrənilən növlərin 3 toxum tipinə aid olması müəyyən edilmişdir. Aşkar edilən konstant əlamətlərdən yarımcins və növlərin təyinində və onların statuslarının dəqiqləşdirilməsində istifadə oluna bilər.

Açar sözlər: *Talış, üçyarpaq yonca, toxum, morfologiya, taksonomiya*

Морфологическое изучение семян некоторых видов из подродов (subgen. *Trifolium,* subgen. *Galearia*) рода *Trifolium* L.

А.М. Аскеров, К.А.Мамедярова

Институт генетических ресурсов НАН Азербайджана

На сканирующем электронном микроскопе исследованы микроморфологические особенности шести видов клевера (*Trifolium* L.), относящихся к двум подродам (subgen. *Trifolium,* subgen. *Galearia*). Установлено, что признаки изученных видов клевера относятся к трем морфологическим типам семян. Обнаруженные константные морфологические признаки семян клевера (*Trifolium* L.) могут быть использованы при определении подродов и видов, а также в уточнении их статусов.

Ключевые слова: *Талыш, клевер, семена, морфология, таксономия*

Journal of Life Sciences and Biomedicine, vol. 1 (74), No 1, p. 53-62 (2019)

Engagement of mechanisms of cellular differentiation in formation of memory traces

A.A. Mekhtiev[1*], Sh.M. Asadova[1], Sh.B. Guseinov[1], G.R. Vagabova[2]

[1]Academician A.Garayev Institute of Physiology, Azerbaijan National Academy of Sciences, 78 Sharifzadeh, Baku AZ1100, Azerbaijan
[2]Azerbaijan State Medical University, 23 A.A.Bakikhanov, Baku AZ1022, Azerbaijan
**For correspondence: arifmekht@yahoo.com*
Accepted for publication: 01 October 2019

The article concerns study of the effect of antibody-mediated blockade of serotonin-modulating anticonsolidation protein (SMAP), being in linear relation with serotonin, on the formation of memory in the rats on the conditioned models of alternative running and 2-lever operant differentiation with food reinforcement, as well as on the level of nerve growth factor (NGF) in the brain structures. In the 1st series of studies in the rats, achieved 80% level of correct trials on the model of alternative running, through ELISA-test the level of SMAP was evaluated in the brain occipital and temporal cortex. Significant downregulation ($p<0.001$) of SMAP in the temporal cortex of the trained rats was noticed. In the 2nd and 3rd series of studies a single intra-cerebral administration of the anti-SMAP antibodies prior to learning sessions brought to much quicker ($p<0.001$) formation of the memory (50% level of correct trials), than in the intact and control (non-immune γ-globulins) animals, as well as to a significantly quicker decrease of latency of the first running towards the platform or lever ($p<0.01$). In the 4th series of studies 24 h later since intra-cerebral administration of anti-SMAP antibodies induced downregulation of NGF in the hippocampus ($p<0.001$) and left parietal cortex ($p<0.001$), whereas 3 days later downregulation of NGF in the left parietal cortex ($p<0.001$) and its upregulation in the hippocampus ($p<0.001$) were noticed. It is proposed that, promoting effects of antibodies-mediated blockade of SMAP on the formation of memory traces are related to its negative regulation of cellular differentiation.

Keywords: *Serotonin-modulating anticonsolidation protein, antibodies, memory, indirect ELISA-test, nerve growth factor, hippocampus, left parietal cortex*

INTRODUCTION

In spite of long-term history of studies of the role for serotonin in the processes of memory, up to now still there is no complete clearness of understanding concerning character of its engagement in these processes, as besides tremendous amount of publications showing promoting effects of serotonin on memory formation (Harvey, 1995; Barrionuevo et al., 2000; Cassel, 2010), there are literature data as well about blocking effects of abundant level of serotonin on these processes (Essman, 1974; Getsova et al., 1980; Vanderwolf, 1989; Santucci et al., 1996). Furthermore, of not less importance is exploration of the mechanism of participation of serotonin in the process of memory consolidation.

Presently the widely accepted is a statement saying that in the basis of memory formation lies advent of novel synaptic connections between neurons involved into the process of remembering. In experimental way this standpoint is supported by the results of ultra-structural investigations revealing increase of a number of dendritic spines in the brain cortex of the trained animals or animals kept under informational-enriched conditions (Leuner, Shorts, 2004).

The studies undertaken by different researchers last years, demonstrate engagement of newly-formed neurons in the brain structures of

the mature organisms (neoneurogenesis) in the formation of memory traces (Sherstnev et al., 2010; Sherstnev et al., 2015).

Earlier conducted studies showed that intracerebral administration of serotonin-modulating anticonsolidation protein (SMAP), identified in the brain cortex and purified from the whole brains of the rats and being in linear relations with serotonin (Mekhtiev, 2000), impairs processes of memory consolidation in the conditioned models with negative and positive reinforcement (Guseinov, Mekhtiev, 2013; Mekhtiev et al., 2015). Besides, formation of these tasks in the rats till reaching 80% of correct trials leads to pronounced downregulation of SMAP in the brain cortex (Mekhtiev et al., 2015).

Proceeding from the mentioned above data, the attempt of clarification of input of molecular mechanisms underlying differentiation of the precursors of nervous cells, into the formation of traces of long-term memory was undertaken. For the purpose of solving of this problem the effects of antibodies-mediated blockade of SMAP activity on the formation of memory traces in the conditioned models of alternative running and 2-lever operant differentiation with food reinforcement as well as on the levels of nerve growth factor (NGF) in the hippocampus and left and right parietal areas of the brain cortex were analyzed.

MATERIALS AND METHODS

Biochemical methods. SMAP was purified from the cow brains. The brains were homogenized in the extracting buffer containing 0.05 M phosphate buffer (pH 7.2), 0.3 M NaCl, 5 mM EDTA and 0.1% Triton X-100 in a volume ratio of tissue and buffer as 1:4. The main stages of fractionations were as follows: 1) partial precipitation by ammonium sulfate under the final concentration 40%, 2) gel-chromatography on the column (3 X 60 cm) of Sephadex G-150. The process of fractionation and selection of the immunopositive fractions was realized under the control of indirect ELISA-test with application of anti-SMAP polyclonal immunoglobulins (Mekhtiev, 2000).

Anti-SMAP polyclonal immunoglobulins were produced through 5-6-month immunization of the male rabbits of Chincilla species by subcutaneous administration of 300 μg of the purified correspondent protein per animal, in a mixture with complete Freund adjuvant (Sigma, Germany).

Measurements of the levels of SMAP and NGF in the brain cortex and hippocampus were carried out by indirect ELISA-test (Antibodies Volume II: Practical Approach) on the polysterene plates with moderate level of adsorption (Sigma, Germany) with application of rabbit polyclonal immunoglobulins to SMAP and NGF (2.5 S; Sigma Immunochemicals, Germany). Owing to involvement of brain cortex in the formation and storage of memory traces, during realization of the ELISA-test total proteins of the occipital cortex (processing and storage of visual information) and parietal (participation in associative learning) cortex of the brain were used. The animals had been anesthetized and sacrificed, and the hippocampus and left and right areas of parietal cortex were removed and frozen under a temperature of -70°C. Prior to the beginning ELISA-test, the water-soluble proteins were extracted from the studied samples. Those proteins were extracted in the extraction buffer (pH 7.3) and their concentrations were brought up to 20 μg/mL with 0.1 M Tris-HCl buffer (pH 8.6). Each sample was repeated three times and on finalization of the reaction the average values of three samples were calculated. The concentrations of the total proteins were measured on Bredford technique with application of 0.01% solution of Coumassi G-250 on the wavelength 595 nm. Immunoglobulins to SMAP and NGF (2.5 S; Sigma Immunochemicals, Germany) were used as the first antibodies, while goat anti-rabbit immuneglobulins with conjugated horseradish peroxidase (Sigma Immunochemicals, Germany) were used as the second antibodies. Visualization of the reaction was realized with application of substrate of horseradish peroxidase – 0.05% orthophenilendiamine in 0.05 M citrate-phosphate buffer (pH 4.5). The reaction was stopped 30 min later from addition of substrate by addition of 3 M solution of NaOH. The results of the reaction were digitalized in the photometer for the ELISA-test "Spectra Max 250" (Molecular Devices Co., USA) on the wavelength 492 nm.

Anti-SMAP polyclonal antibodies were purified from the solution of anti-SMAP immunoglo-

bulins through a technique of immune-affinity chromatography performed on the column (0.5 X 3 cm) of CNBr-Sepharose (Sigma, Germany) with covalently immobilized SMAP (Mekhtiev, Asadova, 2018). After application of anti-SMAP immunoglobulins onto the column, it was thoroughly washed with 20 column volumes of 0.01 M phosphate buffer (pH 7.2) and under the extinction control (method by Bradford) specifically bound anti-SMAP antibodies were eluted by chaotropic agent 3 M KCNS. The eluted antibodies were dialyzed against 0.15 M NaCl, buffered up to the value of pH 7.2, and frozen. In a single cycle, up to 12 mg antibodies were eluted from the affinity column.

Physiological methods. In the 1st series of studies the behavioral experiments were carried out on the 5-6-month-old Wistar male rats on the difficult for acquisition conditioned model of alternative running with food reinforcement (Semyonova, 1976). The experimental box was made from organic glass with dimensions 60 X 60 cm. The platforms of sizes 20 X 10 cm were secured to the left and right corners of the box, at the height of 16 cm from the bottom of the box. The animals were culled into 2 groups: 1) control group (n=13); 2) experimental group (n=12). The animals of the experimental group were put onto the start platform at the entrance of the experimental box and their running and climbing onto the left and right platforms were reinforced by food pellets of mass 200 mg, placed on them and composed of sunflower oil, millet flour, ground corn grains and combined fodder. After animal's running towards the platform and eating the fodder on one side, it was placed again onto the starting platform and its running to the opposite side was reinforced. The pellets were placed onto the platforms at the time, when animal could not see it.

The learning sessions lasted for 7 days, daily, 20 trials each day. The trial was considered as correct, if after returning to the starting platform the next trial was done towards opposite side. Criterion of successful learning was calculated on ratio of a number of correct trials to a total amount of trials during single learning session. The learning was lasted up to reaching 80% of correct trials, the animals were sacrificed, the occipital and parietal areas of the brain cortex were removed and frozen. The animals of the control group as well as the animals of the experimental group were deprived of food and put into the experimental box without learning for a timeframe correspondent to the timeframe of the experimental animals.

In the 2nd series the studies were also carried out on the model of alternative running. In this series of studies the rats were culled into 3 groups: (1) intact group (n=13); (2) control group – rabbit non-immune γ-globulins (n=13); (3) experimental group – rabbit anti-SMAP antibodies (n=12). The animals were anesthetized with natrium etaminali (40 mg per 1 kg of body mass) and administered with 10 μl of preparations at a concentration of 1.5 mg/ml in the saline buffered to pH value of 7.2 into the brain left lateral ventricle. The learning sessions were undertaken 24 h after administration of the preparations till reaching by the animals of 50% criterion of correct trials. In this case, the latencies of the first trials towards the platform and ratio of correct trials to total amount of trials in percent were measured. The animals of the control group as the animals of the experimental group were deprived for food and placed into the experimental box for the time similar to the time of the animals of the experimental group.

In the 3rd series the studies were carried out on the model of 2-level operant differentiation model. The rats were culled into 3 groups: 1) intact group (n=13), 2) control group – rabbit non-immune γ-globulins (n=13) and 3) experimental group – anti-SMAP antibodies (n=12). During the learning sessions the animals were trained to press the right lever of the two levers secured to the back wall of the experimental box close to each other to get food pellet as reinforcement. The animals in this series of studies were administered the preparations the same way and the time interval between injections and beginning of learning sessions were the same as in the 2nd series of studies.

In the 4th series of studies the effect of administration of anti-SMAP antibodies into the brain left lateral ventricle on the levels of NGF in the hippocampus, right and left parietal cortex of the rats was analyzed. The rats were culled into 3 groups: 1) intact group (n=7), 2) control group – rabbit non-immune γ-globulins (n=8) and 3) experimental group – anti-SMAP antibodies (n=7). The animals in this series of studies were administered the preparations the same way and the time inter-

vals between injections and onset of learning sessions were the same as in the 2nd and 3rd series of studies. 24 h or 3 days later the rats were sacrificed, hippocampus, right and left parietal cortex were removed from the brain, water-soluble proteins were extracted and used as antigens in the indirect ELISA-test whose stages are detailed above.

The results of the 2nd, 3rd and 4th series of studies were grouped and analyzed by Student's t-criterion.

RESULTS

In the 1st series of studies after animals' reaching 80% criterion of correct trials in the model of alternative running the following regularities were revealed. In the course of elaboration of the task permanent increase of correct turn-by-turn trials to left and right platforms, climbing onto them and consuming food pellets were observed. In this case in the 1st day of learning sessions in the first 1-2 min later from putting the animals into the box, they stayed mostly in one of the corners demonstrating the mere signs of anxiety in the form of uninterrupted trembling and freezing. 2-3 min later they started to thorough exploration and sniffing of the box, looking for food and in different timeframes the animals climbed onto one of the platforms and consumed the food pellet. On the 2nd day after putting into the box the animals on the first minute again demonstrated the signs of anxiety, but thereafter they quickly passed to thorough exploration of the box. Beginning from the 4th experimental day the animals very quickly entered the box, without delay came up to the platforms and climbed onto them.

In the 1st series of studies evaluation of SMAP levels in the occipital and parietal cortex of the brain revealed significant downregulation (by 25.3%) of SMAP in the parietal cortex of the animals of the experimental group, reached 80% criterion of correct trials on the alternative running model relatively to the rats of the control group ($p<0.001$ on Student's t-criterion; Fig.1). In the occipital cortex no changes of SMAP level in the trained animals in comparison to the control values were noticed (Fig. 1).

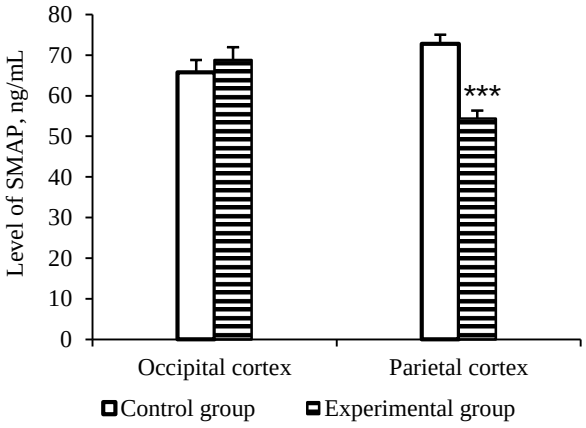

Fig. 1. The levels of SMAP in the occipital and parietal cortex of the rats, reached 80% criterion of correct trials in the alternative running model.
*** - $p<0.001$.

In the 2nd series of studies administration of anti-SMAP antibodies into the brain lateral ventricle of the rats 24 h prior to learning sessions in the conditioned model of alternative running significantly facilitated elaboration of the task. In particular, if the animals of the intact and control groups reached 50% learning criterion on the 7th experimental day, then under the effect of anti-SMAP antibodies the animals of the experimental group reached this criterion on the 4th day ($p<0.001$ on Student's t-criterion; Fig. 2).

Furthermore, though the dynamics of downregulation of the latencies of the first trial towards the platform was observed in the all studied groups, nevertheless in the experimental group this downregulation bore steeper character ($p<0.01$; Student's t-criterion; Fig. 3). So, the obtained data indicate to stimulating effect of anti-SMAP antibodies on memory formation and, correspondently, to negative character of regulation of this process by SMAP.

In the 3rd series of studies administration of anti-SMAP antibodies into the brain lateral ventricle of the rats 24 h prior to learning sessions in the complicated and time-consuming conditioned 2-lever operant differentiation model significantly promoted and strengthened the formation of memory.

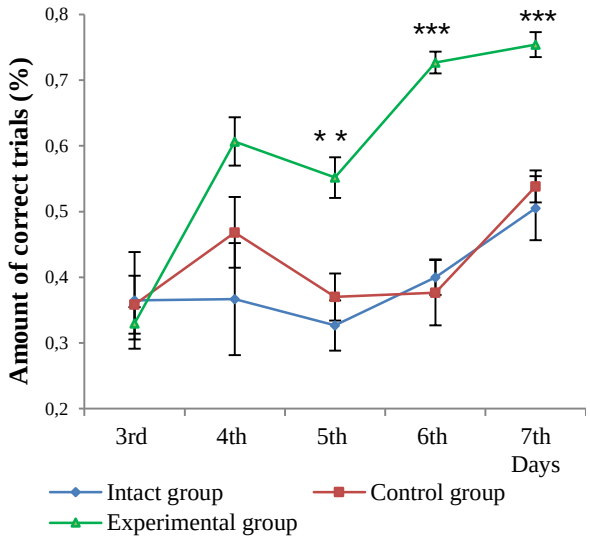

Fig. 2. Effects of anti-SMAP antibodies on the dynamics of memory formation in the alternative running model. ** - p<0.01; *** - p<0.001.

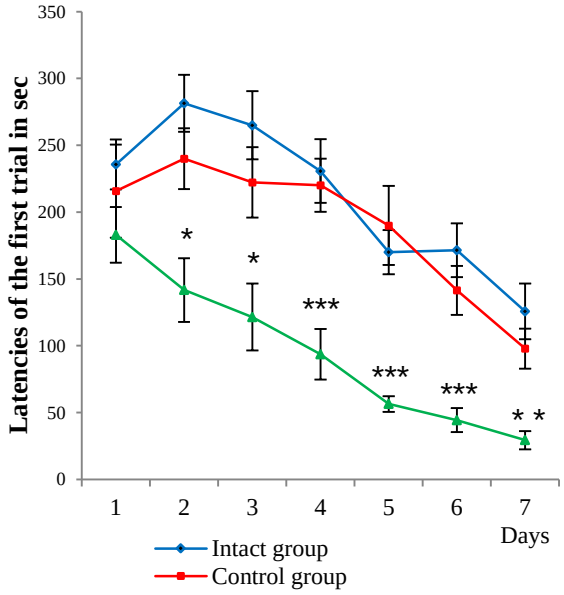

Fig. 3. Effects of anti-SMAP antibodies on the latencies of the first trial in the alternative running model. * - p<0.05; ** - p<0.01; *** - p<0.001.

If the animals of the intact group reached 50% criterion of correct trials on the 7th experimental day and the control animals reached this criterion on the 6th day, then the animals of the experimental group reached the level of 50% correct trials on 4th day (p<0.001; Student's t-criterion; Fig. 4). Besides of a hallmark of the rate of achieving 50% learning criterion, each group had its upper limit of correct trials (plateau), no matter how long the learning sessions lasted. So, the plateau for the animals of the intact group made 50%, the plateau for the control rats – 55%, and the plateau for experimental group – 80% (Fig. 4).

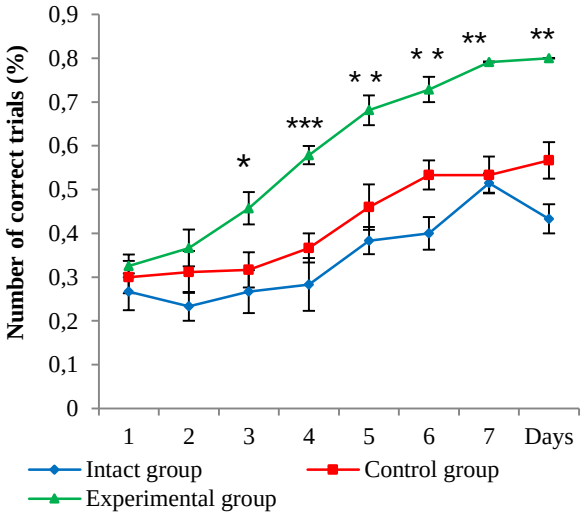

Fig. 4. Effects of anti-SMAP antibodies on the dynamics of memory formation in the model of 2-lever operant differentiation. * - p<0.05; ** - p<0.01; *** - p<0.001.

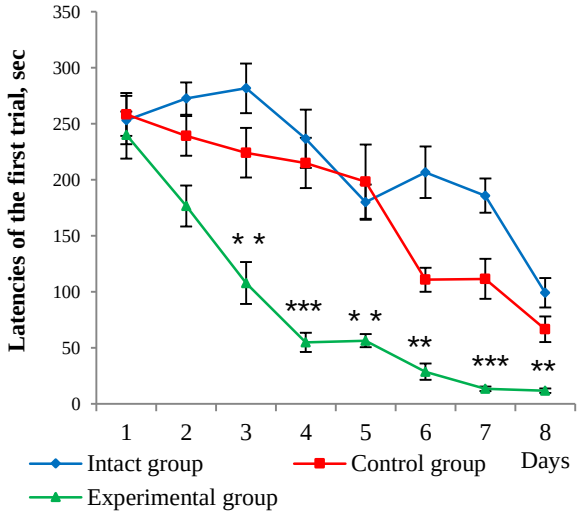

Fig. 5. Effects of anti-SMAP antibodies on the latencies of the first trial in the model of 2-lever operant differentiation. **- p<0.01; *** - p<0.001.

As in the 4th series, the dynamics of downregulation of the latencies of the first trial towards the lever was observed in the all studied groups, however, in the experimental group this downergulation had much steeper character ($p<0.01$; Student's t-criterion; Fig. 5).

In the 4th series of studies the effect of intracerebral administration of anti-SMAP antibodies on the levels of NGF in the hippocampus, brain right and left parietal cortex was evaluated. It was shown that 24 h later since intra-cerebral administration of anti-SMAP antibodies, downregulation of NGF in the hippocampus ($p<0.001$ on Student's t-criterion; Fig. 6) and left parietal cortex ($p<0.001$ on Student's t-criterion; Fig. 6) was revealed, whereas in the right parietal cortex the level of NGF did not change.

At the same time, 3 days later from intra-cerebral administration of anti-SMAP antibodies downregulation of NGF in the left parietal cortex having still been maintained ($p<0.001$ on Student's t-criterion; Fig. 7), although in the hippocampus its significant upregulation was revealed ($p<0.001$ on Student's t-criterion; Fig. 7).

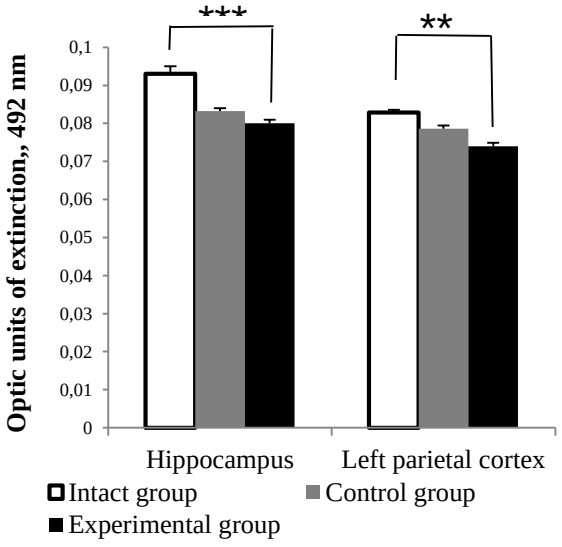

Fig. 6. Effects of anti-SMAP antibodies on the level of NGF in the hippocampus and left parietal cortex 24 h after antibodies administration. *** - $p<0.001$.

So, the obtained results in these series of studies indicate to downregulation of SMAP in the parietal cortex of the brain through elaboration of the conditioned alternative running model. Besides, the results indicate to accelerating and strengthening the formation of memory traces in the rats on the complicated conditioned models under antibodies-mediated blockade of SMAP. Moreover, 24 h later after intra-cerebral administration of SMAP downregulation of NGF in the hippocampus and left parietal cortex of the rat brain, though 3 days after their administration downregulation of NGF was noticed in the left parietal cortex, while in the hippocampus its upregulation was revealed.

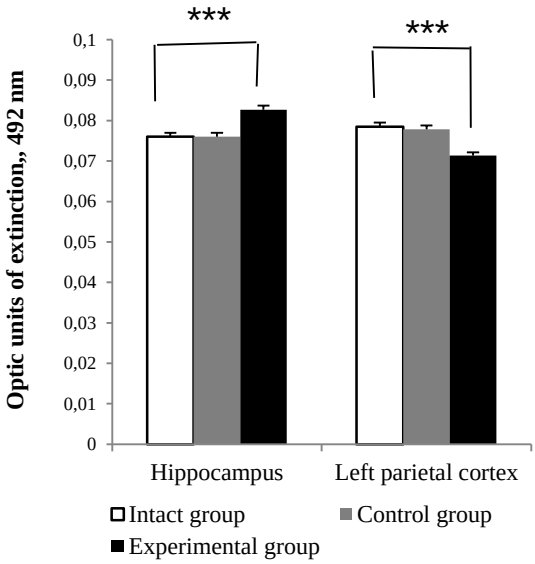

Fig. 7. Effects of anti-SMAP antibodies on the level of NGF in the hippocampus and left parietal cortex 3 days after antibodies administration. *** - $p<0.001$.

DISCUSSION

While considering downregulation of SMAP in the brain cortex of the trained animals in the many-time conditioned model of alternative running with food reinforcement and in the earlier undertaken studies on the shuttle box model with electroshock reinforcement (Guseinov, Mekhtiev, 2013) as well as promoting effect of anti-SMAP antibodies on the formation of memory traces on the model of alternative running and 2-lever operant differentiation, one can come to a reasonable conclusion about existence of SMAP-mediated negative regulation of the formation of memory traces. The revealed promoting effects of anti-SMAP antibodies on the formation of memory coincide with the earlier obtained data on the bloc-

king effects of intra-cerebral administration of SMAP itself on elaboration of the task in the shuttle box model (Guseinov, Mekhtiev, 2013) and in the model of alternative running (Mekhtiev et al., 2015).

The studies conducted by different researchers revealed that formation of memory traces induces the formation of novel cellular elements in the brain structures of the mature organisms (neoneurogenesis; Sherstnev et al., 2010; Deng et al., 2010; Sherstnev et al., 2015; Yau & So, 2015). Furthermore, the newly-formed neurons should pass through the stages of differentiation and specialization and, finally, be integrated into the functioning of the brain structures, that have already been formed in ontogenesis. For this purpose these neurons should sprout their axons and form new synaptic connections with other neurons, i.e. they should become a part of new neuronal circuits.

In the embryonic period of development of the organism, neurogenesis in the brain cortex is realized through migration of neuroblasts, formed in generative ventricular zone, i.e. in the zone of hippocamp, towards cortical plate along certain glial cells, called "radial glia" and realizing the role of the cellular conductors (Nadarajah et al., 2003). Radial glia realizes this function by "directional" molecules, in particular molecules of cellular adhesion, obviously, lined along the designed migration route of neuroblasts. The neuronal precursors are formed in the hippocampus also in postnatal ontogenesis (neoneurogenesis), however, in the mature organisms they migrate towards the cortex through another mechanism. In this case the neuronal precursors within the rostral migratory stream migrate first into bulbus olfactorius, where they are directed further to the points of their final localization (Sawada et al., 2011; Kaneko et al., 2017). Interestingly, the phenotypic peculiarities of the differentiated newly-formed neurons are generated in their cellular precursors before the beginning of migration and do not change after its finalization and arrival of the cells to the point of destination (Merkle et al., 2007). Hence, under the effect of molecular signals, released from the microenvironment of precursor cells in the course of migration and in the point of their arrival, their phenotypic profiles do not change. In the light of processes of formation of long-term memory this fact, probably, means that the neuronal precursors, modified under the effect of elaborated task in the hippocampus, are capable to maintain differentiated changes till the end of migration.

Presently it is revealed that ablation of the bulbus olfactorius in the animals brings to noticeable changes in their behavior, including impairment of memory storage, worsening with time course passed since the operation (Yamamoto et al., 1994; Yamamoto, Watanabe, 1997). In this case, it was found that bulbectomized rats had morphological changes in the form of the atrophy of dendritic spines and significant decrease of the total length of dendrites in the hippocampus and piriform cortex as well as downregulation of cellular proliferation in the dentate gyrus of the hippocampus (Morales-Medina et al., 2013). Proceeding from the revealed rough impairment of memory storage in the animals through bulectomy and taking into account engagement of bulbus olfactorius in migratory processes, one can propose that these disturbances are as well related to the impairment of migration of newly-formed neurons in the mature animals.

The literature data demonstrate that downregulation of NGF in the brain structures of the mature organisms promotes strengthening of differentiation processes of the precursors of the nervous cells, though its upregulation reflects strengthening of proliferative activity of precursor cells (Liu et al., 2014). The significant downregulation of NGF in the hippocampus and left parietal cortex in the rats 24 h later since intra-cerebral administration of anti-SMAP antibodies, revealed in the 4th series of studies, apparently, reflects strengthening of the processses of differentiation of the precursors of the cellular elements. Furthermore, the observed 3 days later downregulation of NGF in the left parietal cortex is, perhaps, related to continuing mighty cell differentiation, though parallel upregulation of NGF in the hippocampus, perhaps, induces increased proliferative activity. Probably, the precursor cells, starting their differentiation 24 h later from administration of SMAP, migrate from the hippocampus into the brain cortex. Moreover, 3 days later from the administration of antibodies, in the hippocampus the processes of cellular differentiation are strengthened for the purpose of restoration of a part of the pool of the precursor cells lost due to their migration into the cortex.

Perhaps, the revealed stimulatory effect of the antibodies-mediated blockade of SMAP on the formation of memory traces in the complex conditioned models is directly related to its negative regulatory activity regarding to differentiation of cellular elements. Besides, earlier on the model of embryonic development of *Xenopus laevis* we demonstrated that addition of anti-SMAP antibodies to the incubation medium of the embryos accelerates noticeably their passing through the stage of metamorphosis (Aminov, Mekhtiev, 2017). Hence, on the basis of the results obtained in this study and earlier undertaken studies one can make a conclusion that in the course of consolidation of the obtained information in the brain structures of the mature organisms differentiation and functional specialization of the newly formed neurons occur, and these processes last continuously throughout the whole lives of the individuums.

REFERENCES

Aminov A.V., Mekhtiev A.A. (2017) Application of embryonic models for elaboration of anticarcinogenic preparations of desired action. *Hematology and Medical Oncology*, **2(4):** 1-4.

Antibodies Volume II: A Practical Approach Press. (1989) Edited by D.Catty. Oxford University Press, IRL Press, Oxford. pp. 259.

Barrionuevo M., Aguirre N., Del Río J., Lasheras B. (2000) Serotonergic deficits and impaired passive avoidance learning in rats by MDEA: A comparison with MDMA. *Pharmocol. Biochem. Behav.*, **65(2):** 233–240.

Cassel J.-Ch. (2010) Experimental studies on the role(s) of serotonin in learning and memory functions. *Handbook Behav. Neurosci.*, **21:** 429–447.

Deng W., Aimone J.B., Gage F.B. (2010) New neurons and new memories: how does adult hippocampal neurogenesis affect learning and memory? *Nat. Rev. Neurosci*., **11(5):** 339-350.

Essman W.B. (1974) Brain 5-hydroxytriptamine and memory consolidation. *Adv. Biochem. Psychopharmacol*., **11:** 265–274.

Getsova V.M., York P., Vettsel V. (1980) About mechanisms of participation of serotonin in consolidation of temporary relations. *Journal of Highest Nerous Activity*, **30(5):** 988–990 (in Russ.)]

Guseinov Sh.B., Mekhtiev A.A. (2013) Study of the role of serotonin-modulating anticonsolidation protein in formation of the task on the rats in shuttle box model. *Neuroscience and Behavioral Physiology*, **43(5):** 551-556.

Harvey J.A. (1995) Serotonergic regulation of associative learning. *Behav. Brain Res.*, **73(1–2):** 47–50.

Kaneko N., Sawada M., Sawamoto K. (2017) Mechanisms of neuronal migration in the adult brain. *J. Neurochem*., **141:** 835-847.

Leuner B., Shorts T.J. (2004) New spines, new memories. *Mol. Neurobiol*., **29(2):** 117-130.

Liu F., Xuan A., Chen Y., Zhang J., Xu L., Yan Q., Long D. (2014) Combined effect of nerve growth factor and brain-derived neurotrophic factor on neuronal differentiation of neural stem cells and the potential molecular mechanisms. *Molecular Medicine Reports*, **10:** 1739-1745.

Mekhtiev A.A. (2000). Revealing in the brain of rats the protein possessing anticonsolidation properties. *Bulletin Exper. Biol. Med*., **129(8):** 147-150 (in Russ.)

Mekhtiev A.A., Asadova Sh.M. (2018) Dual-way of suppressive action of antibodies to serotonin-modulating anticonsolidation protein on drug addiction in rats. Neuropsychiatry (London). 8(4):739-749.

Mekhtiev A.A., Panahova E.N., Rashidova A.M., Guseinov Sh.B. (2015) Engagement of serotonin-modulating anticonsolidation protein in memory formation and suppression of drug addiction and epileptic seizures. New Developments in Serotonin Research (ed. M.D. Li). New York: Nova Science Publishers, p. 123-143.

Merkle F.T., Mirzadeh Z., Alvarez-Buylla A. (2007) Mosaic organization of neural stem cells in the adult brain. *Science*, **317:** 381-384.

Morales-Medina J.C., Juarez I., Venancio-García E., Cabrera S.N., Menard C., Yu W., Flores G., Mechawar N., Quirion R. (2013) Impaired structural hippocampal plasticity is associated with emotional and memory deficits in the olfactory bulbectomized rat. *Neuroscience*, **236:** 233-243.

Nadarajah B., Alifragis P., Wong R.O.L., Parnavelas J.G. (2003) Neuronal migration in the developing cerebral cortex: observations based on real-time imaging. *Cerebral Cortex*, **13:** 607-611.

Santucci A.C., Knott P.J., Haroutunian V. (1996) Excessive serotonin release, not depletion to memory impairments in rats. *Eur. J. Pharmacol*., **295(1):** 7–17.

Sawada M., Huang Sh., Hirota Y., Kaneko N., Sawamoto K. (2011). Neuronal migration in the adult brain. In: Neurogenesis in the Adult Brain I: Neurobiology (eds. T.Seki et al.), Springer, p. 337-355; DOI 10.1007/978-4-431-53933-9-14.

Semyonova T.P. (1976) Method of study of memory on the rats, based on inborn reaction of sequential changing of right-side and left-side running. *Journal of Highest Nerous Activity*, **26(6):** 1322-1324 (in Russ.).

Sherstnev V.V., Gruden M.A., Golubeva O.N., Alexandrov Yu.I., Solovyeva O.A. (2015) Newly-formed long-living neurons in the mature brain are engaged into support of processes of learning and memory. *Neurochemistry*, **2(1):** 19-26. (In Russ.)

Sherstnev V.V., Yurasov V.V., Storozheva Z.I., Gruden M.A., Proshin A.T. (2010) Neurogenesis and apoptosis in mature brain in formation and strengthening of long-term memory. *Neurochemistry*, **27(2):** 130-137 (in Russ.).

Vanderwolf C.H. (1989) A general role for serotonin in the control of behavior: Studies with intracerebral 5.7-dihydroxytryptamine. *Brain Res*., **504(2):** 192-198.

Yamamoto T., Jin J., Watanabe Sh. (1997). Characteristics of memory dysfunction in olfactory bulbectomized rats and the effects of cholinergic drugs. *Behav. Brain Research*., **83(1-2):** 57-62.

Yamamoto T., Kitajima I., Hironaka K., Ueki S., Watanabe Sh. (1994) Olfactory bulbectomy leads to learning/memory impairments in 3-panel runway and 3-lever operant tasks. *Nihon Shinkei Seishin Yakurigaku Zasshi*, **14(4):** 279-290.

Yau S., Li A., So K.-F. (2015) Involvement of adult hippocampal neurogenesis in learning and forgetting. *Neural Plasticity*, **Article ID 717958**, 13 p.

Yaddaş izlərinin yaranması prosesində hüceyrə differensiasiyası mexanizmlərinin iştirakı

A.Ə. Mehdiyev[1], Ş.M. Əsədova[1], Ş.B. Hüseynov[1], Q.R. Vahabova[2]

[1]AMEA akademik A.Qarayev adına Fiziologiya İnstitutu
[2]Azərbaycan Tibb Universiteti

Məqalə qida möhkəmlənməsi ilə yaranan növbəli qaçış və instrumental differensiasiya şərti-reflektor modellərində erkək siçovullarda yaddaş yaranmasına, həmçinin beyin strukturlarında sinir böyümə faktoru (SBF) miqdarına serotonin ilə düz mütanasib əlaqədə olan serotonin-modullu antikonsolidasiya zülalının (SMAZ) anticisimlər vasitəsilə blokadasının təsirinin öyrənilməsinə həsr olunub. Tədqiqatların 1-ci seriyasında növbəli qaçış modelində düzgün cavabların 80% səviyyəsinə çatmış siçovulların beyin qabığının ənsə və təpə nahiyələrində SMAZ-ın miqdarı müəyyən edilib. Öyrənilmiş siçovulların beyin qabığının təpə nahiyəsində SMAZ-ın miqdarının ciddi dərəcədə azalması ($p<0.001$) müşahidə olunur. Tədqiqatların 2-ci və 3-cü seriyalarında təlim seanslarından əvvəl siçovullara SMAZ-a qarşı anticisimlərin beyindaxili birdəfəlik yeridilməsi kontrol (qeyri-immun γ-qlobulinlər) və intakt heyvanlara nisbətən onlarda vərdişlərin daha tez yaranmasına ((düzgün cavabların 50%-lı meyarı; $p<0.001$), habelə platformaya və ya qola doğru birinci qaçışın latent dövrünün daha tez azalmasına ($p<0.01$) gətirib çıxarır. Tədqiqatların 4-cü seriyasında siçovullara SMAZ-a qarşı anticisimlərin beyindaxili yeridilməsi 24 s sonra hippokampda ($p<0.001$) və baş beynin sol təpə nahiyəsində ($p<0.001$) SBF-nun miqdarının azalması ilə nəticələnir. Halbuki, 3 gün sonra SBF-nun miqdarının sol təpə qabığında azalması ($p<0.001$), hippokampda isə artması ($p<0.001$) müşahidə olunur. Güman edilir ki, SMAZ-ın anticisimlər ilə blokadasının yaddaş izlərinin yaranmasına stimuləedici təsiri onun hüceyrə elementlərinin differensiasiyasını neqativ tənzimləməsi ilə əlaqədardır.

Açar sözlər: *Serotonin-modullu antikonsolidasiya zülalı, anticisimlər, yaddaş, dolayı immuno-enzim analizi, sinir böyümə faktoru, hippokamp, sol təpə qabığı*

Участие механизмов клеточной дифференциации в процессе формирования следов памяти

А.А. Мехтиев[1], Ш.М. Асадова[1], Ш.Б. Гусейнов[1], Г.Р. Вагабова[2]

[1]Институт физиологии им. академика А.Гараева НАН Азербайджана,
[2]Азербайджанский медицинский университет

Статья посвящена изучению влияния блокады антителами активности серотонин-модулируемого антиконсолидационного белка (СМАБ), находящегося в прямой зависимости от уровня серотонина, на формирование памяти у крыс-самцов в условно-рефлекторных моделях чередования побежек и инструментального дифференирования с пищевым подкреплением, а также на уровень фактора роста нервов (ФРН) в структурах головного мозга. В 1-й серии исследований в затылочной и теменной областях коры головного мозга крыс, достигших 80% -го уровня правильных ответов, в модели чередования побежек методом иммуноферментного анализа определяли уровень СМАБ. Было обнаружено заметное снижение ($p<0.001$) уровня СМАБ в теменной области коры у обученных животных. Во 2-й и 3-й сериях исследований однократное внутримозговое введение антител к СМАБ крысам до сеансов обучения приводило к значительно более быстрому формированию у них навыков (50%-й критерий правильных ответов), чем у контрольных (неиммунные γ-глобулины) и интактных животных ($p<0.001$), а также к более быстрому снижению латентного периода первой побежки к платформе или к рычагу ($p<0.01$). В 4-й серии исследований внутримозговое введение крысам антител к СМАБ через 24 ч вызывало снижение уровня ФРН в гиппокампе ($p<0.001$) и левой теменной области ($p<0.001$) головного мозга, тогда как через 3 суток – снижение уровня ФРН в левой теменной коре ($p<0.001$) и повышение его уровня в гиппокампе ($p<0.001$). Возможно, что стимулирующее влияние блокады СМАБ антителами на формирование следов памяти обусловлено его негативной регуляцией дифференциации клеточных элементов.

Ключевые слова: *Серотонин-модулируемый антиконсолидационный белок, антитела, память, непрямой иммуноферментный анализ, фактор роста нервов, гиппокамп, левая теменная область коры головного мозга*

Journal of Life Sciences and Biomedicine, vol. 1 (74), No 1, p. 63-68 (2019)

Species composition of anamorphic fungi on medicinal plants in Azerbaijan

K.F. Bakhshaliyeva[1], N.R. Namazov[2], A.A. Yusifova[3], S.M. Jabrailzade[3], P.Z. Muradov[1]*

[1] *Institute of Microbiology, Azerbiajan National Academy of Sciences, 103 M.Mushfig, Baku AZ1004, Azerbaijan*
[2] *Sumgayit State University, 43rd block, Sumgayit AZ 5008, Azerbaijan*
[3] *Azerbaijan State Pedagogical University, Uzeyir Hajibayli 68, Baku AZ 1000, Azerbaijan*
**For correspondence: mpanah@mail.ru*
Accepted for publication: 01 October 2019

This work was devoted to the study of mycobiota of the medicinal plants included in the flora of Azerbaijan, and pathologies caused by the anamorphic fungi. The results demonstrated that the anamorphic mycobiota of the medicinal plants (57 species) in the conditions of Azerbaijan is abundant and various and the mycobiota of the medicinal plants of Azerbaijan consists of 110 species of anamorphic fungi belonging to 22 genera. The most representative genus consisting of 10 and more species in each type are: *Septoria* – 14, *Penicillium* – 12, *Ascochyta* – 11, *Fusarium* – 10, *Aspergillus* – 10, other types are represented by 1-8 species. It was also demonstrated that the discovered fungi include the species which cause the different diseases (ascochitosis, septorioz, necrosis, spotting, rubigo, powdery mildew, botritis disease, wilting, phomosis etc.), and the frequency of occurrence of the activators of these pathologies varies greatly within 0.001-17.6%. Among the fungi found on medicinal plants, there are few toxigenic species. The presence of toxigenic fungi and their mycotoxins on the plants used for medicinal purposes is unfavorable and justifies the development of missing or non-existing approaches regulating both the presence of fungi and the quantity of their mycotoxins

Keywords: *Medicinal plants, mycobiota, anamorphic fungi, fungal diseases, frequency of occurrence*

INTRODUCTION

It is commonly known that currently the plant kingdom includes about 0.5 mln species. About 16% of these plants are medicinal, and many of them are used in the folk medicine over a long time (Chen et al., 2016). Idea does not correspond to the cited literature, also type of citation is unusual. However, many of these plants did not pass the screening for detection of medicinal properties, with the assumption that about 4/5 of global population administer the plant preparations and demand for such preparations increases every year (Ivanise et al., 2018; Noudèkè et al., 2017). Regardless of this fact the reserves of plants used for receiving the same preparations are limited gradually (Yuan et al., 2016). On the one hand, it is associated with the biological diversity depletion, and on the other hand – with intense, irrational and insufficiently controlled preparation of raw materials. It should be also noted that some medicinal plants are used for other purposes (feeding, food and technical) that plays a certain role in limiting the reserves of these plants. Together with it, it is necessary to consider the diseases of these plants caused by the fungi, even regardless of that many medicinal plants have the antifungal and antibacterial action (Safarova et al., 2018; Sarkhosh et al., 2018). As a result, all this negatively affects the resources of medicinal plants. That is why studying the regularity of the occurrence and distribution of the phytopathogenic properties of fungi in relation to the medicinal plants is also important in this context.

The natural vegetation of the Republic of Azerbaijan differs by great variety and reflects not only the impact of the set of modern natural and historical conditions and human but also the complex and long-term historical path of formation backgrounded by the change of geological period. Almost all large types of vegetation found on the

globe are represented at comparatively small territory. Currently, about 4700 species belong to the flora of Azerbaijan (Mehdiyeva, 2011). Together with the species of plants widely found in Caucasus and other countries the flora of Azerbaijan has the significant number of species specific only for Azerbaijan (Hirkan figs - *Ficus hyrcana* A.Grossh. T.). Special attention shall be paid to the relict plants (iron wood – *Parrotia persica* (DC.) C.A.Mey., silk tree – *Albizia julibrissin* Durazz., chestnut-leafed oak – *Quercus castaneifolia* C.A.Mey., boxwood – *Buxus* L., etc.) which appeared about 70 million years ago.

It should be noted that the flora includes many species considered as useful among which the special place is occupied by the medicinal plants (about 1500 species). The medicinal plants include all the life forms (grasses, bushes and trees), both wild-growing and cultivated species. In addition, the medicinal plants of Azerbaijan also include the endemic and relic species (pomegranate – *Punica* L. and fig tree – *Ficus carica L.*). Some medicinal plants belonging to the flora of Azerbaijan are widely used for feeding (*Trifolium pratense* L., *Zea mays* L.), food (*Cucurbita* L., *Zea mays* L., *Solanum L.*) and technical (*Fagus orientalis* Lipsky, *Pinus* L., *Populus* L. etc.) purposes (Mehdiyeva, 2011).

Regardless of that the flora consists of many medicinal plants they are studied insufficiently, especially in the mycological context. In this relation, this work was aimed at studying the mycobiota of the medicinal plants belonging to the flora of Azerbaijan and pathologies caused by the anamorphic fungi.

The selection of anamorphic fungi is stipulated by that, first, the fungal pathologies are more common among the plants compared to bacteria and, second, the most of phytopathogenic fungi belong namely to these species (Doehlemann et al., 2017).

MATERIALS AND METHODS

The medicinal plants of Azerbaijan were used as the material for this study. The samples of medicinal plants were collected during the 10th expedition (2010-2018) at the different territories of Azerbaijan (Great Caucasus, Talysh mountains, Kura-Araks lowland, part of the territory of Lesser Caucasus not occupied by Armenia).

In all cases, rice agar (RA), potato agar (PA) were used from the wort agar (WA), agar medium Czapek (AMC) (Handbook of Mycological Methods, 2006). It was also used during the hiding of workers' cultures from these nurturing environments.

When identifying fungi taken into a pure culture from the abovementioned nutrient media, determinants based on cultural-morphological and physiological characters were used (Sutton et al., 2001; Klich, 2002; Kirk et al., 2008). For the taxonomy and the name of the fungus, the data indicated on the official website of IMA (Crous et al., 2004; Robert et al., 2005; Vincent et al., 2013). The determination of pathology caused by fungi was also carried out as in Horst (Horst, 2013).

The frequency of occurrence (P) of the species (diseases) was evaluated (%) using the following formula: $P=(n/N) \times 100$, where n - is a number of samples on which this species of fungi (type of disease) are detected, N - is a total number of samples.

RESULTS AND DISCUSSION

The results demonstrated that the anamorphic mycobiota of the medicinal plants in the conditions of Azerbaijan is abundant and various which is confirmed by the data specified in table 1. As it can be seen, the mycobiota of the medicinal plants of Azerbaijan consists of 110 species of anamorphic fungi belonging to 22 genera. Some of the representative genera consist 10 and more species: *Septoria* – 14, *Penicillium* – 12, *Ascochyta* – 11, *Aspergillus* – 10; other genera are represented by 1-8 species. Therefore, above mentioned 4 genera make up about 42.7% of detected mycobiota and include 47 species.

The selectivity in the distribution of micromycetes by 57 species of host plants also were characterized in different manner and the largest number of micromycetes (more than 10 species) was detected mainly on the plants of three genera: *Solanum* (11 species of anamorphic fungi), *Trifolium* (15 species) and *Zea* (10 species). 1-8 species of anamorphic fungi were detected on other 54 species of plants.

As it is shown in table 1 numerous micromycetes detected on plant genera. Associations between fungi and plant most probably could be explained by ecological conditions of different study territories within Azerbaijan.

It is known that many fungi cause spotting in plants, the causative agent of which are representatives of different genera. The results of our studies showed that most of fungi detected on medicinal plants also cause spotting, and the frequency of occurrence of which relative to the total number of plants studied is average 17.6%.

Such pathologies are specific for *Septoria* fungi in relation to which during the study it was established that the species of this genus cause the spotting of leaves in the plants of 15 genera. The detected fungi include *S.astericola* Ellis et Everh., *Septoria alliorum* West., *S. carotae* Nagorny., *S.leucanthemi* Sacc et Speg, *S. lucopersici* Speg and *S.petroselini* (Lib) Desm, which are common in the territory of Azerbaijan, and they are characterized by a relatively high frequency of occurrence (4.0-6.0%), that such species as *S. iridis* C.Massal., *S.primulae* Buckn., *S.cacaliae-aconitifoliae* Ziling., *S.senecionis* Westend., *S.violae* Rabenh., *S. flagellifera* Ell. et Ev., *S.glycines* T.Hemmi. and *S.valerianae* Sacc.et Fautrey (0.001-1.0%). The range of feeding plants for the most of detected *Septoria* species is limited to one genus of the host plant, except for *S.violae* which were detected on two species of *Viola* (*V.arvensis* Murr. and *V.odorata* L.).

Table 1. Distribution of fungal genera and species on host plants.

№	Fungal genera	Number of species	Genera of host plants
1	*Acremonium*	1	*Rosa*
2	*Alternaria*	8	*Agropyrum, Brassica, Calendula, Datura, Heliantus, Iris, Malva, Nicotiana, Senecio, Punica, Solanum, Trifolium, Verbascum, Zea*
3	*Ascochyta*	11	*Aconitum, Iris, Primulla, Punica, Senecio, Trifolium,Valeriana, Verbascum, Zea*
4	*Aspergillus*	10	*Agropyrum, Calendula, Datura, Heliantus, Malva, Nicotiana, Senecio, Punica, Solanum, Trifolium, Verbascum, Zea*
5	*Biopolaris*	1	*Iris*
6	*Botrytis*	2	*Iris, Trifolium, Zea,*
7	*Cercespora*	2	*Foeniculum, Viola*
8	*Cladosporium*	3	*Achillea, Carum, Ficus, Datura, Trifolium, Zea*
9	*Colletotrichum*	8	*Aloe, Cucurbita, Euphorbi, Ficus, Pimpinella, Nepeta, Viola, Zea*
10	*Fusarium*	10	*Artemisia, Asparagus, Malva, Magnolia, Petroselinum, Satureja, Solanum, Trifolium, Tulipa, Zea*
11	*Gliocladium*	1	*Tulipa*
12	*Marssonina*	1	*Rosa*
13	*Penicillium*	12	*Astrodaucus, Datura, Dorema, Ficus, Leucanthemum, Ocimum, Phlomis, Punica, Satureja, Trifolium, Tripleurospermum, Tulipa, Zea, Zosima*
14	*Phoma*	8	*Anethum, Artemisia, Brassica, Carum, Chenopodium, Daucus, Ficus, Medicago, Paeonia Stachys, Valerian, Verbascum, Zea*
15	*Phomopsis*	4	*Sambucus, Solanum*
16	*Ramularia*	5	*Galega, Gentiana, Iris, Magnolia,Viola*
17	*Rhizoctonia*	1	*Zea*
18	*Sclerotium*	2	*Laurus, Leucanthemum, Teucrium*
19	*Septoria*	14	*Carum, Daucus, Ficus, Heracleum, Iris, Laurus, Mentha, Primulla, Rhamnus, Senecio, Solanum, Tanacetum, Valeriana, Viola*
20	*Stemphylium*	3	*Achillea, Ficus, Punica, Senecio, Leucanthemum*
21	*Trichothecium*	1	*Anthemis, Rosa*
22	*Verticillium*	2	*Teucrium, Trifolium, Zea*

One of the genus characterized by the rich species diversity is *Ascochyta*. They also affect the different (vegetative and generative) organs of medicinal plants and cause the spotting (or disease- ascochytosis). The detected species (*A. anethicola* Sacc., *Asc. iridis* Oudem., *A. malvicola* Sacc., *A. primulae* Trail., *A. pseudopinodella* Bond.-Mont et Wassil., *Asc. pinodes* Jones. and *Asc. berberidina* Sacc.) are characterized by narrow substrate specifics, i.e. the most of detected species are stenotrophic, though the fungi of this type include also the conditionally stenotrophic species (*Asc. allii-cepae* Punith. and *Asc. phaseolorum* Sacc.) and eutrophic (*Asc.cucumeris* Faurtr. et Roum. and *Asc.doronici* Allesch.).

The fungi of the genus *Alternaria* (*A. alternata* (Fr.: Fr) Keissl., *A.calendulae* Ondfej, *A.cucurnerina* (Ell. et Ev.) Elliot, *A.iridicola* (Ellis et Everh.) J.A.Elliott, *A.longipes* (Ellis et Everh.) E.W.Mason., *A.helianthi* (Hansf) Tubaki et Nishih. and *A. solani* Sorauer.*), Ramularia* (*R.geranii* Fuckel., *R.lactea*(Desm)Sacc., *R. macrospora* Fresen and *R.galegae* Sacc.), *Cladosporium (C.cladosoriodes* (Fresen.) G.A. de Vries, *C.iridis* (Fautrey et Roum.) G.A.deVries and *C.herbarum* (Pers.) Link.), *Colletotrichum* (C. capsici (Syd) Buti et Bisby., *C.circians* (Berk.) Voglino, *C. gloeosporioides* Penz.) Penz. et Sacc., *C.langenarium* (Pass) Ell et Halst., *C.malvarum* (A.Braun et Casp.) Southw, *C. nigrum* Ell. et Halst. *C. orbiculare* (Berk. et Mont) Arx., *C. phomoides* (Sacc)Chest.) also cause the spotting in the medicinal plants. The results demonstrated that the occurrence of these species of fungi is within 0.001-3.2%.

It was shown that only one species of the genus *Botrytis (B. cinerea* Pers) is recoded on the medicinal plants. Despite this, this fungus is one of the most widespread not only throughout Azerbaijan but also in the world (Safaraliyeva, 2019), *B. cinerea* is a significant necrotrophic plant pathogen causing devastating diseases on more than 500 plant species, especially on fresh fruits and vegetables, resulting in the economic losses ranging from $10 billion to $100 billion worldwide (Hua et al., 2018). As a result of our studies, it was shown that the frequency of occurrence of this fungus in Azerbaijan is 4.2%. Affecting the leaves, stalks, flower buds and flowers of the plants they cause the botrytis disease.

According to the table, the *Penicillium* possess rich species diversity, and 12 species (*P. chrysogenum* Thorn., *P. citrinum* Thom., *P. cyclopium* Westl., *P. expansum* Link., *P. funiculosum* Thom., *P.janthinellum* Biourge., *P. lanosum* Westling., *P. olivaseum* Wehmer., *P. puberulum* Bain., *P. rubrum* Stoll. *P. purpurogenum* Stoll. and *P. rubrum* Stoll.) form the mycobiota of the medicinal plants. The certain pathology associated with these fungi are not studied yet (except for the mold formation) but their presence on the medicinal plants weakens them and creates the favorable conditions for other phytopathogens. In addition, the species of this type are able also to synthesize the toxins together with other fungi.

During the study some species causing wilting was detected on the medicinal plants, such as *Verticillium albo-artrum* Reinke and *V.dahliae* Klebahn., fusariosis by F*uzarium moniliforme* J.Sheld., *F.oxysporum* Schlechtend., *F.sambucinum* Fuckel. *F.semitecthum* Berk., *F.solani*(Mart)Sacc., phomosis by *Phoma anethi* (Pers) Sacc., *Ph. cepae* Verwold et Du Plessis, *Ph. exigua* Desm., *Ph. minutella* Sacc. et. Penz., *Ph.rostrupii* Sacc., *Ph.siliguarum* Sacc et Rourn, *Ph. solanicola Prillet.* Delacr. and *Ph.subvelata* Sacc., etc. The occurrence of the activators of these diseases varies within 0.01-2.1%.

It should be noted that the fungi causing one or another pathology not only weaken the biological activity of the plants but also fertilize them by their metabolites which include also the toxic substances. The presence of fungi and their mycotoxins on the plants used for medical purposes is unfavorable and even hazardous because the results of their impact on the health of humans are characterized negatively (Anater et al., 2016). In addition, currently many countries have the normative documents regulating the mycological safety in relation to the use of such materials which do not consider all the details of the actions of the above mentioned groups of fungi that justifies the development of missing or non-existing approaches regulating both the presence of fungi and the quantity of their mycotoxins.

CONCLUSION

Thus, in the studies it was found that the anamorphic mycobiota of medicinal plants in Azerbaijan is abundant and diverse. Mycobiota of medicinal plants of Azerbaijan consists of 110 species of mushrooms of the 22nd genus. Despite the fact that the conducted studies concerned a small part of medicinal plants, the results obtained to some extent expanded the information on anamorphic fungi associated with medicinal plants of Azerbaijan, and many species were first discovered on medicinal plants in Azerbaijan.

REFERENCES

Anater A., Manyes L., Meca G., Ferrer E., Luciano F. B., Pimpão C. T. et al. (2016) Mycotoxins and their consequences in aquaculture: a review. *Aquaculture*, **451:** 1-10. 10.1016/j.aquaculture.2015.08.022

Chen Sh., Yu H., Luo H., Wu Q, Li Ch., Steinmetz A. (2016) Conservation and sustainable use of medicinal plants: problems, progress, and prospects. *Chin. Med.*, **11:** 37. doi: 10.1186/s13020-016-0108-7

Crous P.W., Gams W., Stalpers J.A., Robert V. and Stegehuis G. (2004) MycoBank: an online initiative to launch mycology into the 21st century. *Studies in Mycology*, **50:** 19-22

Doehlemann G., Ökmen B., Zhu W., Sharon A. (2017) Plant Pathogenic Fungi. *Microbiol Spectr.*, **5(1):** doi: 10.1128/microbiolspec. FUNK-0023-2016.

Handbook of Mycological Methods (2006) http://www.fao.org/fileadmin/user_upload/ agns/pdf/coffee/Annex-F.2.pdf

Horst K.R. (2013) Westcott's Plant Disease Handbook. 8th Ed. New York: Springer, 826 p.

Hua L., Yong Ch., Zhanquan Z., Boqiang L., Guozheng Q., Shiping T. (2018) Pathogenic mechanisms and control strategies of *Botrytis cinerea* causing post-harvest decay in fruits and vegetables, *Food Quality and Safety*, **2(3):** 111–119.

Ivanise B.S. et al. (2018) Use of medicinal plants in the treatment of erysipelas: A review. *Phcog Rev*., **12:** 200-207.

Kirk P.M., Cannon P.F., Minter D.W., Stalpers J.A. et al. (2008) Ainsworth & Bisby's Dictionary of Fungi. CAB International, 771 p.

Klich M.A. (2002) Identification of common *Aspergillus* species. Utrecht: CBS, 116 p.

Mehdiyeva N.R. (2011) Biodiversity of medicinal flora of Azerbaijan. Baku: Letterpress, 186 p.

Noudèkè N.D. et al. (2017) Inventory of medicinal plants used in the treatment of diseases that limit milk production of cow in Benin. *Journal of Advanced Veterinary and Animal Research*, **4(1):** 1-14. http://doi.org/ 10.5455/javar.2017.d183

Robert V., Stegehuis G., Stalpers J. (2005) The MycoBank engine and related databases. http://www.mycobank.org

Safaraliyeva E.M. (2019) General characteristics of mycobiota of gray-brown soils affected by various anthropogenic impacts in Azerbaijan. *Int. J. Curr. Microbiol. App. Sci.,* **8(07):** 1712-1718. doi: https://doi.org/10.20546/ijcmas.2019.807.203

Safarova A.Sh. et al. (2018) Mycobiota and fungicide impact of *Alhagi mourorum* Medik. *Sylwan journal* (Poland), **162(4):** 79-84.

Sarkhosh A. et al. (2018) *In vitro* evaluation of eight plant essential oils for controlling *Colletotrichum, Botryosphaeria, Fusarium and Phytoph thora* fruit rots of avocado, mango and papaya. *Plant. Protect. Sci*., **54:** 153-162. doi: 10.17221/49/2017-PPS

Sutton D., Fothergill A., Rinaldi M. (2001) The determinant of pathogenic and conditionally pathogenic fungi. M: The World, 468 p.

Vincent R., Duong V., Ammar B.H.A. et al. (2013) MycoBank gearing up for new horizons. *IMA Fungus*, **4(2):** 371-379.

Yuan H. et al. (2016). The traditional medicine and modern medicine from natural products. *Molecules*, **21:** 559; doi:10.3390/molecules 21050559

Azərbaycanda dərman bitkilərində anamorf göbələklərin növ tərkibi

K.F. Baxşəliyeva[1], N.R. Namazov[2], A.Ə. Yusifova[3], S.M. Cəbrailzadə[3], P.Z. Muradov[1]

[1] AMEA Mikrobiologiya İnstitutu
[2] Sumqayıt Dövlət Universiteti
[3] Azərbaycan Dövlət Pedaqoji Universiteti

Təqdim olunan işin məqsədi Azərbaycan florasına daxil olan dərman bitkilərinin(57 növ) mikobiotasının və anamorf göbələklərin onlarda törətdikləri patologiyaların tədqiqinə həsr edilibdir. Göstərilmişdir ki, Azərbaycanın dərman bitkilərinin mikobiotası zəngin və geniş müxtəlifliyə malikdir, belə ki, Azərbaycanın dərman bitkilərinin anamorf mikobiotasına 110 növə aid 22 cins daxildir. 10 və daha cöx növlə təmsil olunan cinslər: *Septoria* -14 növ, *Penicillium* - 12, *Ascochyta* – 11, *Aspergillus* – 10. Qalan cinsəlr isə 1-8 növlə təmsil olunuralr. Müəyyən edilmişdir ki, qeydə alınan göbələklərin əksəriyyəti dərman bitkilərində müxtəlif xəstəliklər (ləkəlilik, boz çürümə, fusarioz, solma və s.) törədir və həmin patologiyaların rastgəlmə tezliyi güclü şəkildə variasiya edir və 0,001%-17,5% arasında dəyişir. Dərman bitkilərində qeydə alınan bitkilər arasında bəzi toksigen göbələklərə də rast gəlinir. Tibbi məqsədlər üçün istifadə edilən bitkilərdə toksigen göbələklərin və onların mikotoksinlərinin olması əlverişli deyil, bu səbəbdən də göbələklərin həm özlərinin, həm də əmələ gətirdikləri mikotoksinlərin miqdarını tənzimləyən yanaşmaların işlənib hazırlanmasını əsaslandırır.

Açar sözlər: *Dərman bitkiləri, mikobiota, anamorf göbələklər, göbələk xəstəlikləri, rastgəlmə tezliyi*

Видовой состав анаморфных грибов на лекарственных растениях в Азербайджане

К.Ф. Бахшалиева[1], Н.Р. Намазов[2], А.А. Юсифова[3], С.М. Джабраилзаде[3], П.З. Мурадов[1]

[1] Институт микробиологии НАН Азербайджана
[2] Сумгаитский педагогический университет
[3] Азербайджанский государственный педагогический университет

Целью представленной работы явилось изучение микобиоты лекарственных растений, входящих во флору Азербайджана, и патологий, вызванных анаморфными грибами. Показано, что анаморфная микобиота лекарственных растений Азербайджана обильна и разнообразна.Так, в Азербайджане насчитываются относящиеся 22 родам 110 видов анаморфных грибов лекарственных растений. Наиболее полно представленными родами, которые насчитывают по 10 и более видов в каждом роде, являются: *Septoria* - 14 видов, *Penicillium* – 12 видов, *Ascochyta* – 11 и *Aspergillus* – 10 видов. Остальные роды представлены 1-8 видами. Выявлено, что большинство грибов, обнаруженных на лекарственных растениях, вызывают различные болезни (пятнистость, серая гниль, фузариоз, увядание и др.), и частота встречаемости возбудителей этих патологий сильно варьирует и находится в пределах 0,001-17,6%. Среди грибов, встречающихся на лекарственных растениях, существует несколько токсигенных видов. Наличие токсигенных грибов и их микотоксинов на растениях, используемых в медицинских целях, является неблагоприятным и оправдывает разработку подходов, регулирующих как наличие грибов, так и количество их микотоксинов.

Ключевые слова: *Лекарственные растения, микобиота, анаморфные грибы, грибные болезни, частота встречаемости*

Journal of Life Sciences and Biomedicine, vol. 1 (74), No 1, p. 69-76 (2019)

Optimization of culture conditions for higher production of antimicrobial compounds by AZ-130 bacterial strain isolated from soil of Azerbaijan

A.G. Aghayeva

Institute of Molecular Biology and Biotechnologies, Azerbaijan National Academy of Sciences, 11 Izzat Nabiyev, Baku AZ1122, Azerbaijan; For correspondence: aytanaghayeva@gmail.com
Accepted for publication: 08 November 2019

AZ-130 bacterial strain was isolated from soil sample collected from Azerbaijan in 2014. After preliminarily culture and supernatant screenings for novel antibacterial compounds, AZ-130 showed strong gram-positive activity against pathogenic *Staphylococcus aureus* and *Enterococcus faecalis* strains. Based on range of its activity, AZ-130 strain that produces AZ-130 antibacterial compound was selected for the further characterization. The main goal of this study is to optimize growth conditions for AZ-130 to determine the optimal medium, incubation temperature and time point in which the production of the antimicrobial compound is highest. To achieve this goal, 4 different media types at 4 different temperatures, in total 16 different growth conditions were tested. Supernatants were collected and clarified at day 1, 2 and 3 or 5. All collected supernatants were analyzed by spot test and broth microdilution method against *S.aureus*. According to the spot test and broth microdilution results, AZ-130 produces the most antimicrobial compound in TB + 2% Glucose medium at 32°C; incubation time is 2 days.

***Keywords*:** *Antimicrobial activity, antibiotics, bioactive molecules, culture conditions, medium optimization, natural products, primary metabolite, secondary metabolite, pathogenic bacteria*

INTRODUCTION

The bacterial metabolism is a combination of all biochemical reactions occurring in a microbial cell lifelong. Metabolism ensures the reproduction of all cellular material and includes two opposite processes pathways - catabolism (destructive) and anabolism (constructive). Metabolites are the intermediates and products of metabolism. Depending on functional properties and metabolic pathways, metabolites classified into 2 groups - primary and secondary metabolites. Primary bacterial metabolites (nucleotides, amino acids, sugars, organic acids, vitamins) are low molecular weight compounds directly involved in growth, development or reproduction of the producing organism and present in every living cell. They serve as a primary source of energy for various biochemical and physiological functions necessary for the life and growth of the cell. Secondary bacterial metabolites (antimicrobial, antiparasitic and antitumor agents; enzymes and enzyme inhibitors etc.) are bioactive substances at low molecular weight that are in most cases not necessary for the life cycle of the producer. They play a role in the survival of producer organism in its ecosystem serving as poisons against competitors (Gokulan et al., 2014; Demain et al., 2000).

Antibiotics are one of the very important for human health secondary metabolites. Since 1928 - the year penicillin was discovered by A. Fleming - antibiotics have been the foremost weapon for combating such pathogenic microorganisms as *Staphylococcus aureus, Acinetobacter baumannii*, *Pseudomonas aeruginosa*, *Enterobacteriaceae* and others (Jones et al., 2017). However, during recent years the rapid emergence of antibiotic-resistant bacteria is occurring worldwide, and, unfortunately, nearly all available for treatment antibiotics are losing their effectiveness (Johnning et al., 2018). Bacterial infections caused by methicillin-resistant *Staphylococcus aureus* (MRSA), carbapenem-resistant *Acinetobacter baumannii* (CRAB), multidrug-resistant *Pseudomonas aeruginosa* (MDR) are becoming a critical threat to global health (Johnning et al., 2018; Lerminiaux et al., 2019;

Otto, 2013). Consequently, there is an urgent need to develop new, safe and effective antibiotics against bacterial infections. And considering that a majority of antibiotics used in the clinic today have been isolated from living organisms or are modified compounds which core structures derived from nature (Jones et al., 2017), it is very important to identify novel antibiotic producer strain.

Discovery and development of a new medicine, from target identification through approval for marketing is a very long and expensive process (Ekins, 2019). One of the main steps in antibiotics development is the optimization of growth conditions of the producer strain to maximize the final metabolite yield. Media components and their levels are crucial for the production of secondary metabolites. Even small changes in growth medium may affect not only the quantity of target-metabolite, but also the overall metabolic profile of producer strain. That is why before any large scale production of metabolites necessary to optimize growth condition of producer strain (Singh et al, 2017; Arul Jose et al., 2013; Wang et al., 2011).

The main objective of this study is to optimize growth conditions for AZ-130 bacterial strain to determine the optimal media, temperature and time point in which the production of the target AZ-130 antimicrobial compound is highest.

MATERIALS AND METHODS

To determine the optimal medium, temperature and time point in which the production of the AZ-130 compound is highest, 2 different media types (TSB - Tryptic Soy Broth and TB - Terrific Broth) +/- 2% Glucose at 4 different temperatures (18°C; 25°C; 32°C; 37°C) were tested (Table 1). To start all media with the same density of colonies, we made a preculture of AZ-130 strain and grown it at 32°C 250 RPM for 2 h. After 2 h, all 4 media (TB +/- Glucose; TSB +/- Glucose) were inoculated with 1mL of preculture of AZ-130 and grown at respective temperatures (18°C; 25°C; 32°C and 37°C). At time points of 24 h, 48 h and longer 1 mL of culture were collected. Bacteria-free culture supernatants were clarified by centrifugation at 10,000xg for 15 min at 4°C and filtering through 0.22 μm PES. Initially, all collected supernatants were tested for an inhibitory activity against *S.aureus* by the soft-agar overlay method as described by Hockett (Hockett et al., 2017) with some modifications. 10 μl of collected supernatants were spotted onto an agar plate of confluent indicator organisms. Plates were incubated at 37°C overnight and examined for the presence of inhibition zones in the place the supernatant has been spotted. The range of antibacterial activity was evaluated by measuring the diameter of the inhibition zone. Then, active in spot-test supernatants were analyzed by broth microdilution assay (Coyle et al., 2005). For broth microdilution assay 100 μl of supernatant was added to the first well of row and diluted 1:1 across the row. Then, 50 μL of *S.aureus* at required concentration, to obtain a final concentration of $5x10^4$ cells per well, was added into each well. As controls we used: positive 100% growth control – 50 μL of medium plus 50 μL of indicator organism; negative no cells control – 100 μL of medium. Microtiter plates were incubated at 37°C overnight in open biohazard bag (to hold moisture inside). After overnight incubation OD was read at 650 nm using Molecular Devices Spectra MaxPlus microplate reader. Data were analyzed and plotted.

Table 1. Components of TSB and TB media

Media componenets:	
TSB	**TB**
Casein peptone (pancreatic) - 17 g/L	Tryptone (pancreatic digest of casein) - 12 g/L
Dipotassium hydrogen phosphate - 2.5 g/L	Yeast extract 24 g/L
Glucose - 2.5 g/L	K_2HPO_4 9.4 g/L
Sodium chloride - 5 g/L	KH_2PO_4 2.2 g/L
Soya peptone (papain digest.) - 3 g/L	

RESULTS AND DISCUSSION

This research was carried out at Fraunhofer USA Center for Molecular Biotechnology. About 30 soil samples were collected from different areas of Azerbaijan during 2014-2018 years and sent to the Fraunhofer CMB for bacterial isolation and screening. A total of 578 bacterial strains were isolated from 30 soil samples and all of them were screened for antibacterial activity against two gram-positive (*Staphylococcus aureus*, *Enterococcus faecalis*) and two gram-negative (*Escherichia coli*) pathogenic strains by growth inhibition assay. After preliminarily culture screening 62 isolates showed an antibacterial activity against at least one pathogenic indicator organism. All 62 "active in culture" isolates were screened for an activity in cell-free culture supernatant. 14 isolates demonstrated an inhibitory activity in supernatant. They were categorized as "isolates of interest" and chosen for the further characterization. AZ-130 strain that produces antibacterial compound (AZ-130) is one of "isolates of interest". It showed a strong antibacterial activity of 7 mm in supernatant against *S.aureus* during initial supernatant screening.

The effect of four different culture media at four different temperatures on bacterial growth was studied. Supernatants obtained from AZ-130 culture grown at respective temperatures were clarified and analyzed for an antibacterial activity against *S.aureus* by the growth inhibition assay (Fig. 1–Fig. 4).

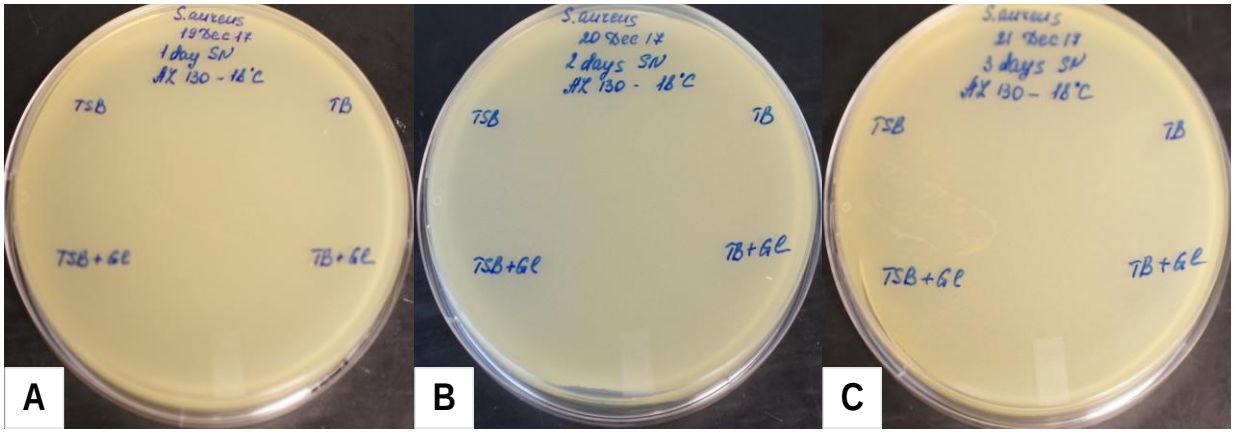

Fig. 1. Inhibitory effect of AZ-130 supernatants collected from cultures grown at 18°C against *S.aureus*. A) Supernatants collected at day 1. B) Supernatants collected at day 2. C) Supernatants collected at day 3.

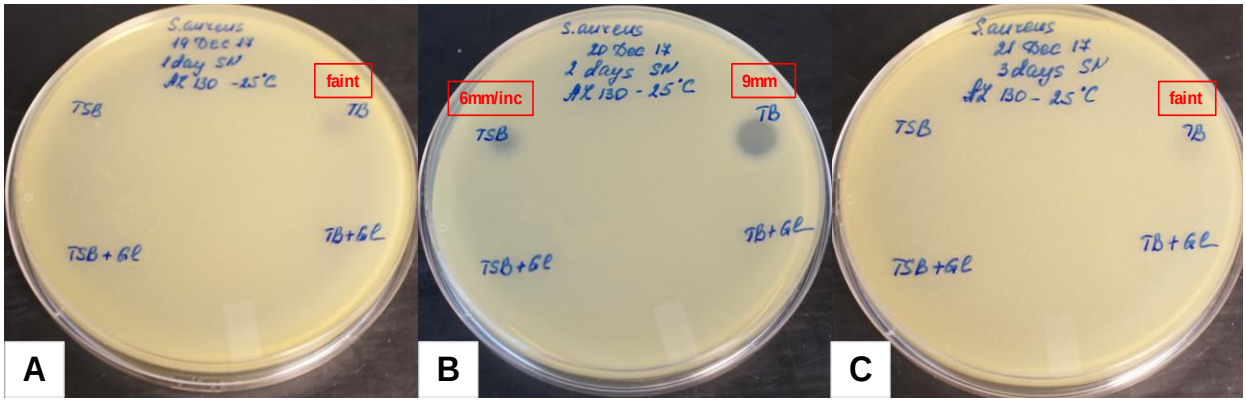

Fig. 2. Inhibitory effect of AZ-130 supernatants collected from cultures grown at 25°C against *S.aureus*. A) Supernatants collected at day 1. Only supernatant clarified from TB medium showed faint activity. B) Supernatants collected at day 2. Supernatants clarified from TSB and TB media showed respectively 6 mm/incomplete and 9 mm activity. C) Supernatants collected at day 3. Supernatant clarified from TB medium showed faint activity.

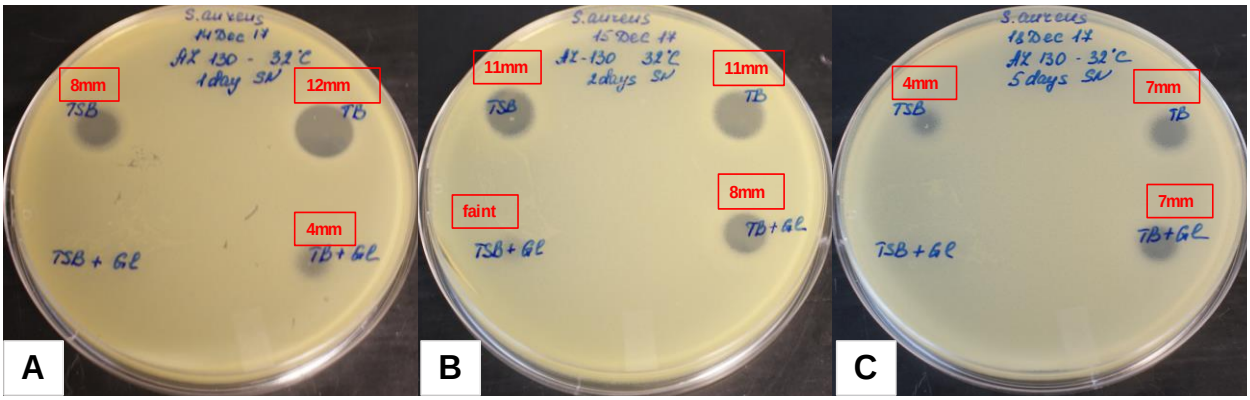

Fig. 3. Inhibitory effect of AZ-130 supernatants collected from cultures grown at 32°C against *S.aureus*. A) Supernatants collected at day 1. Supernatants clarified from TSB, TB and TB + 2% Glucose media showed respectively 8 mm, 12 mm and 4 mm activity. B) Supernatants collected at day 2. All clarified supernatants had an activity: TSB – 11 mm, TB – 11 mm, TSB + 2% Glucose – faint, TB + 2% Glucose – 8 mm. C) Supernatants collected at day 5. Supernatants clarified from TSB, TB and TB + 2% Glucose media showed respectively 4 mm, 7 mm and 7 mm activity.

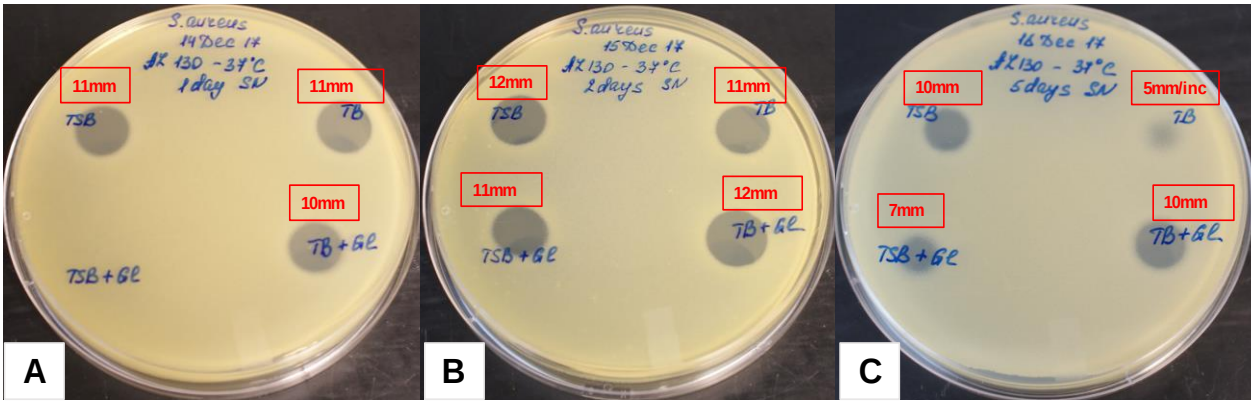

Fig. 4. Inhibitory effect of AZ-130 supernatants harvested from cultures grown at 37°C against *S.aureus*. A) Supernatants collected at day 1. Supernatants clarified from TSB, TB and TB+2% Glucose media showed respectively 11 mm, 11 mm and 10 mm activity. B) Supernatants collected at day 2. All clarified supernatants had an activity: TSB – 12 mm, TB – 11 mm, TSB + 2% Glucose – 11 mm, TB + 2% Glucose – 12 mm. C) Supernatants collected at day 5. All clarified supernatants had an activity: TSB – 10 mm, TB – 5 mm/incomplete, TSB + 2% Glucose – 7 mm, TB + 2% Glucose – 10 mm.

As can be seen from the Fig. 1 AZ-130 didn't produce any antimicrobial compound with gram-positive activity when it grown at 18°C; all supernatants collected at day 1, 2 and 3 didn't show any activity. In three other tested temperatures production of antimicrobial compound depends on media components and incubation time (Fig. 2-Fig. 4).

The production of AZ-130 compound by AZ-130 strain grown in TSB medium rises as the incubation time and temperature goes up (ZOI at day 1: 25°C – none, 32°C – 8 mm, 37°C – 11 mm; ZOI at day 2: 25°C – 6 mm/incomplete, 32°C – 11 mm and 37°C – 12 mm), before declining at day 3 or 5 (ZOI at 25°C – none, 32°C – 4 mm and 37°C – 10 mm).

The secretion of AZ-130 compound by AZ-130 strain grown in TB medium also fluctuates depending on growth temperature. Faint activity observed at day 1 from culture grown at 25°C sharply increases to strong 11-12 mm activity at 32°C and 37°C. The same upward trend in supernatants activities was observed at day 2 (ZOI at 25°C – 9 mm, at 32°C – 11 mm, at 37°C – 11 mm). AZ-130 partially loses its activity at day 3 or 5 (ZOI at 25°C – faint, 32°C – 7 mm, 37°C – 5 mm/incomplete).

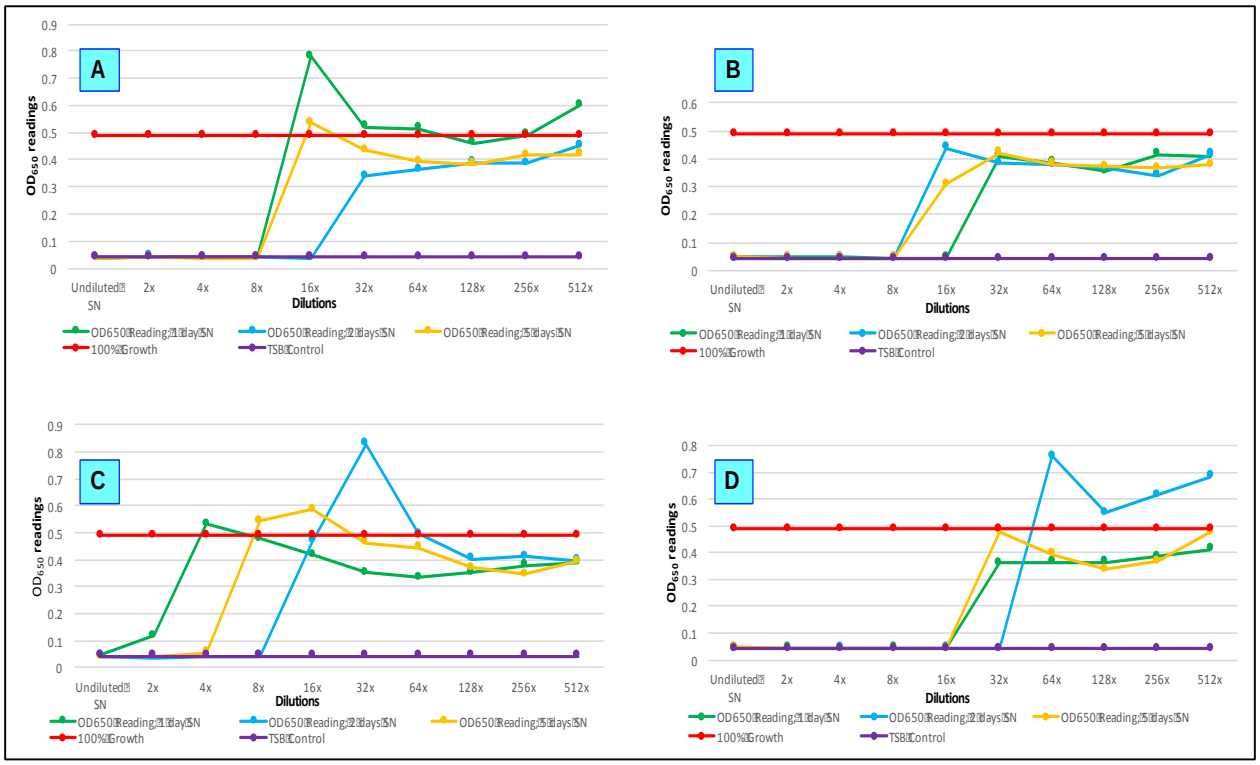

Fig. 5. Growth kinetics of *S.aureus* in the presence of AZ-130 supernatants (32°C) clarified from: A) TSB medium; B) TB medium; C) TSB + 2% Glucose; D) TB + 2% Glucose.

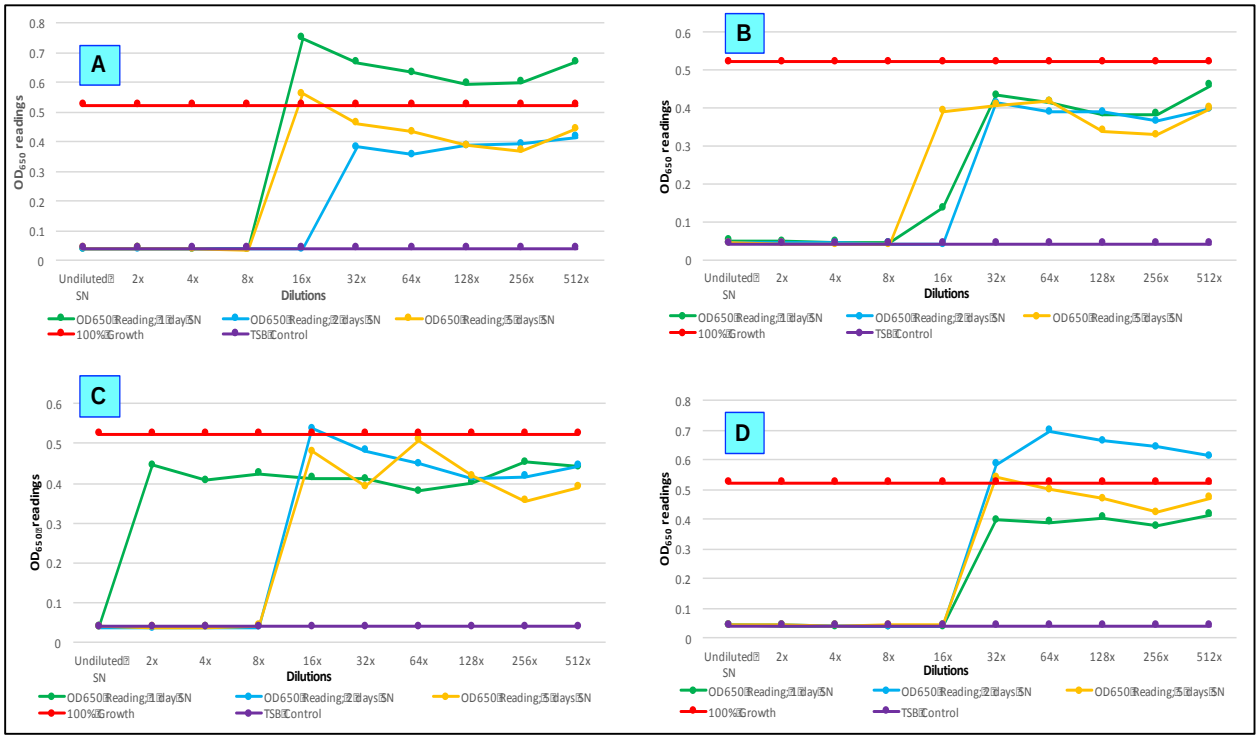

Fig. 6. Growth kinetics of *S.aureus* in the presence of AZ-130 supernatants (37°C) clarified from: A) TSB medium; B) TB medium; C) TSB + 2% Glucose; D) TB + 2% Glucose.

AZ-130 strain grown in TSB + 2% Glucose medium doesn't produce enough compound at day 1, however, at day 2 the concentration of compound grows as the temperature rises (ZOI at 25°C – no activity, 32°C – faint, 37°C – 11 mm) and decreases again at day 3 or 5 (ZOI at 25°C - none, 32°C – none and 37°C – 7 mm).

In terms of TB + 2% Glucose medium AZ-130 strain produces an antimicrobial compound when it grown at 32°C and 37°C. The activity of AZ-130 increases from 4 mm at day 1 to 8 mm at day 2 and slightly drops to 7 mm at day 5 (32ºC). Similar tendency in activity of AZ-130 observes at 37°C (ZOI at day 1 – 10 mm, day 2 – 12 mm and day 5 – 10 mm).

To summarize spot-test results, AZ-130 strain produces the most antimicrobial compound when it grown at 32°C and 37°C. We didn't observe any activity in supernatants collected from AZ-130 cultures grown at 18°C. We observed some activity in supernatants collected from AZ-130 cultures grown at 25°C, but those activities weren't as strong as they were in supernatants collected from cultures grown at 32°C and 37°C. In the next step, to be able to compare the concentration of bactericidal units in active supernatants, collected from cultures grown at 32°C and 37°C, they were analyzed by broth microdilution assay. Results of broth microdilution assay are presented in the Fig. 5 and Fig. 6.

As we see from the Fig. 5 in three out of four tested media at 32°C the highest production of AZ-130 observes at day 2. Supernatant collected from TSB + 2% Glucose active after eight-fold, from TSB after sixteen-fold and from TB+2% Glucose after thirty-two-fold dilution. Supernatant collected from TB medium shows its maximum activity of sixteen-fold at day 1.

From the Fig. 6 (growth of AZ-130 at 37°C) it's clear that the activity of sixteen-fold diluted AZ-130 compound collected from TB + 2% Glucose is stable even after five days of incubation. Supernatants of AZ-130 collected from TB and TSB media showed maximum activity of sixteen-fold at day 2; supernatants collected from TSB + 2% Glucose showed maximum activity of eight-fold at day 2 and day 5.

In summary, AZ-130 produces the most antibacterial compound when it grown in TB+2% Glucose medium at 32°C for 2 days. Observed activities are strong and stable, since AZ-130 biomolecule doesn't lose activity even after 5 days of incubation.

Summarized results of spot-test and broth microdilution assay are given in the Table 2.

Table 2. Summary of spot test and broth microdilution assay results.

Temperature	Medium	Agar spot test results ZOI, mm			Broth Microdilution results Active supernatants' dilution		
		SN at day 1	SN at day 2	SN at day 3 / day 5	SN at day 1	SN at day 2	SN at day 5
18°C	**TSB**	none	none	none			
	TB	none	none	none			
	TSB+2 % Glucose	none	none	none			
	TB +2 % Glucose	none	none	none			
25°C	**TSB**	none	6 /inc	none			
	TB	faint	9	faint			
	TSB + 2% Glucose	none	none	none			
	TB + 2% Glucose	none	none	none			
32°C	**TSB**	8	11	4	*8*	*16*	*8*
	TB	12	11	7	*16*	*8*	*8*
	TSB + 2% Glucose	none	faint	none	*undiluted*	*8*	*4*
	TB + 2% Glucose	4	8	7	**16**	**32**	**16**
37°C	**TSB**	11	12	10	*8*	*16*	*8*
	TB	11	11	5 /inc	*8*	*16*	*8*
	TSB + 2% Glucose	none	11	7	*undiluted*	*8*	*8*
	TB + 2% Glucose	10	12	10	**16**	**16**	**16**

CONCLUSION

Discovery and development of a new antimicrobial compound, from target identification through approval for marketing, is a very long and expensive process (Ekins S., 2019). One of the main steps in antibiotics development is the optimization of growth conditions of the producer strain to maximize the final metabolite yield (Singh et al, 2017; Arul Jose et al., 2013; Wang et al., 2011).

The results obtained fully confirm the importance of optimizing even the most insignificant parameters of growing medium. Temperature, incubation time, media components play significant role in the production of AZ-130 biomolecule by AZ-130 bacterial strain.

According to the spot-testing and 96-well plate microdilution assay results, AZ-130 strain produces the most antimicrobial compound in TB + 2% Glucose at 32°C; incubation time is 2 days. The production of AZ-130 compound in this medium is at least twofold higher in compare with all other tested conditions.

Further characterization of AZ-130 compound will involve the isolation/purification of secreted bioactive compound from cell-free culture supernatant, determination of MIC values against pathogenic lab and clinical strains, determination the chemical structure of novel biomolecule and confirmation the antimicrobial activity in vivo.

ACKNOWLEDGEMENTS:

The article was prepared based on results of experiments carried out during 2014-2018 years at the Fraunhofer USA Center for Molecular Biotechnology. The presented work is a part of the doctoral thesis to be submitted to the Institute of Molecular Biology and Biotechnologies of Azerbaijan NAS. The author would like to thank prof. I.M.Huseynova (Institute of Molecular Biology and Biotechnologies of Azerbaijan NAS), prof. V.M.Yusibov (Institute of Molecular Biology and Biotechnologies of Azerbaijan NAS); Indiana Biosciences Research Institute, IN, USA), prof. S.J.Streatfield (Fraunhofer Center for Molecular Biotechnology, DE, USA), prof. J.Karczew-ski (Fraunhofer Center for Molecular Biotechnology, DE, USA), prof. S.Goldman (Evolva, CA, USA) and C.M.Morris (Hygiena/Qualicon Diagnostics LLC, DE, USA) for their support and assistance.

REFERENCES

Arul Jose P., Sivakala K.K., Jebakumar S.R. (2013) Formulation and statistical optimization of culture medium for improved production of antimicrobial compound by *Streptomyces* sp. JAJ06. *Int. J. Microbiol.* **2013:** Article ID 526260.

Coyle M.B. et al. (2005) Manual of Antimicrobial Susceptibility Testing. AS for Microbiology.

Demain A.L., Fang A. (2000) The natural functions of secondary metabolites. *Adv. Biochem. Eng. Biotechnol.,* **69:** 1-39.

Ekins S., Puhl A.C., Zorn K.M., Lane T.R., Russo D.P., Klein J.J, Hickey A.J., Clark A.M. (2019) Exploiting machine learning for end-to-end drug discovery and development. *Nature Materials*, **18:** 435–441.

Gokulan K., Khare S., Cerniglia C. (2014) Production of secondary metabolites of bacteria. *Encyclopedia of Food Microbiology*, **2nd Ed.** Elsevier, p. 561-569.

Hockett K.L., Baltrus D.A. (2017) Use of the soft-agar overlay technique to screen for bacterially produced inhibitory compounds. *J. Vis. Exp.*, **119:** 55064.

Johnning A., Karami N., Tång Hallbäck E. et al. (2018) The resistomes of six carbapenem-resistant pathogens - a critical genotype-phenotype analysis. *Microbial Genomics*, **2018:** 4

Jones M.B., Nierman W.C., Shan Y., Frank B.C., Spoering A., Ling L., Peoples A., Zullo A., Lewis K., Nelson K.E. (2017) Reducing the bottleneck in discovery of novel antibiotics. *Microbial Ecology*, **73(3):** 658-667.

Lerminiaux N.A., Cameron A.D.S. (2019) Horizontal transfer of antibiotic resistance genes in clinical environments. *Can. J. Microbiol.,* **65(1):** 34-44.

Otto M. (2013) Community-associated MRSA: what makes them special? *Int. J. Med. Microbiol.,* **303(6-7):** 324-30.

Singh V., Haque S., Niwas R., Srivastava A., Pasupuleti M., Tripathi C.K. (2017) Strategies for fermentation medium optimization: An in-depth review. *Front. Microbiol.,* **7:** 2087.

Wang Y., Fang X., An F., Wang G., Zhang X. (2011) Improvement of antibiotic activity of *Xenorhabdus bovienii* by medium optimization using response surface methodology. *Microb. Cell Fact.*, **14(10):** 98.

Azərbaycan torpaqlarından ayrılmış AZ-130 bakteriya ştamının yüksək miqdarda antibakterial birləşmənin sintezi üçün böyümə şəraitinin optimallaşdırılması

A.Q. Ağayeva

AMEA Molekulyar Biologiya və Biotexnologiyalar İnstitutu

2014-cü ildə Azərbaycandan toplanmış torpaq nümunəsindən AZ-130 ştamı ayrılmışdır. Yeni antibakterial birləşmələrin aşkarlanması üçün aparılmış ilkin kultura və supernatant skrininqinin nəticəsində AZ-130 ştamı *Staphylococcus aureus* və *Enterococcus faecalis* qram-müsbət patogenlərə qarşı güclü fəallıq göstərmişdir. Onun fəallığını nəzərə alaraq, AZ-130 antibakterial birləşməni istehsal edən AZ-130 ştamı xüsusiyyətlərinin daha dərin öyrənilməsi üçün seçilmişdir. Aparılmış tədqiqat işinin məqsədi antimikrob birləşmənin istehsalının ən yüksək olduğu optimal mühit, inkubasiya temperaturu və zaman nöqtəsini müəyyənləşdirmək üçün AZ-130 ştamının böyümə şəraitinin optimallaşdırılmasıdır. Bu məqsədə, 16 fərqli böyümə şəraiti (4 fərqli temperaturda 4 fərqli mühit növü) yoxlanılmışdır. Supernatantlar 1-ci, 2-ci və 3/5-ci günlərdə toplanaraq təmizlənmişdir. Toplanan bütün supernatantlar bakteriyanın böyüməsinin inhibə edilməsi və mikrodurulaşdırma metodları ilə təhlil edilmişdir. Əldə edilmiş nəticələrə əsasən, AZ-130 biomolekulunun ən yüksək istehsalı AZ-130 ştamının 32°C-də TB + 2% glükoza mühitində müşahidə edilir.

Açar sözlər: *Antimikrob fəallıq, antibiotiklər, bioaktiv molekullar, kultural mühit, böyümə mühitinin optimallaşdırılması, təbii məhsullar, ilkin metabolit, ikinci metabolit, patogen bakteriyalar*

Оптимизация условий культивирования для более высокой продукции антимикробных соединений бактериальным штаммом AZ-130, выделенным из почвы Азербайджана

А.Г. Агаева

Институт молекулярной биологии и биотехнологий НАН Азербайджана

Штамм AZ-130 был изолирован из образца почвы, отобранного в Азербайджане в 2014 году. После предварительного скрининга на наличие антимикробной активности в культуре и в супернатанте, AZ-130 показал сильную грамположительную активность против патогенных *Staphylococcus aureus* и *Enterococcus faecalis* штаммов. Учитывая активность штамма AZ-130, который продуцирует антибактериальное соединение AZ-130, он был выбран для более детального изучения его характеристик. Основной целью данной работы являлась оптимизация условий выращивания штамма AZ-130, т.е. определение оптимальной среды, температуры инкубации и времени культивирования, при которых синтез антимикробного соединения достигает наивысших значений. Для достижения поставленной цели были протестированы 16 различных условий культивирования (4 разных типа среды при 4 разных температурах). Супернатант клеточной культуры собирали и очищали в 1-й, 2-й и 3-й/5-й дни. Очищенные супернатанты анализировали методом подавления роста и микроразведения в бульоне. Согласно полученным результатам, штамм AZ -130 продуцирует наибольшее количество антимикробного соединения AZ -130, в условиях. когда культивирование осуществляется в течение 2-х дней при температуре 32°C на среде TB с добавлением 2% глюкозы.

Ключевые слова: *Антимикробная активность, антибиотики, биоактивные молекулы, условия культивирования, оптимизация среды, натуральные продукты, первичный метаболит, вторичный метаболит, патогенные бактерии*

Journal of Life Sciences and Biomedicine, vol. 1 (74), No 1, p. 77-83 (2019)

Comparative characteristics of the facial skull size of an adult, depending on the shape of the nose

V.B. Shadlinsky*, S.A. Aliyeva

*Department of Human Anatomy and Medical Terminology, Azerbaijan Medical University, 1 S.Vurgun str., Baku AZ1022, Azerbaijan; *For correspondence: medun91@mail.ru*
Accepted for publication: 22 August 2019

The craniometrical indicators of the facial skull were studied in 40 specially selected human skulls from the craniological collection of the fundamental museum of the human anatomy department of the Azerbaijan Medical University. It was established that among the studied skulls, mesoproseps prevail in the shape of the facial skull, and leptorrhines in the shape of the nose. In the female series, a significant asymmetry was determined by the nazion-zygomaxillary indicator for chamerins left-sided, for leptorrhines right-sided, whereas in the mezorin group the asymmetry was right-sided and insignificant. A steady trend towards left-sided asymmetry was found in almost all indicators of the "side fan" in the men's series. The only exception was the distance from the point of the zygomaxillary to the lowest point of the pear-shaped hole, along which the right-sided asymmetry was noted in the male series.

Keywords: *Asymmetry, facial skull, fan morphometry method, superscript face*

INTRODUCTION

Asymmetry of the face - an important factor in the individuality of beauty. According to the literature, it can be noted that the asymmetry of the face is caused by changes in the soft tissues, facial vessels, muscles, including changes in the bones of the skull, but if there are many articles devoted to soft tissue structures and a range of diagnostic and therapeutic manipulations is directed to them, then the bone structure is not studied so far.

If a lot of scientific papers are devoted to soft tissue structures (Ponomareva, 2010; Hwang et al., 2012; Nur et al., 2014; Starbuck et al., 2016), the asymmetry of the bone structures on different forms of the skull, especially in the sexual aspect, has been little studied (Nikolayeva, 2007; Zhang et al., 2013). It should be noted that among the diversity of the bony structures of the facial skull and its formations, the external nose occupies a central place as the most cosmetically and aesthetically important formation, the shape and size of which determine not only the beauty of the human face, but are paramount in the formation of facial asymmetry (Khrappo and Tarasova, 1999; Gayvoronsky et al., 2009).

The aim of the work was to study the size of the facial skull in an adult, depending on the shape of the nose.

MATERIALS AND METHODS

Individual and gender differences in craniometrical indices of the facial skull were studied on 40 specially selected human turtles from the craniological collection of the fundamental museum of the human anatomy department of the Azerbaijan Medical University.

To realize this goal, a comprehensive study was conducted. The essence of which lies not only in the measurement of the morphometric parameters of the facial skull, but also in the assessment of the size between standard and non-standard points by the original method.

The measurements were carried out according to the method of R. Martin in compliance with the existing craniometrical requirements used in anthropological research (Martin, 1928). For the measurement of the relevant parameters, thickening, coordinate, and sliding compasses were used, as well as a soft flexible ruler. The measurement accuracy reached 0.5 mm. The work

mainly used standard craniometrical points, some of which are used in clinical practice.

The following dimensions of the facial skull and nasal area are measured:

1. Upper face width - the distance between the points of the fronto-molar-temporal (between the outermost points of the frontal-zygomatic suture);
2. Zygomatic diameter - the greatest distance between the outer surfaces of the zygomatic arches;
3. The upper height of the face - the distance between the nasion point and the alveolar point - the lowest point of the upper jaw alveolar edge between the medial incisors;
4. Dacrial width - the distance between the points of the orbit (dacrion), located at the junction of the frontal and lachrymal bones with the frontal process of the upper jaw;
5. The upper front pointer;
6. Nose width - the greatest distance between the outer edges of the pear-shaped hole;
7. Nasal index - the ratio of the zygomatic width to the upper height of the face expressed as a percentage.

According to the nasal index, the studied skulls were divided into 3 groups (Martin, 1928):

1. Leptorrhines (narrow nose) (ind. nose <43.5 - 47.5);

2. Mezorins (average width of the nose) (ind. nose 47.6 - 52.1);

3. Chamerins (wide nose) (ind. nose> 52.2).

The characteristic of the group of skulls that we study was carried out on the basis of the upper index of the face. The upper index of the face is the ratio of the upper height of the face (the distance between the nazion and the most prominent point of the lower jaw) to its width (the distance between the extreme points of the zygomatic bones) multiplied by 100 (Martin, 1928).

All the studied skulls on the superscript of the face were divided into 3 groups: Wide-faced (Eiren) (ind. <49.9), average face width (mezen) (ind. 50.0 - 54.9), narrow-faced (leptin) (ind.> 55.0).

To study the asymmetry of the facial skull and was used “fan method of morphometry” (Gayvoronsky, 2009). The proposed method allows us to estimate the asymmetry in different parts of the facial skull. All studied parameters were divided into three “fans” - “upper”, “lower”, “lateral”, outgoing from three standard points: Nazion (N is the point located on the nasal seam), subspinal (Ss is the point located under the front nasal spine), zygomaxillary (Zm - point located in the lower part of the jaw joint).

The digital data of our study were subjected to statistical processing, observing the general provisions for medical and biological research. The data were processed by a variation-statistical method using the Statistical application package (Statsoft, 1999) and Microsoft Excel Windows-7 (Borovikov, 2015).

RESULTS AND DISCUSSION

We have established that leptorrhines predominate in the total sample, mezorines are in second place in terms of frequency, and chamerins are in third place in frequency. Thus, it can be concluded that mesoproteins predominate in the shape of the facial skull, but in the shape of the leptorrhine nose (Table 1).

To characterize the facial skull and nasal region, 14 standard linear dimensions and 2 indices (upper facial and nasal) were included.

All studied parameters were divided into three "fans" - "upper", "lower" and "lateral", coming from the following standard points: nasion, subspinale, zygomaxillary (n is a point located on the nasaloneal suture, ss is a point, located under the anterior nasal spine, zm is the point located in the lower part of the zygomatic-jaw seam).

A comparative analysis of unpaired indicators by sex and depending on the width of the nose indicates the following:

1) The width of the nasal bones at the level of the nasal-frontal suture (n-fr).

This indicator varies, on average, from 9.2±0.8 mm for hamerins to 11.7±0.4 mm for leptorrhines in the female skull series and from 11.7±1.8 mm for hamerins to 13.1±0.5 mm for leptorrhines in the male series of skulls, with an average value in the total sample of 12.2±0.6 mm.

Table 1. Quantitative distribution of the studied group of skulls depending on the size of the nasal index.

No		The value of the index (in one)	Characteristics of the skulls in the total sample	
			Quantity (in one)	Quantity (in %)
1	Leptorrhines	<43.5-47.5	19	47.5
2	Mezorins	47.6-52.1	14	35.0
3	Chamerins	>52.2	7	17.5

Table 2. Statistical indicators of women with various forms of the external nose.

No	Investigated trait	Research side	Statistical indicators					
			Chamerins	Difference between states	Mezorins	Difference between states	Leptorrhines	Difference between states
1	n-zm	right	63.30±0.75	-0.90	66.07±0.96	0.14	72.70±0.98	5.01
		left	64.20±0.80		65.93±0.94		67.69±1.05	
2	n-fmt	right	51.85±0.80	0.35	53.25±0.69	0.04	53.48±0.48	0.08
		left	51.50±0.84		53.21±0.60		53.40±0.46	
3	n-ft	right	49.10±0.64	-0.05	48.86±0.52	-1.43	49.88±1.02	-0.86
		left	49.05±0.63		50.29±0.69		50.74±0.45	
4	n-ap. inf	right	46.27±0.67	-0.28	48.09±0.87	-0.37	48.81±0.73	-0.29
		left	46.55±0.68		48.46±0.79		49.10±0.69	
5	n-ap.lat	right	41.10±0.62	-0.05	42.94±0.69	-0.02	44.42±0.71	0.51
		left	41.15±0.60		42.96±0.62		43.91±0.69	
6	n-infr	right	39.80±0.80	-0.65	41.96±0.86	-0.10	43.15±0.77	-0.05
		left	40.45±0.83		42.06±0.83		43.20±0.83	
7	n-max width	right	24.45±1.08	-0.36	27.16±0.71	-0.77	27.36±0.65	0.35
		left	24.81±1.12		29.93±0.61		27.01±0.79	
8	n-da	right	14.95±0.61	-0.63	16.19±0.40	0.65	15.78±0.32	-0.06
		left	15.58±0.75		15.54±0.79		15.84±0.31	
9	n-min width	right	8.13±0.42	0.26	10.19±0.42	-0.05	9.69±0.33	0.61
		left	7.77±0.42		10.24±0.41		9.08±0.32	
10	n-fn seam	right	6.67±0.58	-0.01	7.61±0.56	0.05	7.67±0.25	-0.29
		left	6.68±0.59		7.56±0.58		7.96±0.33	

2) Nose length (n-rhin). The value of this non-standard indicator in mm varies, on average, from 23.1±0.7 mm for leptorrhines to 17.7±1.4 mm for chamerins in the men's skull series, with an average value of this indicator in the total sample of 21.0±0 , 7 mm and from 20.4±0.7 mm in leptorrhines to 19.8±0.9 mm in chamerins in the female skull series with an average value of this feature in the total sample of 20.3±0.9 mm.

3) The height of the pear-shaped hole (rliin-sp). This indicator varies across the width of the nose: from 36.4±0.8 mm in leptorrhines to 32.5±1.0 mm in chamerins in the male series of skulls, with an average value of this indicator in the total sample of 32.9±0.8 mm. The following signs on the characteristic of asymmetry of the facial skull of the "upper fan" were measured in pairs to the left and to the right.

Their dimensions in mm were arranged in descending order separately for the male and female series of skulls.

In the women's series, significant asymmetry in terms of the nasion-zygomaxillary indicator of the chamerins is left-sided, in the leptorrhines it is right-sided, while in the group of mezorins, the asymmetry is right-sided and insignificant. With regard to the asymmetry of the nasion-frontotemporal index, there is a weak right-sided asymmetry in chamerins and significant asymmetry in the group of meso and leptorrhines (table 2). The asymmetry of the nasion-nasomaxillary index varies from weak left-sided with chamerins to strong left-sided in the mezorin group, opposite to chemerins.

Of particular interest is the size of the nasion-front-molar-temporal in the male series, where the dimensions on the right vary, on average, from 55.3±1.4 mm for chamerins to 56.4±0.5 mm for leptorrhines, while the average sizes for mezorins make up 56.5±0.51mm.

Table 3. Statistical indicators of men with various forms of the external nose.

№ right/right	Investigated trait	Research side	Statistical indicators					
			Chamerins	Difference between states	Mezorins	Difference between states	Leptorrhines	Difference between states
1	n-zm	right	69.50±0.38	0.60	71.87±0.82	-0.31	67.48±0.67	-5.02
		left	69.40±0.21		72.88±0.86		72.50±0.72	
2	n-fmt	right	55.30±0.43	-0.60	56.51±0.51	-1.73	56.36±0.43	0.23
		left	55.90±0.41		58.24±0.78		56.13±0.45	
3	n-ft	right	51.92±0.95	0.12	53.59±0.54	-0.07	54.83±0.56	1.19
		left	51.80±0.86		53.66±0.47		52.84±0.58	
4	n-ap. inf	right	48.04±0.50	-0.76	49.80±0.75	-0.04	52.52±0.55	-1.45
		left	48.80±0.62		49.84±0.84		53.97±0.46	
5	n-ap.lat	right	43.50±0.40	0.28	45.25±0.64	-0.07	47.03±0.43	-0.08
		left	43.22±0.53		45.32±0.65		47Д2±0.46	
6	n-infr	right	42.20±1.06	-1.04	45.27±0.63	0.25	46.37±0.27	0.42
		left	43.24±0.61		45.02±0.61		45.95±0.37	
7	n-max width	right	31.50±0.35	5.90	27.78±0.68	-0.27	29.07±0.74	-0.46
		left	25.60±0.77		28.05±0.62		29.23±0.70	
8	n-da	right	17.30±0.83	-0.30	17.29±0.40	-0.08	17.74±0.37	0.25
		left	17.60±0.68		17.37±0.23		17.49±0.35	
9	n-min width	right	9.40±1.08	-0.08	10.18±0.49	-0.06	11.09±0.38	1.34
		left	9.48±0.98		10.24±0.45		9.75±0.34	
10	n-fn seam	right	7.94±1.08	-0.04	8.00±0.50	0.02	8.90±0.34	0.06
		left	7.98±1.11		7.88±0.46		8.84±0.31	

Similarly, the left dimensions: from 55.9±1.1 mm for chamerins to 56.1±0.5 mm for leptorrhines, with an average size of 58.2±1.8 mm.

Table 3 shows the dimensions of the facial skull in the shape of the nose in the men's series, asymmetry sizes are calculated according to the indicators of the “upper fan” from the nasion point (table 3).

From the data obtained, it follows that the most significant left-sided asymmetry is observed in terms of nazion-zygomaxillary in leptorrhines in the male skull series, and the most significant right-sided asymmetry is observed in terms of nazion-naxomaxillary in chamerins in the same group.

Further, a significant left-sided asymmetry can be noted in terms of the nazion-front-molar-temporal variable in the mezorins in the male series of skulls.

In terms of the nasion-frontotemporal and distance from the nasion point to the junction of the nasal bones, significant right-sided asymmetry is observed in the male skull series in leptorrhines and the distance from the point to the lowest point of the pear-shaped hole – significant left-sided asymmetry in leptho and chamerins in the same group.

In a comparative analysis of the female and male series of skulls, it can be noted that in terms of the nasion-zygomaxillary indicator, the leptorrhines in the female series have a significant right-sided asymmetry, while the leptorrhines in the men's series have significant left-sided asymmetry. In terms of the nasion-front-wheel-molar-temporal index, in the female series, there is a slight right-sided asymmetry in all three groups, while in the male series, for chamerins and mezorins, there is left-sided asymmetry and for leptorrhines, there is insignificant right-sided asymmetry.

In terms of the nasion-frontotemporal index, in the female series, there is significant left-sided asymmetry in meso- and leptorrhines, whereas in the men's series, in leptorrhines, there is significant right-sided asymmetry.

In terms of the indicator from the nazion point to the lowest point of the pear-shaped hole, there is left-sided asymmetry in the women's and masculine series, and this is slightly pronounced in the women's series, and significantly in the masculine series.

In terms of the nion-infraorbital indicator, wide-bearing men and women show significant left-sided asymmetry. In terms of the nasion-naso-maxillary indicator, a significant left-sided asym-

metry is observed in the female skull series with medium nose sizes, whereas in the male series, the left-sided asymmetry is negligible.

Wide-nosed men have a very significant right-sided asymmetry. Whereas, in the female skull series it is insignificant and left-sided. In terms of the distance from the nasion point to the junction of the nasal bones, narrow-pointed men and women show significant right-sided asymmetry.

The fact of asymmetry in the external structure of the face and body of man has been known since ancient times to artists and sculptors of the ancient world, and was used by them to impart expressiveness and spirituality to their works (Alekseyev and Alekseyeva, 1989).

All human asymmetries are divided into static (proportions, dimensions, weight, volume, etc.) and functional: motor (motor), sensory (sensitive) and, mental or sensual (Kibkalo, 2006).

Among the morphological asymmetries of the face, the deviation of the nose to the right is expressed in right-handers and to the left in left-handers; the right half of the face most people have more than the left half (Koff and Borod, 1981).

The data obtained indicate that in the female series, significant asymmetry is determined by the nazion-zygomaxillary indicator for left-sided chamerins, left-sided in leptorrhines, while asymmetry in the mezorin group is right and minor.

According to I.V.Gayvoronsky and S.Y.Baybakov (2008) points of the infraorbital and zygomaxillary are the attachment points of the mimic muscles. Consequently, the difference in size for these parameters is due to the functional asymmetry of the mimic muscles along the "side fan" asymmetry is almost negligible, both left and right (Gayvoronsky and Baybakov, 2008).

When analyzing the data obtained, a steady trend towards left-sided asymmetry can be noted in almost all indicators of the "side fan" in the men's series. The only exception is the distance from the point of the zygomaxillary to the lowest point of the pear-shaped hole, along which the right-sided asymmetry is noted in the men's series.

According to Y.I.Dubovik (2009), the asymmetry of the dimensions of the "side fan" is influenced by the mimic muscles of the muscle. Thus, the tone of the facial muscles raising the upper lip, zygomatic, nasal and cheek muscles causes a change in the shape and size of the bony structures of the facial skull (Dubovik, 2009).

CONCLUSIONS

1. Among the studied skulls, mesoprozeps predominate in the shape of the facial skull, and not the nose form leptorrhines.
2. In the female series, significant asymmetry is determined by the nasion-zygomaxillary index in skulls with a wide nose with left-sided, in skulls with a long nose-right-sided, whereas in the group of skulls with a nose-like asymmetry a slight right.
3. A steady trend towards left-sided asymmetry in almost all indicators of the "side fan" in the men's series. The only exception is the distance from the point of the zygomaxillary to the lowest point of the pear-shaped hole, along which the right-sided asymmetry is noted in the men's series.

REFERENCES

Alekseyev V.P., Alekseyeva T.I. (1989) Anthropology in medicine. M.: Publ. Moscow University, 243 p.

Borovikov V.P. (2015) Popular introduction to modern data analysis in the system STATISTICA. Moscow: Telecom, 288 p.

Dubovik Y.I. (2009) Asymmetry of the facial skull in its various forms in an adult: *PhD. Thesis.* St. Petersburg: 156 p.

Gayvoronsky I.V., Baybakov S.Y. (2008) Individual anatomical variability: Historical and methodological aspects. *Journal of Experimental and Clinical Surgery*, **1:** 65-72.

Gayvoronsky I.V., Dubovik Y.I., Kraynik I.V. (2009) Morphometric indicators of the asymmetry of the facial skull in an adult. *Morphology*, **2:** 74-79.

Hwang H., Yuan D., Jeong K. et al. (2012) Three-dimensional soft tissue analysis for the evaluation of facial asymmetry in normal occlusion individuals. *Korean J. Orthod.*, **42(2):** 56-63.

Khrappo N.S., Tarasova N.V. (1999) Nose in whole-skull system. Samara: San. SMU, 172 p.

Kibkalo A.P. (2006) Know Your Face. Volgograd. 150 p.

Koff E., Borod J.C., White O. (1981) Asymmetries for hemiface size and mobility. *Neuropsychologic*., **19(6):** 825-830.

Martin R. (1928) Kraniologie a кraniometrische technik. Auft., Jena: 214вd

Nikolayeva Y.Y. (2007) Influence of the asymmetry of the facial skeleton on the severity of anomalies of the dental system and its orthodontic correction: *Abstract. of PhD. Thesis.* Tver: 21 p.

Nur R., Çakan D., Arun T. (2016) Evaluation of facial hard and soft tissue asymmetry using cone-beam computed tomography. *Am. J. Orthod. Dentofacial Orthop*., **149(2):** 225-237.

Ponomareva T.V. (2010) Formation of functional asymmetries in early ontogenesis: *PhD Thesis.* Krasnodar: 163 p.

Starbuck J., Ghoneima A., Kula K. (2014) Facial soft-tissue asymmetry in three-dimensional cone-beam computed tomography images of children with surgically corrected unilateral clefts. *J. Craniofac. Surg.*, **25(2):** 476-480.

Zhang Y., Che B., Ni Y. et al. (2013) Three-dimensional condylar positions and forms associated with different anteroposterior skeletal patterns and facial asymmetry in Chinese adolescents. *Acta Odontol Scand.*, **71(5):** 1174-1180.

Burunun formasından asılı olaraq insanın kəlləsinin ölçülərinin müqayisəli xüsusiyyətləri

V.B. Shadlinski, S.A. Əliyeva

Azərbaycan Tibb Universitetinin İnsan anatomiyası və tibbi terminologiyası kafedrası

Üz kəlləsinin kraniometrik göstəriciləri Azərbaycan Tibb Universitetinin insan anatomiyası və tibbi terminologiya kafedrasının əsas muzeyinin kranioloji kolleksiyasından xüsusi seçilmiş 40 insan kəlləsi üzərində tədqiq edilmişdir. Müəyyən edilmişdir ki, öyrənilən kəllələr içərisində üz kəlləsinin formasına görə üzlülər, burunun formasına görə ensiz burunlar üstünlük təşkil edir. Qadın kəllələri içərisində nasion-ziqomaksilyar məsafənin göstəricisinə burunun enli formalarında sol tərəfli, uzun formalarında sağ tərəfli, orta formalarında zəif sağ tərəfli asimmetriya müəyyən edilmişdir. Kişi kəllələrində "Yan yelpik"in bütün göstəricilərində sol asimmetriyaya meyllilik aşkar edilmişdir. Ancaq ziqomaksilyar nöqtədən armudu dəliyin aşağı nöqtəsi arasındakı məsafədə sağ tərəfli asimmetriya müşahidə edilmişdir.

Açar sözlər: *Asimmetriya, üz kəlləsi, kraneometryanın yelpik üsulu, üzün yuxarı indeksi*

Сравнительная характеристика размеров лицевого черепа у взросло человека в зависимости от формы носа

В.Б. Шадлинский, С.А. Алиеав

Кафедра анатомии человека и медицинской терминологии Азербайджанского медицинского университета

Краниометрические показатели лицевого черепа были изучены на 90 специально подобранных черепах людей из краниологической коллекции фундаментального музея кафедры анатомии человека Азербайджанского медицинского университета. Установлено, что среди изученных черепов по форме лицевого черепа преобладают мезопрозепы, а по форме носа лепторины. В женской серии определяется значительная асимметрия по показателю назион-зигомаксилляре: у черепов широким с носом - левосторонняя, у черепов с длинным носом - правосторонняя, тогда как в группе черепов со средним носом - асимметрия незначительная правосторонняя. Устойчивая тенденция к левосторонней асимметрии отмечена практически по всем показателям «бокового веера» в мужской серии. Исключение составляют расстояние от точки зигомаксилляре до наиболее нижней точки грушевидного отверстия, по которой отмечается правосторонняя асимметрия в мужской серии.

Ключевые слова: *Асимметрия, лицевой череп, веерный метод морфометрии, верхний индекс лица*

Journal of Life Sciences and Biomedicine, vol. 1 (74), No 1, p. 84-88 (2019)

Features of the density of the location and changes in the cellular composition of the lymphoid formations of the vaginal vestibule of rats after a treatment course of naphthalan baths

S.V. Shadlinskaya*

*Department of Human Anatomy and Medical Terminology, Azerbaijan Medical University, 1 M. Sanani str., Baku AZ1022, Azerbaijan; *For correspondence: sh.sabina23@gmail.com*
Accepted for publication: 14 August 2019

The purpose of the study was to analyze the changes in the quantity and qualitative composition of the lymphoid tissue of the walls of the rat's vaginal vestibule after a treatment course of naphthalan baths. The lymphoid formations of the walls of the vaginal vestibule of sexually mature female Wistar rats subjected to naphthalan baths were investigated. Obtained digital data were subjected to statistical processing. Morphological analysis showed that in the mucous membrane of the vaginal vestibule in rats of both experimental groups, as well as in the control, all forms of lymphoid tissue are present. Lymphoid formations of the vaginal vestibule are located near the initial parts of the glands. The lymphoid formations of the mucous membrane of the vaginal vestibule of rats do not actually change quantitatively and qualitatively after the course effect of freshwater baths, which indicates their safety. The treatment course of naphthalan baths causes an increase in the number of cells of the lymphoid tissue in all lymphoid formations, activation of lymphocytopoietic processes, a decrease in the level of cellular degeneration of lymphoid tissue.

Keywords: *The vaginal vestibule, the lymphoid nodules, the diffuse lymphoid tissue*

INTRODUCTION

Vaginal pathology is a significant medical and social problem that requires the development of new and the updating of existing means of treatment, prevention and rehabilitation (Scherbina and Lamia, 2016). Significant importance in the organization of therapeutic and preventive measures is given to balneological procedures, especially with the use of naphthalan baths, the effectiveness of which has been repeatedly proved in gynecological practice (Kyazimov, 2009). The effect of naphthalan, according to the prevailing opinion, is mainly caused by the presence in its composition of polycyclic naphthenic hydrocarbons, which are also present in the composition of various hormones, bile acids, vitamin D and some other biologically active substances (Badalov, 2003). The anti-inflammatory effect of naphthalan oil is provided by its anti-allergic effects (Sizyakova, 2010).

At the same time, there are almost no experimental studies of the effectiveness and safety of naftalan effects in the scientific literature, there have been almost no experimental morphological studies on this subject, or they have been extremely superficial. At present, it has been established that one of the most adequate markers of any external environmental influences is lymphoid tissue (Nikityuk and Klochkova, 2015).

The purpose of the study was to analyze the changes in the quantity and qualitative composition of the lymphoid tissue of the walls of rat's vaginal vestibule after a course of naphthalan baths.

MATERIALS AND METHODS

The lymphoid formations of the walls of the vaginal vestibule of adult Wistar rats subjected to experimental exposure to naphthalan baths (30 rats) were investigated according to the schemes adopted in modern balneological practice. Lymphoid formations of the vaginal vestibule were also studied in rats subjected to a fresh bath course (30 rats) and in intact 30 rats (control). Analysis of the vaginal smear confirmed the same state of the ovarian cycle (Oransky, 1998). The total dura-

tion of the treatment course of naphthalan and fresh baths is similar - 20 days. The duration of one exposure (bath) was 8–10 minutes, the bath temperature was 37-38°C. From the experiment, rats were derived simultaneously (by decapitation, in compliance with ethical norms). After fixation of the material in neutral formalin, subsequent alcohol wiring and paraffin embedding at the level of the anterior, middle and back third walls of the vaginal vestibule, 5–7 μm thick transverse sections were made and stained with hematoxylin-eosin and picrofuxin according to van Gieson

For the lymphoid tissue of the walls of the vaginal vestibule, the percentage of lymphoid nodules with a reproduction center was determined (the total set of lymphoid nodules on the cut was taken as 100%), the length, width and area of the cut at the lymphoid nodules with and without reproduction center, as well as the length, width and area of reproduction centers themselves. The density of the cells of the lymphoid series (their number on an area of 880 μm² cut) in the composition of the diffuse lymphoid tissue, lymphoid nodules without centers of reproduction, in the centers of reproduction and the mantle of lymphoid nodules was determined.

Obtained during the study of digital data were subjected to statistical processing. At the same time, general recommendations for medical and biological research were followed (Glantz, 1999).

RESULTS AND DISCUSSION

Morphological analysis showed that the mucosa of the vaginal vestibule in rats of both experimental groups, as well as in the control, contains all forms of lymphoid tissue, including intraepithelial lymphocytes, diffuse lymphoid tissue, lymphoid nodules with and without reproduction centers. Lymphoid mucous membranes of the vestibule are always located near the initial parts of the glands, accompanied by their excretory ducts in the form of a rim.

The performed morphometric analysis showed an almost complete absence of changes with respect to the control, after a course of fresh baths. On the contrary, naphthalan baths provide activation of lymphoid tissue formation processes. Thus, the proportion of lymphoid nodules with a center of reproduction (the most functionally mature form of lymphoid tissue) increases as a result of the bath course relative to the control, by 1.9 times ($p < 0.05$).

Localization density of lymphoid cells as part of lymphoid nodules without a reproduction center in the walls of the vaginal vestibule in rats of the experimental group as a result of a course of naphthalan baths, in the walls of the anterior third of the vestibule 1.39 times ($p < 0,05$), middle third 1.33 times ($p < 0.05$), and the back third - 1.29 times ($p < 0.05$) and for the vaginal vestibule as a whole - 1.33 times more ($p < 0.05$), compared with the control (Table 1).

In the reproduction centers, as a result of the treatment course of naphthalan baths, in the walls of the anterior third of the vestibule 1.31 times more ($p < 0.05$), in middle third - 1.32 times more ($p < 0.05$), in the back third is 1.45 times more ($p < 0.05$) and for the vaginal vestibule as a whole - 1.35 times more ($p < 0.05$), in comparison with the control (Table 2).

Table 1. The density of the lymphoid cells in the lymphoid nodules without a center of reproduction in the vaginal vestibule of rats after the treatment course of action naphthalan baths (X±Sx; min-max).

Nature of the effects	n	Part of the vaginal vestibule			
		Anterior third	Middle third	Posterior third	The vaginal vestibule as a whole
Naphthalan baths	30	29.2±0.5 21-33	29.5±0.5 24-36	32.6±0.5 27-38	30.4±0.4 26-35
Fresh baths	30	20.2±0.3 16-23	22.1±0.3 19-25	25.3±0.5 18-28	22.5±0.4 17-26
Control	30	20.9±0.4 15-24	22.1±0.4 18-26	25.3±0.5 19-29	22.8±0.4 17-26

Table 2. The density of the cells of the lymphoid series in the centers of reproduction of lymphoid nodules in the vaginal vestibule of rats after a treatment course of naphthalan baths (X±Sx; min-max).

Nature of the effects	n	Part of the vaginal vestibule			
		Anterior third	Middle third	Posterior third	The vaginal vestibule as a whole
Naphthalan baths	30	22.2±0.4 16-24	22.5±0.4 16-24	23.6±0.3 24-31	22.7±0.3 23-30
Fresh baths	30	16.2±0.3 13-20	16.1±0.3 13-20	16.3±0.3 15-21	16.2±0.3 13-20
Control	30	16.9±0.3 14-21	17.1±0.3 14-21	16.3±0.4 14-22	16.8±0.3 14-21

The result of the treatment with naphthalan baths is an increase in the percentage of lymphocytes (1.1-1.2 times, $p < 0.05$). There is an increase in the number of lymphoid cells with signs of mitosis (1.3-1.5 times), which indicates the activation of lymphocytopoiesis; the level of cellular destruction decreases - the number of cells with signs of degeneration (1.2-1.6 times, relative to the control). Similar changes in the cellular composition of the lymphoid tissue, as a result of the course action of iodine-bromine and organic bituminous baths, have previously been shown in the rat larynx lymphoid apparatus as an example (Seidova, 2001). Similar materials are cited by other authors who have studied the lymphoid apparatus of the larynx (Shadlinski and Movsumov, 2002; Movsumov, 2004), the trachea and the main bronchi (Huseynov, 2011), the lymphoid structures of the extrahepatic biliary tract (Allahverdiev, 2008).

Thus, the conducted studies revealed significant formative changes of the lymphoid apparatus of rat's vaginal vestibule after a course of naphthalan baths, proving the safety of these effects.

CONCLUSIONS

1. Lymphoid formations of the mucous membrane of the vaginal vestibule are always oriented mainly near the small glands of this area. Both for experimental and control observation groups, significant individual variations in the number of lymphoid cells in all morphogenetic forms of lymphoid tissue are typical.
2. Lymphoid formations of the mucous membrane of the vaginal vestibule of rats (do not differ from the control) quantitatively and qualitatively do not change after the course effect of fresh baths.
3. The treatment with naphthalan baths causes an increase in the number of cells of the lymphoid tissue in all the lymphoid formations of the vestibular mucosa, the activation of lymphocytopoietic processes, a decrease in the level of cell degeneration of lymphoid tissue.

REFERENCES

Allahverdiev M.K. (2008) Structural and functional characteristics and patterns of morphogenesis of the glandular and lymphoid apparatus of the extrahepatic biliary tract of a person in postnatal ontogenesis *Avtoref. dis ..... Dr. med.* Baku, 40 p.

Badalov N.G. (2003) Derezinated naphthalan and its complexation with other physical factors in the medical rehabilitation of patients with psoriatic arthritis *Avtoref. Dis ..... Dr. of Medicine*, Moscow, 28 p.

Glantz S.T. (1999) Medical and biological statistics: Translated from English. Edited by N.E. Buzikashvili and D.V.Samoylova. Moscow: Practice, 200 p. (in Russian).

Huseynov B.M. (2011) Morphological features of the glands and lymphoid structures of the trachea and main bronchi in humans in postnatal ontogenesis and in an experiment in rats when exposed to water procedures with different salt composition *Avtoref. dis ..... Dr. med.* Baku, 40 p. (in Russian).

Kyazimov G.A. (2009) Innovative technologies in naphthalanotherapy (balm naftalan for baths). *Theses of scientific works of the III All-Russian Congress of Dermatovenerologists*. Kazan: (in Russian).

Movsumov N.T. (2004) The morphogenesis of the glands of the human larynx at norm and in experiments with some balneological effects. *Author. Dis ..... Doctor of Medicine*., Baku, 35 (in Russian).

Nikityuk D.B., Klochkova S.V., Alekseeva N.T. (2015) Modern ideas about the general laws of macromicroscopic anatomy of lymphoid organs. *Journal of Anatomy and Histopathology*, **4(2):** 9-13. (in Russian).

Oransky I.E. (1998) Natural healing factors and biological rhythms., Moscow: Medicine, 288 p. (in Russian).

Scherbina NA, Lamia A. (2016) Comparative effectiveness of methods for the conservative correction of genital prolapsed in perimenopausal women. *Wschodnioeuropejskie Czasopismo Naukove*, **12(16):** 39-41.

Seidova Z.R. (2001) Lymphoid apparatus of the larynx of rats at influence of water procedures with different salt composition. *Author. Ph.D.* Baku, 23 (in Russian).

Shadlinski V.B., Movsumov N.T. (2002) The glandular lymphoid apparatus of the larynx of rats with balneological influences (experimentally-morphological studies). Baku: Nurlan, 131 p. (in Russian).

Sizyakova L.A. (2010) Rehabilitation treatment of patients with prolonged pneumonia using natural naphthalan: *Avtoref. Dis ..... Cand. med. sci.*, Moscow, 26 p. (in Russian).

Naftalan vannaları kursunun qəbulundan sonra siçovulların uşaqlıq yolu dəhlizi limfoid törəmələrinin hüceyrə tərkibinin yerləşmə sıxlığının və dəyişməsinin xüsusiyyətləri

S.V. Şadlinskaya

Azərbaycan Tibb Universitetinin İnsan anatomiyası və tibbi terminologiyası kafedrası

Tədqiqat üçün cinsi yetişkənliyə çatmış, eksperimental olaraq naftalan vannalarının təsirinə məruz qalmış Vistar xətti siçovullarının uşaqlıq yolu dəhlizi divarlarının limfoid törəmələri öyrənilmişdir. Morfoloji analiz göstərmişdir ki, siçovuların uşaqlıq yolu dəhlizinin selikli qişasında həm eksperimental qrupda, həm də nəzarət qrupunda limfoid toxumanın bütün formalarına rast gəlinir. Siçovulların uşaqlıq yolu dəhlizinin selikli qişasının limfoid törəmələri adi su vannalarının təsirinə məruz qaldıqdan sonra, kəmiyyət və keyfiyyət baxımından dəyişmirlər ki, bu da onların təhlükəsizliyini göstərir. Naftalan vannalarının qəbulu bütün limfoid törəmələrdə limfoid toxuma hüceyrələrinin sayının artmasını, limfositopoetik proseslərin aktivləşməsini, limfoid toxumanın hüceyrə degenerasiya səviyyəsinin enməsini şərtləndirir.

Açar sözlər: *Uşaqlıq yolu dəhlizi, limfoid düyüncüklər, diffuz limfoid toxuma*

Особенности плотности расположения и изменения клеточного состава лимфоидных образований преддверия влагалища крыс после курса нафталановых ванн

С.В. Шадлинская

Кафедра анатомии человека и медицинской терминологии
Азербайджанского медицинского университета

Исследованы лимфоидные образования стенок преддверия влагалища половозрелых крыс-самок линии Вистар, подвергнутых экспериментальному воздействию нафталановых ванн. Морфологический анализ показал, что в слизистой оболочке преддверия у крыс обеих экспериментальных групп, как и в контроле присутствуют все формы лимфоидной ткани. Лимфоидные образования слизистой оболочки преддверия влагалища крыс после курсового действия пресных ванн фактически количественно и качественно не изменяются, что свидетельствует об их безопасности. Курс нафталановых ванн обуславливает увеличение количества клеток лимфоидной ткани во всех лимфоидных образованиях, активацию лимфоцитопоэтических процессов, снижение уровня клеточной дегенерации лимфоидной ткани.

Ключевые слова: *Преддверие влагалища, лимфоидные узелки, диффузная лимфоидная ткань*

Journal of Life Sciences and Biomedicine, vol. 1 (74), No 1, p. 89-95 (2019)

Comparative studies of pelviometric traits in different age groups with narrow female pelvis

E.A. Khydyrov*, S.F. Ganbaeva

*Department of Human Anatomy and Medical Terminology, Azerbaijan Medical University, 23 Bakikhanov str., Baku 1008, Azerbaijan; *For corresspondence: medun91@mail.ru*
Accepted for publication: 30 August 2019

Pelviometric studies of 36 female pelves of a narrow configuration (18 pelves with a uniformly constricted shape and 18 - with a transversely narrowed) were conducted. The change in the dimensional characteristics of these pelves was studied depending on age (age range 16-60 years). It was found that both groups of constricted pelvic forms were not characterized by high variability in the age aspect and their sizes were relatively stable throughout life. At the same time, it was found that the parameters of the transversely shaped forms of the pelves were more susceptible to changes than the dimensions of the uniformly constricted configurations.

Keywords: *Female pelvis, pelviometric signs, age morphodynamics, analysis of variance*

INTRODUCTION

Currently, the problem of analyzing the size characteristics of narrow female pelvis remains in the focus of attention of researchers of various medical profiles. There is evidence (Kovalev, 2003) that a functionally narrow pelvis is found in every tenth parturient woman. Specialists in various fields of medicine indicate a significant increase in the risk of disability and morbidity in a child with an anatomically narrowed pelvis (Shmedyk and Trufanov, 2016; Mudrov and Chatkis, 2017; Savelieva and Sukhikh, 2018), childbirth aggravated in such cases of perinatal pathology and early neonatal mortality is noted (Rebrova, 2002; Kiselevich and Slukhina, 2012). However, despite the relevance, the age dynamics of the osteometric parameters of the female pelvis remains a poorly developed topic. Based on the analysis of literature data and having a sufficiently large osteological material, we set a goal to study the age-related morphodynamics of pelviometric signs of women in the range from 16 to 60 years.

MATERIALS AND METHODS

The research material was the osteological collection from the museum of the department of Human Anatomy of the Azerbaijan Medical University (more than 100 preparations of mounted female pelvis preparations). The passport age of these objects, according to the museum register, ranged from 16 to 60 years and corresponded to the adolescent age period (16-21), as well as the I (22-35) and II (36-60) maturity periods. From this material were selected (using osteometric procedures) preparations that morphologically corresponded to narrow forms of the pelvis. Tazy with a transverse diameter of less than 11.8 cm. and the transverse diameter of the exit of the pelvis less than 10.5 cm. were attributed to cross-contracted forms of the pelvis, according to the recommendations used in gynecology (Chernukha and Volobuev, 2005). There were 18 such objects in the collection. In addition, the objects that had osteometric characteristics (true conjugate, diagonal conjugate, transverse diameter, ridge spacing, transverse size of the wide part, etc.) differing from the average downwards by 1.5 cm. and more were attributed to general uniformly constricted pelvic forms. The selection was carried out on the basis of a comparison of their sizes with the standards of average parameters, which are given by many authors as average values of pelviometric characteristics in women of the European race (Handa and Lockhar, 2006; Shmedyk and Trufanov, 2016; Radzinskiy and Fuks, 2019). As a result, the pelvis with a general uniform form also turned

out to be 18. Preparations classified as narrow pelvic forms were distributed by age categories evenly and thus, in both groups, 6 objects corresponded to the adolescent age period, 6 - I period of maturity, and 6 - II period maturity. On each anatomical preparation of the bone pelvis, 15 pelviometric features were measured according to the generally accepted standard procedure (Avtandilov, 1990). A list of these signs is given in the tables below. The actual data collected using osteometric procedures were processed by simple methods of variation statistics (Glantz, 1999). The necessary statistical calculations were carried out using the appropriate Microsoft Excel software package (version 2016).

RESULTS AND DISCUSSION

As a result of osteometric studies, corresponding pelviometric characteristics were obtained, which were recorded in special pelviometric blanks. These parameters were grouped and entered into the spreadsheet environment of Microsoft Excel. Then, for the entire studied osteological sampling, the corresponding variational-statistical parameters were calculated. Using the results obtained, it was necessary to clarify the behavior of pelviometric signs in the age dynamics taking into account the configuration features of the pelvis. That is, it was necessary to determine how the osteometric parameters of the female pelvis correlate with each other in three age categories with its transversely contracted and generally uniformly constricted configuration. As we already noted in the studied collection of pelvic preparations, the configuration of which was classified as transverse-contracted forms, there were a total of 18 objects. These pelvic preparations were characterized by small transverse dimensions. When objects were distributed from this population, 6 pelvic preparations were in each of the age groups under consideration. For transversely shaped pelvic forms, there was a large variation in metric indices. The most varying features were such signs as anatomical and true conjugates, the straight and transverse size of the wide part of the pelvis, as well as oblique diameter, the transverse size of the narrow part of the pelvis, the intercrest distance and the height of the pelvis. At the same time, the last four signs in different age periods differ by more than 1 cm, and the difference in the size of the pelvis height between the age groups of the first and second mature periods is more than 4 cm. Also, a sharp increase in parameters in the second mature period was characteristic of the transverse size of the narrow part pelvis and intercrest distance. However, all other metric indicators with this form of the pelvis change little with age. The transverse size of the inferior aperture of lesser pelvis, diagonal conjugate, the straight size of narrow part of pelvis and transverse diameter had the most stable dimensional characteristics.

The greatest interval of variability in all three age categories was observed in such signs as the straight size of the narrow part of the pelvis, the distance of the symphosacralis, the true conjugate, the longitudinal size of the inferior aperture of lesser pelvis and the intercrest distance. The maximum range of numerical indicators (taking into account the average value of the parameter in the sample) was noted at the intercrest distance ($27.3>X>22.9$; $28.5>X>21.9$ and $30.0>X>23.3$, respectively, to the increase in age rank). In addition, high variability was observed in both mature periods in the longitudinal size of the inferior aperture of lesser pelvis ($11.8>X>8.3$ and $11.5>X>8.1$) and in the straight size of the narrow part of the pelvis ($12.3>X>8.3$ and $12.2>X>9.0$).

Thus, there are no sufficient grounds for confident statements about the variability over time of pelviometric signs in case of transverse-constricted forms of the pelvis. Perhaps the most interesting is a sharp increase in the parameters of the height of the pelvis, intercrest distance and the transverse size of the narrow part of the pelvis in the last age category (36-60 years). However, all these characteristics can be considered in some way relative due to the small number of objects studied. Therefore, for a more weighty argument of the statements made, the analysis of variance was carried out.

In this case, the differences were checked at a 5% significance level ($P<0.05$). The corresponding critical value F from the Snedekor and Gokhran tables [11] in this case was equal to 3.24. Statistical indicators of the investigated signs and the results of the F-test are presented below in table 1. The results of analysis of variance revealed differences between age categories and in this case, according to four signs - pelvis height, anatomical

conjugate, straight size of the wide part of the pelvis and oblique diameter. At the 7% level of significance, differences between age groups are also found in the transverse size of the narrow part of the pelvis. At the same time, even a slight increase in sensitivity to differences (P <0.02) leads to the loss from the cohort of signs differentiating the selected age periods, such parameters as oblique diameter and straight size of the wide part of the pelvis.

Minor discrepancies are characteristic of two signs characterizing the dimensions of the sagittal direction and one vertical parameter. Thus, it can be said that with a general transverse narrowness of the pelvic configuration, morphodynamic changes in latitudinal parameters are extremely insignificant. Differences are observed only in longitudinal and high-altitude pelviometric traits, and even in one parameter (oblique diameter), which has an intermediate position between the main anatomical axes of the horizontal plane.

Based on the results of analysis of variance, we can conclude that transverse-constricted pelvic configurations are generally conservative. Interestingly, along with the wide parameters, the longitudinal parameters also change little with increasing age. Almost indifferent in this context are the interspinous distance, the transverse and longitudinal dimensions of the inferior aperture of lesser pelvic cavity, the straight size of the narrow part of the pelvis and the transverse diameter. Thus, it is thought that the factors that caused the transverse narrowness of the pelvis continue to act until old age.

Table 1. Pelviometric characteristics in various age groups and analysis of variance according to the same characteristics in various age groups with a cross-shaped pelvis.

Stastistical parameter		Anatomic conjugata	Transverse diameter	Conjugata vera(true)	Conjugata diagonalis	Diameter obliqua	Direct size of the wide part of the pelvis	Tramsverse size of the wide part of the pelvis	Tramsverse size of the narrow part of the p pelvis	Direct size of the narrow Part of the pelvis	Transverse diameter of the lesser pelvic outlet	Longitudinal size of the lesser pelvic outlet	Distantia symphosacralis	Distantia spinarum	Distantia cristarum	Height of the pelvis
16-21	X	10.58	10.28	11.50	11.6	11.68	11.1	11.48	9.88	10.55	9.55	9.50	10.93	10.90	25.4	19.6
22-35	X	10.72	10.27	10.82	11.3	12.73	12.1	12.30	10.2	10.30	9.47	10.18	10.57	10.78	25.5	19.5
36-60	X	9.97	10.73	11.82	11.6	12.78	11.4	11.68	11.2	10.28	9.83	9.62	10.05	10.32	28.1	23.6
16-21	S	0.40	0.50	1.07	0.94	0.97	0.53	0.61	0.56	0.70	0.83	0.94	1.36	1.17	1.79	1.40
22-35	S	0.51	1.04	1.01	0.67	0.56	0.67	0.84	0.89	1.64	0.84	1.50	0.81	0.81	2.58	1.85
36-60	S	0.16	1.12	0.71	0.53	0.36	0.47	0.53	1.16	1.24	0.61	1.19	0.92	1.01	2.55	1.79
16-21	S(r)	0.16	0.20	0.44	0.38	0.40	0.22	0.25	0.23	0.28	0.34	0.38	0.56	0.48	0.73	0.57
22-35	S(r)	0.21	0.43	0.41	0.27	0.23	0.27	0.34	0.36	0.67	0.34	0.61	0.33	0.33	1.05	0.76
36-60	S(r)	0.07	0.46	0.29	0.22	0.15	0.19	0.22	0.48	0.51	0.25	0.49	0.38	0.41	1.04	0.73
16-21	min	10.2	9.6	9.6	9.9	10.2	10.3	10.6	9.1	9.6	8.2	8.4	9.3	9.5	22.9	18.0
22-35	min	10.2	9.4	9.6	10.3	11.8	11.5	10.9	9.4	8.3	8.3	8.3	9.7	9.6	21.9	17.5
36-60	min	9.8	9.4	10.6	10.6	12.3	11.0	11.2	9.1	9.0	9.0	8.1	9.4	9.0	23.3	21.0
16-21	max	11.3	10.9	12.5	12.3	12.6	11.7	12.1	10.5	11.4	10.6	11.0	12.5	12.1	27.3	21.6
22-35	max	11.5	12.1	12.2	12.2	13.3	13.3	13.3	11.3	12.3	10.4	11.8	11.8	11.9	28.5	21.7
36-60	max	10.2	12.0	12.6	12.1	13.2	12.3	12.6	12.5	12.2	10.6	11.5	11.7	11.7	30.0	26.5
D(inter)		0.961	0.421	1.567	0.194	2.315	1.58	1.087	2.652	0.134	0.222	0.802	1.182	0.572	13.8	32.5
D(inside)		0.149	0.866	0.894	0.537	0.461	0.315	0.456	0.821	1.574	0.588	1.517	1.12	1.01	5.447	2.9
F		6.461	0.485	1.752	0.361	5.025	5.016	2.385	3.229	0.085	0.377	0.528	1.055	0.566	2.534	11.3
P		<0.01	<0.63	<0.21	<0.7	<0.02	<0.02	<0.13	<0.07	<0.92	<0.69	<0.60	<0.37	<0.58	<0.11	<0.01

Note (hereinafter): 16-21, 22-35, 36-60 - age groups; N is the number of pelvic preparations; X is the average value of the trait; S is the standard deviation; S (r) is the error of the standard deviation; D (inter) - the value of intergroup dispersion; D (inside) is the value of intragroup dispersion; F - the calculated value of the Fisher criterion; P - probability of validity of the null hypothesis.

And perhaps for this reason, morphodynamic changes are observed only in signs of non-transverse direction. Among the investigated osteological objects, as mentioned above, a group of pelvises were also impressed out, which, by their configuration, were classified as general uniformly constricted forms. There were 18 such preparations of the pelvis in the studied collection, moreover, in each age group, as in the previous case, 6 objects also presented.

Pelviometric signs in the group of general uniformly constricted forms have shown themselves to be the most variable indicators. The average size of more than half of the signs (anatomical and diagonal conjugates, transverse and oblique diameter, straight and transverse size of the wide part of the pelvis, as well as the distance of the symphosacralis and the straight size of the narrow part of the pelvis) in different age periods differ greatly from each other, and the difference between their values It is more than 1 cm. Two more signs - the height of the pelvis and interspinous distance – also differ significantly in terms of parameters almost as high as a centimeter (the difference is 0.98 cm in average and 0.99 cm respectively).

The transverse size of inferior aperture of lesser pelvic cavity (Xavg=8.85, Xavg=9.53 and Xavg=9.57, respectively, increasing age) and the intercrest distance (Xavg=25.25, Xavg=25.67 and Xavg=24.98), for which the difference in averages was approximately 0.7 cm.

These data suggest that having the most minimal values of pelviometric signs, general uniformly constricted pelvic forms have the greatest variability.

Table 2. Pelviometric characteristics in various age groups and analysis of variance on the same lines in various age groups with a uniformly reduced form of the pelvis

Stastistical parameter		Anatomic conjugata	Transverse diameter	Conjugata vera(true)	Conjugata diagonalis	Diameter obliqua	Direct size of the wide part of the pelvis	Tramsverse size of the wide part of the pelvis	Tramsverse size of the narrow part of the p pelvis	Direct size of the narrow Part of the pelvis	Transverse diameter of the lesser pelvic outlet	Longitudinal size of the lesser pelvic outlet	Distantia symphosacralis	Distantia spinarum	Distantia cristarum	Height of the pelvis
16-21	X	8.85	11.52	8.87	8.63	10.10	8.70	8.57	8.52	9.80	8.85	8.50	10.9	9.90	25.3	22.25
22-35	X	9.75	11.55	9.67	10.6	11.90	9.07	9.88	9.13	8.77	9.53	9.22	10.7	9.92	25.7	21.88
36-60	X	9.60	10.23	8.97	9.68	10.93	9.77	10.12	8.60	9.40	9.57	9.43	9.75	8.93	25.0	21.27
16-21	S	0.67	0.87	1.09	1.14	1.54	0.74	1.10	0.71	1.12	1.22	0.60	1.27	0.98	1.90	2.70
22-35	S	1.47	0.55	1.03	2.12	1.84	1.50	1.97	1.79	1.76	1.06	0.84	1.30	1.92	2.20	2.75
36-60	S	1.44	0.48	1.36	1.95	1.79	1.65	2.00	1.26	1.54	1.10	1.32	1.78	0.87	2.75	3.10
16-21	S(r)	0.27	0.36	0.45	0.46	0.63	0.30	0.45	0.29	0.46	0.50	0.24	0.52	0.40	0.77	1.10
22-35	S(r)	0.60	0.22	0.42	0.87	0.75	0.61	0.80	0.73	0.72	0.43	0.34	0.53	0.78	0.90	1.12
36-60	S(r)	0.59	0.20	0.56	0.79	0.73	0.67	0.81	0.52	0.63	0.45	0.54	0.73	0.35	1.12	1.27
16-21	min	7.9	10.3	7.3	7.5	7.8	7.4	7.5	7.1	7.9	7.3	7.8	8.7	8.2	22.6	18.5
22-35	min	7.4	10.7	8.3	7.7	8.3	7.6	7.9	6.8	7.1	8.0	7.9	8.5	7.2	21.8	17.7
36-60	min	7.4	9.9	7.6	7.8	8.7	7.8	7.4	6.9	7.3	8.1	7.7	7.5	7.4	22.0	16.9
16-21	max	9.6	12.2	10.5	9.8	11.9	9.4	9.7	9.0	10.9	10.6	9.2	12.2	11.0	27.5	25.5
22-35	max	11.3	12.3	11.0	12.6	13.1	11.9	12.5	11.0	10.6	10.6	10.1	12.5	12.0	27.1	26.2
36-60	max	11.2	11.2	10.9	11.9	13.1	11.5	12.4	10.5	10.7	10.4	10.8	12.4	9.8	29.5	25.9
D(inter)		1.395	3.382	1.14	5.621	4.869	1.762	4.191	0.672	1.629	0.982	1.432	2.149	1.902	0.712	1.48
D(inside)		1.553	0.43	1.372	3.198	2.989	1.839	3.019	1.769	2.246	1.277	0.935	2.156	1.792	5.332	8.16
F		0.898	7.856	0.831	1.757	1.629	0.958	1.388	0.38	0.725	0.768	1.532	0.997	1.061	1.061	0.18
P		<0.43	<0.01	<0.46	<0.21	<0.23	<0.41	<0.28	<0.69	<0.50	<0.48	<0.25	<0.39	<0.37	<0.37	<0.84

Note that with this configuration, only the parameters of the transverse diameter and height of the pelvis in the first two age categories, as well as the transverse size of the inferior aperture of lesser pelvic cavity and the distance of the symphosacralis in the first period of mature age did not have minimum values compared to other forms of the pelvis. In all other cases, among the entire sample (the osteological collection studied), the smallest indices of pelviometric signs were observed just with the given configurations of the pelvis. The maximum variability of parameters in this group was found in the following pelviometric signs: anatomical conjugate, diagonal conjugate, oblique diameter, and also the transverse dimensions of the wide and narrow part of the pelvis. For these signs, the difference between the minimum and maximum rates was generally above 40% of their average value. It is noteworthy that such an imbalance was more noticeably observed more often in periods of mature age.

For example, significant variability occurred in both mature periods at diagonal conjugates (12.6>X>7.7 and 11.9>X>7.8, respectively, in period I and II), at the transverse size of a wide part of the pelvis (12.5>X>7.9 and 12.4>X>7.4) and at the transverse size of the narrow part of the pelvis (11.0>X>6.8 and 10.5>X>6.9). Interestingly, the greatest variation of parameters (>50% of the average value for a trait) was noted at the distance of the symphosacralis in the second period of mature age - 12.4>X>7.5. However, in previous age categories, the variability of the parameters of this trait is very moderate. In general, in the adolescent age group, for most signs, there was a low variability of dimensional characteristics, which often amounted to less than 25% of the corresponding average value. Only the true conjugate (10.5>X>7.3), oblique diameter (11.9>X>7.8) and the transverse size of inferior aperture of lesser pelvic cavity (10.6>X>7.3) had a rather high variability in this age category. Statistical indicators of the metric characteristics of the pelvis in case of general uniformly constricted forms suggest the presence of certain differences in its size in certain age periods (the variability of signs changes quite synchronously with increasing age). But even here, the comparatively small number of the studied preparations does not allow for the imposition of unconditional judgments. To confirm or refute our assumptions, it was decided to again resort to the use of analysis of variance. The conditions for accepting the null hypothesis and the critical value of F remained unchanged and, using proper calculations, data were obtained from comparative statistical analysis. The values of mean values of pelviometric signs and other variation-statistical parameters, as well as the results of analysis of variance, are presented below in Table 2.

Conducted analysis of variance almost completely confirmed our assumptions about low variability over the age of the size of the pelvis in the group of general uniformly contracted forms. Surprisingly, only the parameters of a single pelviometric trait (transverse diameter) have statistically significant differences when the corresponding sample is broken down into age categories. The remaining parameters, judging by the results of the F-test, have relatively stable parameters from adolescence to old age. Of these parameters, only a diagonal conjugate with a decrease in sensitivity to differences up to 21% of the significance level ($P<0.207$) reveals minor signs of a trait that has differentiated dimensions at different age periods. The diagonal conjugate, as well as the transverse diameter, are the total parameters of the pelvis (as if its dimensions) and correlate little with local dimensions, which in turn are closely related to the development and functions of the internal organs. These signs are subject to sufficiently strong individual variations and are significantly dependent on environmental factors and adaptation. That is, to summarize, it can be said that the general uniformly constricted forms of the pelvis have a greater conservatism of parameters at different age periods compared to its cross-contracted variants.

CONCLUSIONS

The results obtained in the course of this study (parameters of the studied traits, their variability, etc.) are generally comparable with the results obtained by other authors (Khrebtova and Khodova, 2004; Syrova, 2008; Vinogradov, 2012). Nevertheless, there were differences in some mean values of pelviometric characters when compared with the data of some authors (Kurinov, 2007; Gaivoronsky and Bessonov, 2012). Howe-

ver, the revealed differences in the statistical characteristics can be fully explained by the racial-population characteristics of the material studied. Thus, the interpretation of the obtained conclusions with the help of our own analytical constructions can be considered quite legitimate. Summarizing the results of the study of the age-related morphodynamics of the female pelvis in some narrow forms of its configuration, we can say that the design of the pelvis influences, to a certain extent, the variability of pelviometric features in the context of age. Both groups of constricted pelvic forms are not characterized by high variability, and in general-uniformly narrowed forms, almost all pelviometric parameters have the greatest stability by age. It is striking that within the age categories, with this form of the pelvis, the variability of a significant number of pelviometric signs is quite high. Thus, a preliminary analysis of the results allows us to accurately state that the narrow forms of the pelvis of women, in general, are more constant throughout life, although they have a greater range of variability in a considerable number of their metric characteristics.

REFERENCES

Avtandilov A.G. (1990) Medical morphometry: a guide. Moscow: Medicine, 63-65.

Chernukha E.A., Volobuev A.I., Puchko T.K. (2005) Anatomically and clinically narrow pelvis. Moscow: Triad-X, 256 p. (in Russian).

Gaivoronsky I.V., Bessonov N.Yu., Niauri D.A. (2012) Original approaches to the study of the morphometric characteristics of the plane of exit from the small pelvis in adult women. *Journal of Obstetrics and Women's Diseases*. **2;** 20-25 (in Russian).

Glantz S.A. (1999) Biomedical statistics. Moscow, 459 p.

Handa V.L., Lockhart M.E., Fielding J.R. et al. (2008) Racial differences in pelvic anatomy by magnetic resonance imaging. *Obstetrics and Gynecology*. **111(4):** 4-920.

Khrebtova O.M., Khodova L.M. (2004) The size of the pelvis in girls and women aged 13 to 35 years, depending on the somatotype. *Collection of materials of the XIV Scientific Practical Conference of Doctors*. Novosibirsk, p. 25-26 (in Russian).

Kiselevich M.F., Slukhina V.D., Yaprintseva E.G. (2012) The course of pregnancy and childbirth in women with a narrow pelvis. *Scientific Statements of Belgorod State University. A series of medicine, pharmacy*, **4 (123):** 51-54 (in Russian).

Kovalev V.V. (2003) Perinatal aspects of a functionally narrow pelvis. *Author. diss. ... Dr. med sciences*. Moscow, 42 p. (in Russian)

Kurinov S.B. (2007) Radial methods of research in the diagnosis of anatomically narrow pelvis. *Abstract of Diss. ... Cand. med. sciences*. Moscow, 20 p. (in Russian).

Mudrov V.A., Chatkis E.M., Nizhegradtseva D.A. (2017) The role of ultrasonic pelviometry in the diagnosis of anatomically clinically narrow pelvis. *Journal of Obstetrics and Female Diseases*. *Chita*, **66 (6):** 20-29. (in Russian).

Radzinskiy V.E., Fuks A.M., Ch.G. Gagaev Ch.G. (2019) Obstretics Moscow: Geotar-Media, 880 p. (in Russian).

Rebrova O.Yu. (2002) Statistical analysis of medical data. Application software package STATISTICA. Moscow: Media Sphere, 103 p. (in Russian).

Savelieva G.M., Sukhikh G.T., Serov V.N. (2018) Obstetrics. National leadership. Moscow: Geotar-Media, 1048 (in Russian).

Shmedyk N.Yu., Trufanov G.E., Fokin V.A. et al. (2016) Magnetic resonance and external pelvimetry in the diagnosis of the shape and extent of the narrowed pelvis in pregnant women. *Translational medicine*, **3:** 113-124 (in Russian).

Syrova O.V. (2008) Ultrasound anatomy of the internal genital organs of girls 17-19 years old with various forms of the pelvis and body types. *Abstract of Diss ... Cand. med. sciences*. Saratov, 30 p. (in Russian)

Vinogradov S.V. (2006) Sexual and individual morphometric characteristics of the pelvis of an adult. *Thesis ... candidate of medical sciences*. St. Petersburg, 185 p. (in Russian).

Müxtəlif yaş dövrlərində qadın çanağının dar formalarının pelviometrik əlamətlərinin müqayisəli tədqiqi

E.Ə. Xıdırov, Ş.F. Qanbayeva

Azərbaycan Tibb Universitetinin İnsan anatomiyası və tibbi terminologiya kafedrası

Dar formalı 36 qadın çanağı üzərində pelviometrik tədqiqatlar aparılmışdır (18 ümumi-bərabər daralmış formalı, 18 köndələn-daralmış çanaq). Bu çanaqların ölçü xüsusiyyətlərinin dəyişikliyi yaşla əlaqədar (yaş həddi 16-60) öyrənilmişdir. Müəyyən olunmuşdur ki, dar çanağın hər iki forması yaş aspektində yüksək dəyişkənlik ilə xarakterizə olunmur və onların ölçüləri həyat boyu nisbətən sabitdir. Eyni zamanda, köndələn daralmış formalı çanaqların göstəriciləri ümumibərabər daralmış formalı çanaqların göstəricilərinə nisbətən dəyişikliklərə daha çox həssas olduğu müəyyən edilmişdir.

Açar sözlər: *Qadın çanağı, pelviometrik əlamətlər, morfometrik analiz, dispersyion analiz*

Сравнительные исследования пельвиометрических признаков в различных возрастных группах при узких формах женского таза

Э.А. Хыдыров, Ш.Ф. Ганбаева

Кафедра анатомии человека и медицинской терминологии Азербайджанского медицинского университета

Проведены пельвиометрические исследования 36 женских тазов узкой конфигурации (18 тазов с общеравномерносуженной формой и 18 – с поперечносуженной). Изучалось изменение размерных характеристик этих тазов с связи с возрастом (возрастной интервал 16-60 лет). Обнаружено, что обе группы суженных форм тазов не характеризуются высокой изменчивостью в возрастном аспекте и их размеры в течении жизни относительно стабильны. Вместе с тем, установлено, что параметры поперечносуженных форм тазов более подвержены изменениям, нежели размеры общеравномерносуженных конфигураций.

Ключевые слова: *Женский таз, пельвиометрические признаки, возрастная морфодинамика, дисперсионный анализ*

Journal of Life Sciences & Biomedicine, vol. 1(74), No 1, p. 96-104 (2019)

The effect of salt (NaCl) stress on the ultrastructure of mesophyll and bundle sheath cell chloroplasts and the activity of superoxide dismutase in maize plants (*Zea mays* L.)

N.Kh. Aliyeva[1*], E.E.Gafarova[1], D.R. Aliyeva[1], S.Y. Suleymanov[1], F.H. Rzayev[2], E.K.Gasimov[3]

[1]*Institute of Molecular Biology and Biotechnologies, Azerbaijan National Academy of Sciences, 11 Izzat Nabiyev, Baku AZ 1073, Azerbaijan*
[2]*Laboratory of Electron Microscopy, SRC of Azerbaijan Medical University, 163 A Samad Vurgun, Baku AZ1078, Azerbaijan*
[3]*Department of Histology, Embryology and Cytology, Azerbaijan Medical University, 163 A Samad Vurgun, Baku AZ1078, Azerbaijan*
**For correspondence: enahide@rambler.ru*
Accepted for publication: 25 November 2019

The activity and isoenzyme content of superoxide dismutase (SOD) and changes in the leaf ultrastructure have been studied comparatively in chloroplasts of mesophyll and bundle sheath cells isolated from maize plants (*Zea mays* L.) grown in an artificial climate chamber at various concentrations of NaCl (0 mM, 50 mM, 100 mM, 200 mM). The SOD activity was found to increase in plants exposed to 50 mM and 100 mM NaCl, but at 200 mM NaCl it was partly inhibited. The study of the isoenzyme activity of SOD revealed Fe-SOD isoform, which intensity increased with enhancing salt concentrations. The analysis of the ultrastructures of mesophyll (M) and bundle sheath (BS) cell chloroplasts by electron microscopy showed that chloroplasts of M cells were sensitive,whereas chloroplasts of BS cells were tolerant to stress. At the high salt concentration (200 mM), a partial transition of the agranal structure of BS cell chloroplasts to the granal structure occurred.

***Keywords**: Zea mays* L., *salt stress, superoxide dismutase, mesophyll, bundle sheath, chloroplast, ultrastructure*

INTRODUCTION

Maize plants (*Zea mays* L.) use C_4 photosynthetic pathway for the assimilation of CO_2 and this process is divided into two cycles. This division within the leaf is implemented by two specialized photosynthetic cells: M cells surrounded BS cells, located compactly around the veins. BS and M cells differ in their metabolic functions in the maize plant: PEP-carboxylase and C_4 photosynthesis function in M cells, whereas RBP carboxylase and Calvin cycle function in BS cells (Raines, 2003, von Caemmerer and Furbank, 2003). M cell chloroplasts of maize leaves have a granular structure and they possess all components of the electron transport chain, which ensures the photochemical functioning of PS I and PS II. In contrast, the granular structure is not clearly visible in BS cell chloroplasts where mainly PS I functions. Electron microscopy studies revealed differences between the structures of M and BS cells. Thus, M cells are characterized by granal structure, stromal thylakoids and small amounts of starch granules, whereas BS cells are distinguished by their agranal structure and a greater amount of starch granules (von Caemmerer et al., 2003, Shao et al., 2015)

Currently, changes in the molecular, membrane and cellular levels are brought to the fore in the study of the response of living organisms to various extreme conditions. During long-term and intense stress, oxidation of free radicals occurs in the cell (Ramegowda and Senthil-Kumar, 2015). One of the initial responses to stress is the lipid peroxidation process induced by the formation of reactive oxygen species (superoxide anion radical, $O^{2\cdot-}$, - H_2O_2, etc.). Chloroplasts and peroxisomes are the main places for the formation of reactive

oxygen species (ROS) (Asada, 2006). Oxidative stress is often accompanied by photoinhibition. On the other hand, a correlation between the activity of antioxidant enzymes and the inhibition degree of the photosynthetic apparatus was established (Gadjev et al., 2006). Enzymatic antioxidants such as superoxide dismutase (SOD), ascorbate peroxidase (APO) and catalase (CAT) are the main components of the cell antioxidant defense system.

Superoxide dismutase is known to catalyze the reduction of superoxide radical to hydrogen peroxide: $\cdot O_2 + O_2^- + 2H^+ = H_2O_2 + O_2$

Based on recent reports, SOD molecules have several isoforms differing in their cellular localization, primary structure, molecular mass and nature of the metals in the active center – Cu/Zn-SOD, Mn-SOD and Fe-SOD (Alscher et al., 2002; Gill and Tuteja, 2010; Mahanty et al., 2012). Cu / Zn-SOD (30-33 kDa) was found mainly in the cytosol, mitochondria, peroxisome; Mn-SOD (75-94 kDa) - in mitochondria, peroxisome; Fe-SOD (36-48 kDa) - in chloroplasts and cytoplasm of some legumes. Superoxide dismutase was revealed in various organisms, including plants (Kumar et al., 2013). Contrary to SOD in animal cells, plant SOD is distinguished by its numerous isoenzymes. As a result of multiple investigations, it has been found that during the plant protection from oxidative stress, the SOD activity changes depending on the plant species, the stage of development and the degree of the stress effect (Alscher et al, 2002).

The main purpose of the study was to determine the effects of various concentrations of NaCl on the ultrastructure of chloroplasts isolated from mesophyll and bundle sheath cells and the activity of superoxide dismutase in maize leaves.

MATERIALS AND METHODS

Material: Seedlings of the maize plant (*Zea mays* L.), which is a cereal crop, were cultivated in the hydroponic growing mediums – Knop's solution. Seeds were transferred to the filter paper wrapped in roll after being sterilized in 2.5% $KMnO_4$ solution for 15 min. The seeds were germinated in the nutrient medium containing various NaCl concentrations (0 mM, 50 mM, 100 mM, 200 mM NaCl), for 14 days, with a photoperiod of 12h/12, at 25ºC. At the same time, plants grown in soil under phytotron conditions were also used (photoperiod – 14 h/10 h, t – 26ºC, light intensity - 3000 lux).

Isolation of subcellular fractions of chloroplasts from mesophyll and bundle sheath cells: Maize seedlings were used in the experiments after the complete maturation of the second leaf. The plants were exposed to salt stress (0 mM, 50 mM, 100 mM, 200 mM) for 5 days. The differential centrifugation method was used to isolate subcellular fractions (chloroplasts, etc.) from mesophyll and bundle sheath cells of leaf samples. To obtain assimilating tissues, leaves were detached from stems, washed with distilled water and cut into small segments 2-3 mm wide. These segments were homogenized in 25 mM HEPES buffer (pH 7.8) containing 0.3 M sucrose, 1 mM EDTA, 15-20 mM 2-mercaptoethanol (buffer A) using MPW-302 (Poland) mechanical disintegrator, for 4 sec, at 7000 rev/min.

The homogenate obtained was filtered through 4-fold capron and then throughthe Shotov funnel with a pore diameter of 80 μm. The obtained filtrate contained only M cells, the residual part called pulp contained a mixture of M and BS cells. The filtrate was centrifuged for 15 min, at 300 g. The obtained supernatant contained the cytosolic fraction of M cells, whereas the pellet was the chloroplast fraction.The obtained pellet was washed with a buffer A. Then 10 ml of the buffer A without sucrose was added and centrifugation was performed for 15 min, at 300 g. The pellet remained in the filter (pulp) was washed several times with the buffer A, suspended and then homogenized first for 60 sec, at 6000 rev/min and then for 80 sec at 8,000 rev/min. The obtained filtrate was applied to the Shotov funnel with 211 μm diameters of pores. The obtained filtrate contained a mixture of homogenates of M and BS cells. The pellet was suspended in the buffer A and homogenized for 60 sec, at 6,000 rev/min and then for 15 sec, at 8,000 rev/min. The filtrate was centrifuged for 20 min, at 10,000 g. The obtained supernatant contained the cytoplasm of BS cells, whereas the pellet contained chloroplasts of BS cells (Guliev et al., 2003). The pellet was suspended in the buffer A without sucrose, then centrifuged for 20 min, at 10,000 g. This resulted in the

separation of the membrane and stroma of the chloroplasts. All experiments were performed in a cold room with a temperature of 4ºC.

Determination of superoxide dismutase using the spectrophotometric method: The enzyme activity was determined at 450 nm using SOD Assay Kit (Sigma, Aldrich). The enzyme activity was found to be higher in BS cells compared with M cells.

Determination of the isoenzyme content of superoxide dismutase: Electrophoresis on 10% native polyacrylamide gel (PAGE), for 3h, at 4ºC and direct current (30mM) using Tris-glycine (pH 8.3) buffer was performed for the analysis of the isoenzyme content of SOD in maize leaves. After electrophoresis, gel was stained in the darkness for 30 min in 100 ml 1.0 M Tris-HCl (pH 8.2) buffer containing 10 mg NBT, 75 mg EDTA-Na and 3 mg riboflavin.

Ultrastructure of mesophyll and bundle sheath cells: Ultrastructure of M and BS cells were studied using the electron microscope in the 2nd leaves of the maize plant cultivated under artificial climate conditions. The samples were fixed in 0.1 M phosphate buffer (pH 7.4) containing 2% paraformaldehyde, 2% glutaraldehyde and 0.1% picric acid. The samples were kept in the fixative solution for at least one day, then postfixed for 2 hours, in 1% osmium tetroxide solution prepared in phosphate buffer (pH 7.4). Araldite-Epon blocks were made from the material based on general protocols adopted in electron microscopy (Kuo, 2007). Ultra-thin sections (1-2 μm) were made with an ultramicrothome Leica EM UC7, stained with methylene blue, azure II, and basic fuchsin or toluidine blue. Promo Star (Zeiss) microscope was used and the necessary parts were photographed with a Canon D650 digital camera (D'Amico, 2005). The 50-70 nm ultra-thin sections from the same blocks were first stained with 2% uranyl acetate solution, then with 0.6 % pure lead citrate prepared in 0.1 N NaOH solution. Ultra-thin sections were investigated on the electron microscope JEM-1400 at a voltage of 80-120 kw and electronograms were obtained. Morphometric analysis of the image was carried out with TIF format electronograms using computer software (The TEM imaging platform) developed by the German company "Olympus Soft Imaging Solutions Gmbh".

Statistical analysis was performed in 3 biological replicates using the computer program Excel 2016.

RESULTS AND DISCUSSION

Spectrophotometric analysis of mesophyll and bundle sheath cells revealed a higher SOD activity in BS cells compared with M cells (Figure 1). As seen in the figure, the SOD activity did not increase markedly in M and BS cells of the plants grown at 50 mM NaCl compared with the control. However, a significant enhancement in the enzyme activity (55% and 69%, respectively) was observed in both subcellular fractions at 100 mM NaCl and the activity decreased at 200 mM concentration of salt. The enzyme functioning resulted in the formation of the reactive oxygen species H_2O_2, which amount enhanced in the plant cells with the increasing salt concentration. As H_2O_2 is an inhibitor of SOD, its excessive accumulation in the cell at the high salt concentration (200 mM) led to partial inhibition of the enzyme (Jalali-e-Emam et al., 2011) (Figure 1). Omoto et al. (2013) obtained similar results. According to the authors, after emerging the 4th leaf, maize seedlings were watered for 5 days with 3% NaCl solution, which resulted in an increase in the SOD activity both in M and BS cells compared with the control. Whereas, activities of glutathione reductase and monodehydro reductase were observed only in the mesophyll. The ascorbate peroxidase activity and the total amount of ascorbic acid were higher in BS cells exposed to salt stress. According to Hasan et al. (2015), the structure of mesophyll cells in NADP-malic enzyme type (NADP –ME) C_4 plants are more sensitive to salt stress compared with that of bundle sheath cells.

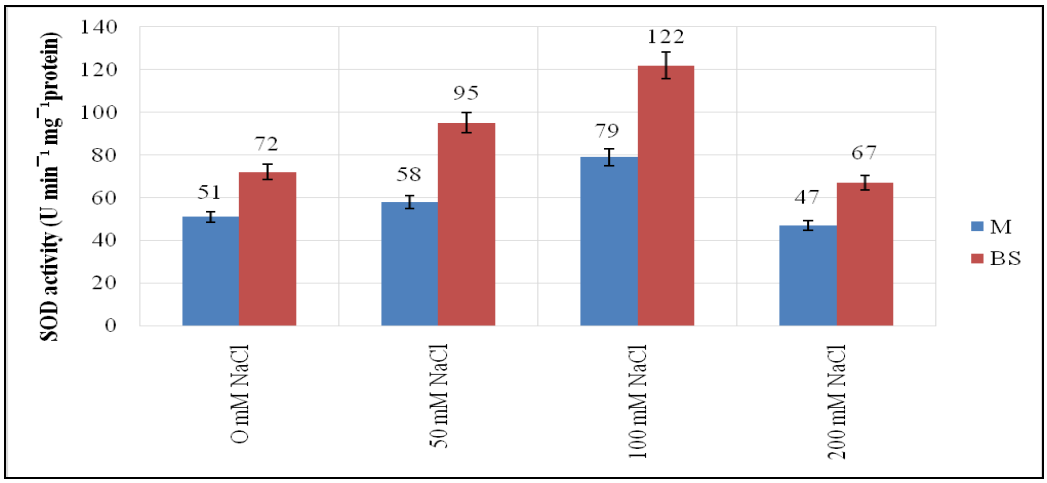

Fig. 1. Changes in the SOD activity in mesophyll and bundle sheath cells of the maize plant depending on the NaCl concentration.

Electrophoretic analysis of mesophyll and bundle sheath cells revealed 1 isoform of the enzyme in BS cells. (Figure 2). Based on literature data, this isoform is suggested to be Fe-SOD (Menezes-Benavente, et al., 2004). As seen in the figure, the isoform intensity increased depending on the salt concentration.

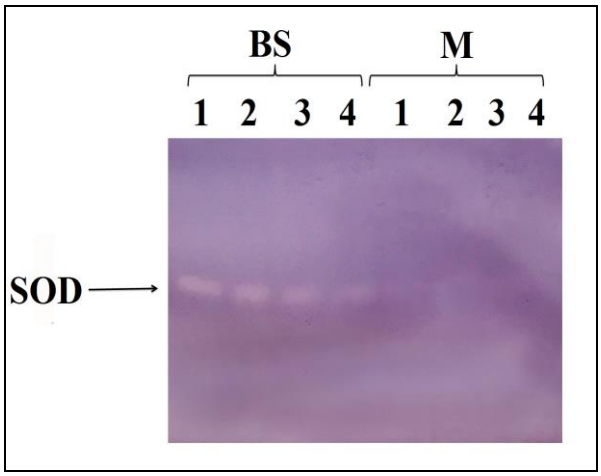

Fig. 2. Isoenzyme content of superoxide dismutase in M and BS cells of the maize plants grown at various NaCl concentrations: 1- 200 mM NaCl, 2 - 100 mM NaCl, 3 - 50 mM NaCl, 4 - 0 mM NaCl.

Changes in the ultrastructure of chloroplasts were analyzed using the electron microscope in leaves of the maize plant grown at various concentrations of NaCl (0 mM, 50 mM, 100 mM, 200 mM) (Figure 3A-D). Mesophyll cell chloroplasts of plants grown under normal conditions have a thylakoid membrane with a well-developed granal structure and a small amount of lipid droplets (plastoglobules) (Figure 3A). Granal thylakoid membranes surrounded by thylakoid membranes, lamellae connecting them and 8 lipid droplets are clearly seen in Figure 3A. Some authors reported the existence of starch granules (Hasan et al. 2005, 2006). But according to electronograms obtained in our research, there is no starch granules in the stroma of the mesophyll cell chloroplasts. As seen in Figure 3B-D, the structure of mesophyll chloroplasts was damaged and swollen after exposure to salt, with the following destruction of the thylakoid membranes (Figure 3). Along with the above ultrastructural changes, chloroplast integrity (external and internal membranes) was also destroyed (Figure 3D). Similar results were obtained by other researchers (Hasan et al. 2005, 2006).

Figure 4 shows changes in the ultrastructure of BS cell chloroplasts of maize plants exposed to salt (NaCl) (4B-D) and in leaves of the control plants (4A). As can be seen, BS cell chloroplasts of the maize plant have a typical NADP-ME structure. As in C_4 plants,they have thylakoid membranes with arganal structures and lipid droplets occur in the stroma (white and black arrows in Figure 4A). It has been established that there is no apparent damage to the thylakoid membrane

system of the BS cell chloroplasts due to salt exposure.The structures of the thylakoids are not destroyed with the increasing salt content (Figure 4B-D). But the volume and number of the lipid droplets increase multiple times (black arrows in Figure 4C, D). It should be noted that salt stress causes a change of the agranal structure to the granal structure in BS cell chloroplasts (white bold arrows in Figure 4C, D).

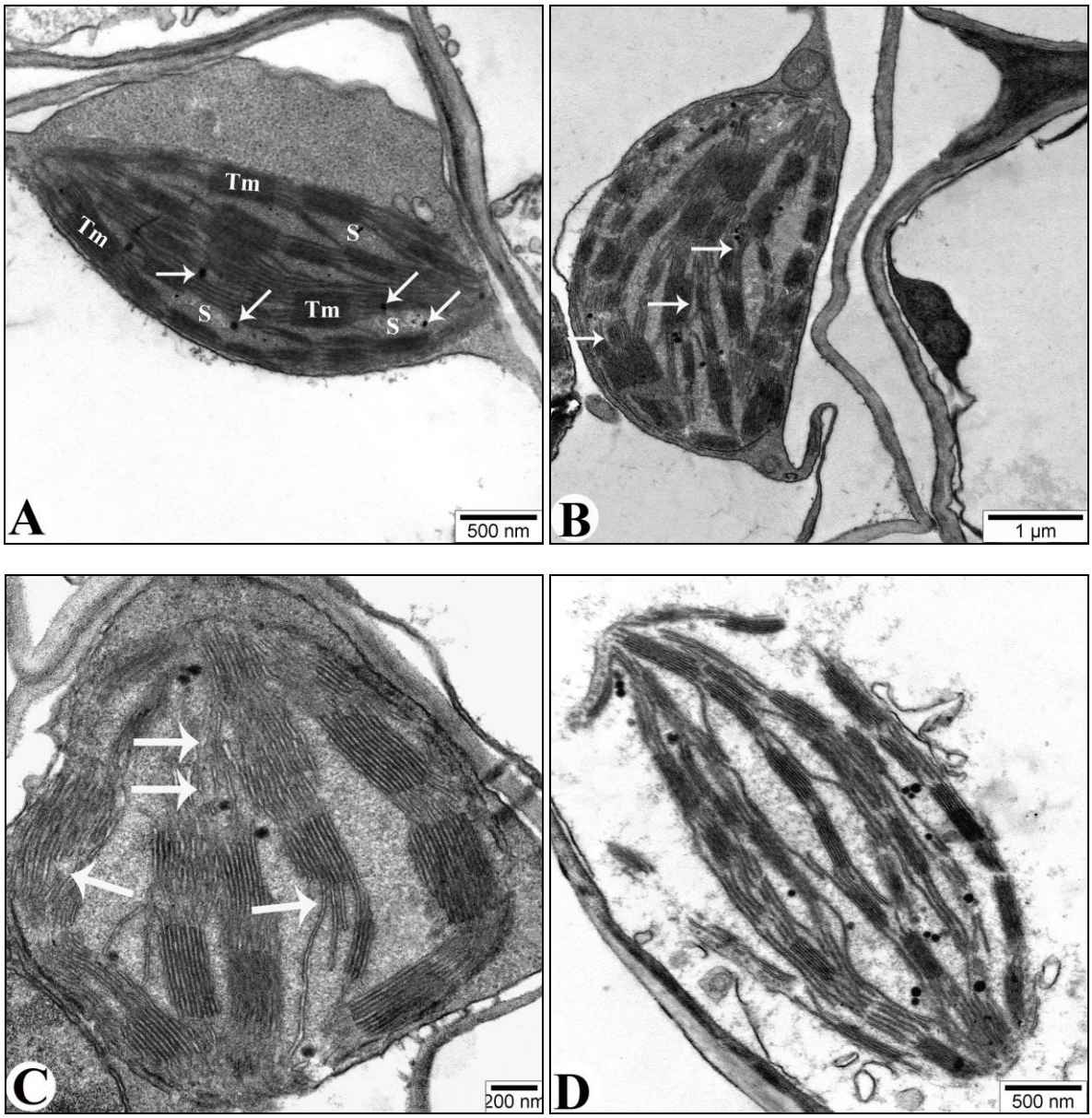

Fig. 3. Ultrastructural changes in mesophyll cell chloroplasts of maize plants exposed to salt stress (B-D) compared with the control group (A). B - 50 mM NaCl; C - 100 mM NaCl; D - 200 mM NaCl; Abbreviations: Tm-thylakoid membrane, S-stroma, white arrows in 3A-lipid droplets (plastoglobules), white arrows in 3B and 3C-formation of spaces between thylakoid membranes with granular structures and damage to the membranes. A-D-Electronograms of ultra-thin sections (50-70 nm). Stain- uranyl acetate and pure lead citrate. The explanation is in the text.

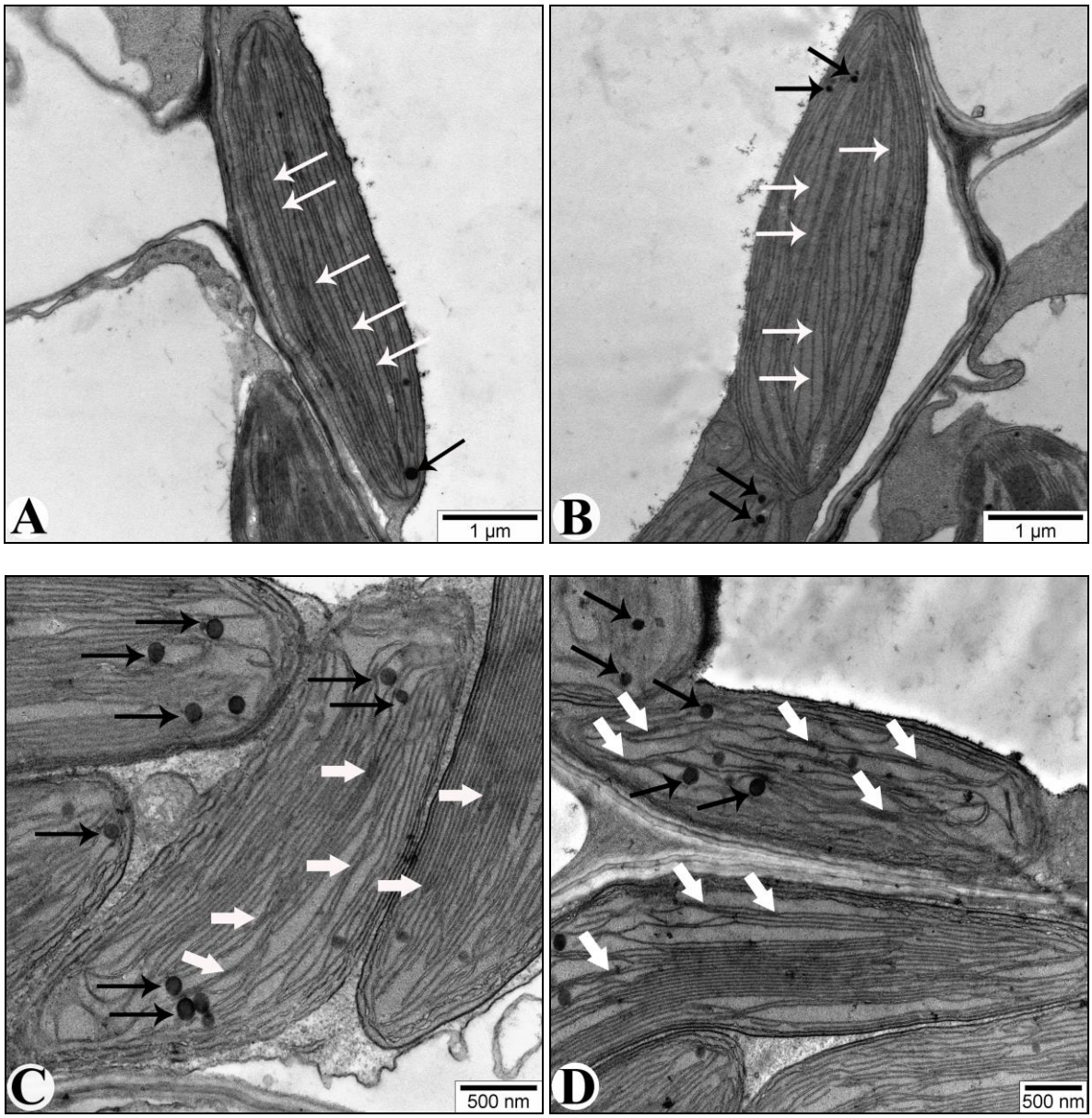

Fig. 4. Ultrastructural changes in bundle sheath cell chloroplasts of maize plants exposed to salt stress (B-D) compared with the control group (A). B - 50 mM NaCl; C - 100 mM NaCl; D - 200 mM NaCl; White arrows in A and B - thylakoid membranes having a granular structures. Black arrows in A, B, C and D - lipid droplets (plastoglobules), Bold white arrows in C and D - zones of the transition of the agranal thylakoid membranes to the granal ones. A-D - Electronograms of ultra-thin sections (50-70 nm). Stain-uranyl acetate and pure lead citrate. The explanation is in the text.

According to the results obtained from the studies, as well as the literature data, M cell and BS cell chloroplasts of C_4 plants contain granal and stromal lamellae, which differ greatly in their biochemical composition, function and localization in the cell. It was found that at low salt concentrations, the activity of SOD - one of the main components of the antioxidant defense system in the cell - enhanced relative to the control. However, at 200 mM concentration of salt, the enzyme activity was partly inhibited. One isoform of the SOD enzyme was observed in BS cells, contrary to M cells. The intensity of this isoform was shown to increase with increasing salt concentrations.

The results of the experiments showed that SOD localized in BS cells plays a major role in the adaptation of maize plants to salt stress. The ultrastructure of chloroplasts in salt-exposed maize leaves was analyzed by electron microscopy. The structure of M cell chloroplasts was shown to be damaged due to salt exposer. They became swollen which led to the destruction of thylakoid membranes. However, there was not such a change in the thylakoid membrane system of BS cell chloroplasts and even apartial transition of the agranal structure to the granal structure occurred.

REFERENCES

Alscher R.G., Erturk N., Heath L.S. (2002) Role of superoxide dismutases (SODs) in controlling oxidative stress in plants. *Journal of Experimental Botany*, **53(372):** 1331-1341.

Asada K. (2006) Production and scavenging of reactive oxygen species in chloroplasts and their functions. *Plant Physiology*, **141(2):** 391-396.

D'Amico F. (2005) A polychromatic staining method for epoxy embedded tissue: a new combination of methylene blue and basic fuchsine for light microscopy. *Biotechnic and Histochemistry*, **80 (5-6):** 207-210.

Gadjev I., Vanderauwera S., Gechev T.S., Laloi C., Minkov I.N., Shulaev V., van Breusegem F. (2006) Transcriptomic footprints disclose specificity of reactive oxygen species signaling in Arabidopsis. *Plant Physiology*, **141(2):** 436-445.

Ghasemi F., Heidari R., Jameii R., Purakbar L. (2013) Responses of growth and antioxidative enzymes to various concentrations of nickel in *Zea mays* leaves and roots. *Rom. J. Biol. Plant Biol.*, **58:** 37-49.

Gill S.S., Tuteja N. (2010) Reactive oxygen species and antioxidant machinery in abiotic stress tolerance in crop plants. *Plant Physiology and Biochemistry*, **48(12):** 909-930.

Guliev N., Babaev G.G., Bairamov Sh.M. et al. (2003) Purification, properties and localization of two carbonic anhydrase from *Amaranhus cruentus* leaves. *Russian Journal of Plant Physiology*, **50(2):** 213-219.

Hasan R., Kawasaki M., Taniguchi M., Miyake H. (2006) Salinity stress induces granal development in bundle sheath chloroplasts of maize, an NADP-malic enzyme-type C4 plant. *Plant Production Science*, **9(3):** 256-265.

Hasan R., Ohnuki Y., Kawasaki M., Taniguchi M., Miyake H. (2005) Differential sensitivity of chloroplasts in mesophyll and bundle sheath cells in maize, an NADP-malic enzyme-type C_4 plant, to salinity stress. *Plant Production Science*, **8(5):** 567-577.

Jalali-e-Emam S.M.S., Alizadeh B., Zaefizadeh M., Zakarya R.A., Khayatnezhad M. (2011) Superoxide dismutase (SOD) activity in NaCl stress in salt-sensitive and salt-tolerance genotypes of Colza (*Brassica napus* L.). *Middle East J. Sci. Res.*, **7:** 7-11.

Kumar M., Kumar A., Dandapat S., Sinha M.P. (2013) Phytochemical screening and antioxidant potency of *Adhatoda vasica* and *Vitex negundo*. *The Bioscan*, **8(2):** 727-730.

Kuo J. (Ed.). (2007) *Electron microscopy: methods and protocols*. Springer Science and Business Media, **Vol.** 369.

Mahanty S., Kaul T., Pandey P., Reddy R.A., Mallikarjuna G., Reddy C.S., Reddy M. K. (2012) Biochemical and molecular analyses of copper–zinc superoxide dismutase from a C_4 plant *Pennisetum glaucum* reveals an adaptive role in response to oxidative stress. *Gene*, **505(2):** 309-317.

Menezes-Benavente L., Kernodle S.P., Margis-Pinheiro M., Scandalios J.G. (2004) Salt-induced antioxidant metabolism defenses in maize (*Zea mays* L.) seedlings. *Redox Report*, ***9*(1):** 29-36.

Menezes-Benavente L., Kernodle S.P., Margis-Pinheiro M., Scandalios J.G. (2004) Salt-induced antioxidant metabolism defenses in maize (*Zea mays* L.) seedlings. *Redox Report*, ***9*(1):** 29-36.

Omoto E., Nagao H., Taniguchi M., Miyake H. (2013) Localization of reactive oxygen species and change of antioxidant capacities in mesophyll and bundle sheath chloroplasts of maize under salinity. *Physiologia Plantarum*, **149(1):** 1-12.

Raines C.A. (2003) The Calvin cycle revisited. *Photosynthesis research*, **75(1):** 1-10.

Ramegowda V., Senthil-Kumar M. (2015) The interactive effects of simultaneous biotic and abiotic stresses on plants: mechanistic unders-

tanding from drought and pathogen combination. *Journal of Plant Physiology*, **176:** 47-54.

Shao R., Xin L., Mao J., Li L., Kang, G., Yang Q. (2015) Physiological, ultrastructural and proteomic responses in the leaf of maize seedlings to polyethylene glycol-stimulated severe water deficiency. *International Journal of Molecular Sciences*, **16(9):** 21606-21625.

Von Caemmerer S., Furbank R.T. (2003) The C_4 pathway: an efficient CO_2 pump. *Photosynthesis Research*, **77(2-3):** 191-207.

Duz (NaCl) stresinin qarğıdalı bitkisinin (*Zea mays* L.) mezofil və örtüktopa hüceyrələrində xloroplastların ultrastrukturuna və superoksiddimutaza fermentinin aktivliyinə təsiri

N.X. Əliyeva[1], E.E.Qafarova[1], D.R. Əliyeva[1], S.Y. Süleymanov[1], F.H. Rzayev [2], E.Kasımov [3]

[1]AMEA Molekulyar Biologiya və Biotexnologiyalar İnstitutu
[2]Azərbaycan Tibb Universitetinin ETM Elektron Mikroskopiya laboratoriyası
[3] Azərbaycan Tibb Universitetinin Histologiya, embriologiya və sitologiya kafedrası

Təqdim olunan işdə NaCl duzunun müxtəlif qatılıqlarında (0 mM, 50 mM, 100 mM, 200 mM) suni iqlim kamerasında becərilən qarğıdalı bitkisindən (Zea mays L.) ayrılmış mezofil və örtüktopa hüceyrələrinin xloroplastlarında superoksiddismutazanın (SOD) aktivliyi, izoferment tərkibi və yarpağın ultrasrukturunda baş verən dəyişikliklər muqayisəli öyrənilmişdir. Aparılan tədqiqatlar nəticəsində müəyyən olunmuşdur ki, stresin təsirindən SOD-un aktivliyi kontrola nisbətən duzun 50 mM və 100 mM qatılığında artmış, lakin 200 mM qatılığında fermentin fəallığı qismən inhibirləşmişdir. SOD fermentinin izoenzim tərkibinin təyini zamanı örtüktopa hüceyrələrində 1 izoforması (Fe- SOD) müşahidə edilmişdir və müəyyən edilmişdir ki, duzun qatılığı artdıqca izoformanın intensivliyi artır. Elektron mikroskopu vasitəsilə mezofil (MH) və örtüktopa hüceyrələri (ÖTH) xloroplastlarının ultrastrukturunun tədqiqi zamanı mezofil xloroplastlarının stresə qarşı daha həssas, ÖTH xloroplastlarının isə nisbətən davamlı olduğu müəyyən olunmuşdur. Duzun yüksək qatılığında (200 mM) ÖTH xloroplastlarının aqranal qurluşunun qismən qranal quruluşa keçməsi aşkar edilmişdir.

Açar sözlər: *Zea mays* L.*, duz stresi, superoksiddismutaza, mezofil, örtüktopa, xloroplast, ultrastruktur*

Влияние солевого (NaCl) стресса на ультраструктуру хлоропластов клеток мезофилла и обкладки проводящих пучков и активность фермента супероксиддисмутазы в растениях кукурузы (*Zea mays* L.)

Н.Х.Алиева[1], Э.Э.Гафарова[1], Д.Р. Алиева[1], С.Ю. Сулейманов[1], Ф.Г. Рзаев[2], Э.К. Касумов[3]

[1]Институт молекулярной биологии и биотехнологий НАН Азербайджана
[2]Лаборатория Электронной микроскопии Азербайджанского медицинского университета
[3]Кафедра гистологии, эмбриологии и цитологии Азербайджанского медицинского университета

В представленной работе было проведено сравнительное изучение активности и состава изоферметов супероксиддисмутазы (СОД) хлоропластов клеток мезофилла и обкладки проводящих пучков, выделенных из растения кукурузы (*Zea mays* L.), выращенной в камере искусственного климата при различных концентрациях NaCl (0 mM, 50 mM, 100 mM, 200 mM), и изменений, происходящих в ультраструктуре листьев. В ходе проведенных исследований было обнаружено, что активность СОД под воздействием солевого стресса при концентрациях NaCl 50 mM и 100 mM возрастала по сравнению с контролем, однако при концентрации соли 200 mM активность фермента частично ингибировалась. При определении состава изоэнзимов была обнаружена 1 изоформа фермента СОД (Fe-SOD) и выявлено, что при повышении концентрации соли интенсивность изоформы возрастает. С помощью методов электронной микроскопии при исследовании ультраструктуры хлоропластов клеток мезофилла и обкладки проводящих пучков было обнаружено, что хлоропласты мезофилла более чувствительны к стрессу, чем хлоропласты обкладки. Также выявлено, что при высокой концентрации соли (200 mM) агранальная структура хлоропластов обкладки частично переходит в гранальную структуру.

Ключевые слова: *Zea mays* L.*, солевой стресс, супероксиддисмутаза, мезофилл, обкладка проводящих пучков, хлоропласт, ультраструктура*

Nəşriyyatın direktoru: *Səbuhi Qəhrəmanov*
Kompüter tərtibçisi: *Rəvanə İlmanqızı*
Bədii tərtibat: *Şəlalə Məmməd*

Formatı 70x100 1/8
Həcmi 13 ç.v.
Tirajı

Ünvan: Bakı şəh., İstiqlaliyyət küç. 28